AD

USAAMRDL TECHNICAL REPORT 71-28

STATIC AND ROTATING AIR/GAS SEAL EVALUATION

By

W. Paladini

June 1971

EUSTIS DIRECTORATE
U. S. ARMY AIR MOBILITY RESEARCH AND DEVELOPMENT LABORATORY
FORT EUSTIS, VIRGINIA

CONTRACT DAAJ02-70-C-0024
CURTISS-WRIGHT CORPORATION
WOOD-RIDGE, NEW JERSEY

UNCLASSIFIED
Security Classification

DOCUMENT CONTROL DATA - R & D

(Security classification of title, body of abstract and indexing annotation must be entered when the overall report is classified)

1. ORIGINATING ACTIVITY (Corporate author)	2a. REPORT SECURITY CLASSIFICATION
Curtiss-Wright Corporation One Passaic Street Wood-Ridge, New Jersey 07075	UNCLASSIFIED 2b. GROUP

3. REPORT TITLE

STATIC AND ROTATING AIR/GAS SEAL EVALUATION

4. DESCRIPTIVE NOTES (Type of report and inclusive dates)

Final Report

5. AUTHOR(S) (First name, middle initial, last name)

W. Paladini

6. REPORT DATE	7a. TOTAL NO. OF PAGES	7b. NO. OF REFS
June 1971	167	19

8a. CONTRACT OR GRANT NO.	9a. ORIGINATOR'S REPORT NUMBER(S)
DAAJ02-70-C-0024 b. PROJECT NO. Task 1G162204A01409 c. d.	USAAMRDL Technical Report 71-28 9b. OTHER REPORT NO(S) (Any other numbers that may be assigned this report) CW-WR-70-024F

10. DISTRIBUTION STATEMENT

Approved for public release; distribution unlimited.

11. SUPPLEMENTARY NOTES	12. SPONSORING MILITARY ACTIVITY
	U.S. Army Mobility Research and Directorate Development Laboratory, Eustis Fort Eustis, Virginia 23604

13. ABSTRACT

This report describes an evaluation of the leakage characteristics of current gas turbine engine air/gas seals and sealing surfaces of small gas turbine engines.

The evaluation included (a) definition of probable air/gas leakage sources and paths in an engine possessing variable compressor and power turbine stator geometry, (b) identification of sealing concepts currently in use, (c) prediction of seal leakage in the small engine, (d) rig testing of several static and rotating seals, and (e) analysis of the effect of leakage on small engine performance.

The rotating shaft seal tests were conducted on a fin-to-fin labyrinth seal and a carbon face contact seal. The casing flange seal tests were conducted on metal-to-metal surfaces and on four metal seals for flanges. The variable-geometry vane trunnion seal tests were conducted on a fluorocarbon bushing and a metal bushing for the compressor and power turbine locations, respectively. Testing included leakage calibrations, and thermal cyclic and mechanical cyclic operation.

The analysis indicated that performance losses in a small engine amounting to an increase in specific fuel consumption of over 10 percent and a loss in power of over 20 percent are possible if leakage is not accounted for in the engine cycle.

DD FORM 1 NOV 68 1473 REPLACES DD FORM 1473, 1 JAN 64, WHICH IS OBSOLETE FOR ARMY USE.

UNCLASSIFIED
Security Classification

DISCLAIMERS

The findings in this report are not to be construed as an official Department of the Army position unless so designated by other authorized documents.

When Government drawings, specifications, or other data are used for any purpose other than in connection with a definitely related Government procurement operation, the US Government thereby incurs no responsibility nor any obligation whatsoever; and the fact that the Government may have formulated, furnished, or in any way supplied the said drawings, specifications, or other data is not to be regarded by implication or otherwise as in any manner licensing the holder or any other person or corporation, or conveying any rights or permission, to manufacture, use, or sell any patented invention that may in any way be related thereto.

Trade names cited in this report do not constitute an official endorsement or approval of the use of such commercial hardware or software.

DISPOSITION INSTRUCTIONS

Destroy this report when no longer needed. Do not return it to the originator.

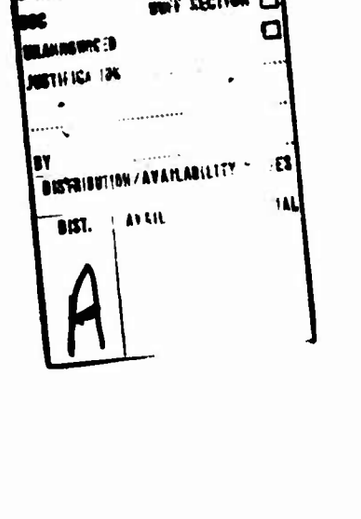

14. KEY WORDS	LINK A		LINK B		LINK C	
	ROLE	WT	ROLE	WT	ROLE	WT
Seals						
Small Gas Turbine Engine						

DEPARTMENT OF THE ARMY
U. S. ARMY AIR MOBILITY RESEARCH & DEVELOPMENT LABORATORY
EUSTIS DIRECTORATE
FORT EUSTIS, VIRGINIA 23604

The research described herein was conducted by Curtiss-Wright Corporation under U. S. Army Contract DAAJ02-70-C-0024. The work was performed under the technical management of Mr. R. G. Furgurson, Propulsion Division, Eustis Directorate, U. S. Army Air Mobility Research and Development Laboratory.

Appropriate technical personnel of this Directorate have reviewed this report and concur with the conclusions contained herein.

The findings and recommendations outlined herein will be considered in planning future programs of small engine or component development.

Task 1G162204A01409
Contract DAAJ02-70-C-0024
USAAMRDL Technical Report 71-28
June 1971

STATIC AND ROTATING AIR/GAS SEAL EVALUATION

Final Report

by

W. Paladini

Prepared by

Curtiss-Wright Corporation
Wood-Ridge, New Jersey

for

EUSTIS DIRECTORATE
U.S. ARMY AIR MOBILITY RESEARCH AND DEVELOPMENT LABORATORY
FORT EUSTIS, VIRGINIA

SUMMARY

The purpose of this program was to provide basic information on the leakage characteristics of current gas turbine engine air/gas seals and sealing surfaces which can be useful in the design and development of small, high-performance gas turbine engines under consideration by USAAMRDL for future Army use.

The approach consisted of (1) definition of all probable air/gas leakage sources and paths in a small, high-temperature, high-pressure gas turbine engine possessing variable compressor and power turbine stator geometry, (2) identification of the various sealing concepts available and currently in use, (3) prediction of the magnitude of leakage of a number of these seals that can be used in the small engine, (4) rig testing of several selected sealing methods to determine leakage rates, and (5) analysis of the effect of this leakage on small engine performance.

The results of the program indicate that performance losses in a small engine amounting to an increase in specific fuel consumption of over 10 percent and a loss in power of over 20 percent are possible if leakages are not predicted and accounted for in the cycle. Overboard leakage produced the largest effect on specific fuel consumption, and leakage bypassing the gas producer turbine had the largest effect on shaft horsepower.

The major source of engine leakage was found to be the labyrinth seals. This was verified both by analytical prediction and by rig testing of a typical labyrinth seal design under simulated engine conditions. The air/gas leakages typical of labyrinth seals constituted more than 75 percent of the total engine performance losses associated with leakages.

The major source of leakage in the compressor case split-lines occurred at the intersections of the horizontal and vertical flanges. Use of static seals at the split-lines produced no significant improvement over the metal-to-metal flanges.

A fluorocarbon bushing used as a variable-geometry compressor vane trunnion seal provided excellent sealing characteristics. The turbine vane trunnion metal bushing leakage was about sixty times higher than the compressor vane seal leakage.

FOREWORD

The work reported herein was performed by Curtiss-Wright under United States Army Contract DAAJ02-70-C-0024 (Task 1G162204A01409) to provide information on the leakage characteristics of current gas turbine engine air/gas seals and sealing surfaces which can be useful in the design and development of small, high-performance gas turbine engines.

The technical guidance of Messrs. H. Morrow, N. Kailos, and R. Furgurson of the Eustis Directorate, U.S. Army Air Mobility Research and Development Laboratory is gratefully acknowledged.

BLANK PAGE

TABLE OF CONTENTS

LIST OF ILLUSTRATIONS

LIST OF ILLUSTRATIONS - Continued

LIST OF ILLUSTRATIONS - Continued

LIST OF ILLUSTRATIONS - Continued

LIST OF TABLES

LIST OF TABLES - Continued

BLANK PAGE

INTRODUCTION

Gas turbine engines contain various air and gas leakage sources which are detrimental to engine performance. The problem is compounded in advanced, high-performance engines by the requirements for higher compressor pressure ratios, higher turbine inlet temperatures, and variable geometry in compressor and turbine stator sections. Furthermore, the problem becomes even more acute in the smaller engines of the 2 to 5 pounds per second airflow range where engine leakage as a percentage of total airflow increases due to the increase in the ratio of engine circumference to flow area.

Typical performance losses in a small turboshaft engine for a leakage of 1 percent of the total engine airflow in each of three major leakage categories are as follows:

	Leakage Percent Total Flow	Percent Loss Horsepower	Percent Increase BSFC
A. Leakage Overboard	1.0	3.8	2.3
B. Leakage Bypassing Turbine	1.0	4.2	1.8
C. Leakage Typassing Combustor	1.0	1.9	0.4
Total	3.0%	9.9%	4.5%

The above leakage classifications are described as follows:

A. Leakage overboard-flow that has been compressed in the compressor and is unavailable to do work in the turbines.

B. Leakage which bypasses the compressor turbine but returns to the mainstream before the power turbine.

C. Leakage which bypasses the combustor but returns to the mainstream before the compressor turbine.

These performance losses are typical of unanticipated leakages occurring in the cycle; they illustrate the importance of minimizing any gas leakage and the serious consequences if leakage is not accurately predicted and accounted for in the cycle.

A wide variety of static and dynamic seals is used in a modern gas turbine engine to prevent or minimize leakage. Static seals include gaskets, O-rings, and metal-to-metal seals as typical representatives. For dynamic seals, both clearance and contact types are used. Clearance types are exemplified by labyrinths, floating rings, and bushings. The contact types include lip seals, piston ring seals, end-face seals, and circumferential seals.

The specific concerns of this program are (1) to identify all probable air/gas leakage sources and paths associated with a small, high-performance gas turbine engine; (2) to investigate typical sealing devices representative of current technology which are most likely to be used at the various leakage sources; (3) to establish the leakage rates which can be expected from these sealing devices; and (4) to determine the effects of these leakages on the performance of a hypothetical, small gas turbine engine with a variable-geometry power turbine nozzle and variable-geometry compressor vanes. The overall objective of the program is to provide the designer of small gas turbine engines with an indication of the serious nature of the leakage problem and a guide to where the emphasis should be placed in reducing the leakage.

The program goals were accomplished in a series of five tasks. The following is a brief description of each task.

Task I - A literature and industry survey was conducted to identify the typical air/gas seals employed in current gas turbine engines and to define their characteristics. Also, all probable air/gas leakage sources were defined on a hypothetical design of a small gas turbine engine which is assumed to possess variable compressor and power turbine geometry, and the magnitude of each leakage source was estimated.

Task II - Testing was conducted under simulated engine conditions to determine the leakage characteristics of a labyrinth seal and a carbon-face seal, which are widely used dynamic seals in current gas turbine engines.

Task III - Testing was conducted under simulated engine conditions to evaluate static sealing configurations for horizontal and vertical case splitlines.

Task IV - Testing was conducted under simulated engine conditions to determine the leakage characteristics of typical variable-geometry vane mechanisms suitable for compressor and turbine applications.

Task V - An analysis was conducted to determine the effect of the various leakage sources on engine performance.

DISCUSSION

LITERATURE AND INDUSTRY SURVEY (TASK I)

Engine Seal Survey

A survey was conducted and information was gathered from various publications and engine and seal manufacturers to identify the typical air/gas seals and sealing surfaces currently used in gas turbine engines and to define their characteristics in terms of leakage and wear rates, limitations and sensitivities, reliability, relative cost, and applicability to a hypothetical gas turbine engine having the characteristics of small size, high temperature, high rotor speeds, and high air/gas pressures. The sources, facilities, and seal manufacturers contacted during this survey are listed in Tables I and II. A list of typical engines surveyed, including their airflow, diameter, and shaft speed, appears in Table III. A summary of the engine seal survey appears in Table IV, which lists the type of seal, engine model, seal location, and significant seal features and limitations.

The following sections summarize the survey information regarding rotating seals, flange seals, and variable-geometry mechanism seals which lead to the selection of the seal configurations tested in Tasks II, III, and IV. These selections are presented in Table V.

Rotating Seals

Rotating seals reviewed in this program can be categorized by their operation as either contact or noncontact seals and by their application as either air (gas) to air (gas), or air (gas) to oil sump.

1. Labyrinth Seals

   Labyrinth seals are noncontact-type rotating seals and fall into two general classes: (1) the straight-through and (2) the double-fin staggered arrangement. The straight-through seal is the least efficient in that it allows some of the fluid to follow a straight line, hence a considerable amount of kinetic energy carry-over from one fin restriction to another. In the staggered fin labyrinth, the shaft and sleeve bore contain thin, sharp-edged circumferential fins. The pitch of the fins on the shaft is mismatched with the pitch of the fins in the sleeve bore such that axial staggering will never allow "straight-through" flow.

   A true staggered seal such as one with fin engagement is difficult to assemble. Consequently, a modified arrangement using a stepped-fin and shroud, or the rub-in type, may be used. The kinetic energy carry-over in either of these labyrinth seals is reduced from that of a straight-through. The rub-in type seal is accomplished by coating the shroud with a soft or low density material and setting a low diametral clearance. The amount of rub-in is determined by the centrifugal growth of the rotor, runout and thermal growth.

TABLE I. TASK I - LITERATURE SURVEY - TYPICAL SOURCES

A. SOURCES

- Defense Documentation Center
- National Aeronautics and Space Administration
- Engineering Index, Inc.
- Institute of Aerospace Sciences
- Society of Automotive Engineers
- American Society of Mechanical Engineers
- Scientific & Technical Aerospace Reports
- American Society of Lubrication Engineers
- Engine Overhaul Manuals
- Curtiss-Wright Service Department
- Various Seal Manufacturers
- General Publications
  - Product Engineering
  - Mechanical Engineering
  - SAE Journal
  - Lubrication Engineering
  - Machine Design
- National Bureau of Standards (Clearinghouse)

B. FACILITIES

- Naval Air Propulsion Test Center, Trenton, New Jersey
- Aeronautical Engine Department, Philadelphia, Pennsylvania
- Curtiss-Wright Engine Overhaul Department, Wood-Ridge, New Jersey

TABLE II. TASK I - SEAL MANUFACTURERS SURVEY

Sealol Inc.
Providence, R. I.

Haskel Engineering and Supply Co.
Burbank, California

Parker Seal Co.
Culver City, California

Gits Brothers Manufacturing Co.
Chicago, Illinois

Clevite Corp.
CGB Division

Simplex Piston Ring Manufacturing Co.
Miami, Florida

Koppers Company Inc.
Baltimore, Maryland

Rex Chainbelt Inc.
Cartriseal Division
Wheeling, Illinois

Crane Packing Co.
Morton Grove, Illinois

Garlock Inc.
Palmyra, New York

Chicago Rawhide Manufacturing Co.
Elgin, Illinois

Borg-Warner Mechanical Seals
Los Angeles, California

Universal Seal Products Corp.
Cleveland, Ohio

Johns-Manville Sales Corp.
New York, New York

United Aircraft Products Inc.
United Metallic O-Ring Divisica
Dayton, Ohio

TABLE III. TASK I - INDUSTRY SURVEY - TYPICAL ENGINE CHARACTERISTICS

Engine Model	Airflow (lb/sec)	Engine Diameter (in.)	Rotor Speed (rpm)
T-63-A-5A	3	-	35,000 L.P. 51,600 H.P.
T-65	3.3	-	57.500
T-53	11	-	25,150
T-58	12.7	18	26,300
T-55-L-7	22	-	18,300
T-64, GE-6	24.5	23.8	16,900
T-56	32	29	13,820
J-85	44	17	16,500
GE-1	77	24	13,000
J-52	120	30	10,500 11,000
TF-30	129	38	9,500 14,500
JT8D	153	44	8,000 11,450
J-79	169	38	7,680
J-57	180	40	6,500 9,500
JT3D	180	-	9,800
TF-41	260	38	8,900 12,700
J-75	265	43	6,500 8,650

BLANK PAGE

TABLE IV. TASK I - GAS TURBINE ENGINE SEALS SUR

Configuration	Engine Model	Location	Fe
I. Rotating			
Straight-through and staggered labyrinth fins	All Models	Compressor discharge air turbine section gas seals	Simplicity, wide materi
	J-65	Nos. 1, 2, & 3 bearings	Operated at velocities,
	T-56	Nos. 2 & 3 bearings	pressure.
	JT-8-D	Nos. 1, 2, 3, & 4 bearings	Requires no
	TF-41	All bearings	
Carbon contact single segmented ring	T-64, J-79, J-85	All bearings	Low leakage
			Accommodat motion.
			Requires s envelope.
Carbon contact multi-split rings	J-57	Nos. 4-1/2 & 6 bearings	Same as ab
	J-75	Nos. 1, 4-1/2, & 6 bearings	Seals betw tric rotat
	JT8-D	Nos. 4-1/2 & 6 bearings	
	TF-30, J-52		
Carbon-face seal with piston ring secondary	J-57, J-52	Nos. 1, 2, 3, 4, & 5 bearings	Low leakag
	J-75	Nos. 2, 3, 4, & 5 bearings	Relatively shaft defl
	JT8-D	No. 1 bearing	Tolerates seal than type since sure balan
	TF-30		

K I - GAS TURBINE ENGINE SEALS SURVEY

Location	Seal Characteristics	
	Features	Limitations
ssor discharge air e section gas	Simplicity, reliability, and wide materials selection.	High leakage rate due to .002 - .020" clearance.
, 2, & 3 bearings & 3 bearings	Operated at high peripheral velocities, temperature and pressure.	
, 2, 3, & 4 bearings	Requires no lubrication.	
arings		
arings	Low leakage. Accommodates large axial motion. Requires small installation envelope.	Limited to low Δ P across seal due to partial pressure balance. Segmented seal is complex and expensive (axial and circumferential springs position seal).
-1/2 & 6 bearings , 4-1/2, & 6 bearings -1/2 & 6 bearings	Same as above. Seals between two concentric rotating shafts.	Requires oil cooling at high rubbing speed to prevent temperature build-up and excessive wear at rubbing faces.
., 2, 3, 4, & 5 igs !, 3, 4, & 5 bearings bearing	Low leakage. Relatively insensitive to shaft deflection. Tolerates higher Δ P across seal than circumferential type since complete pressure balance is possible.	Requires larger installation envelope. Requires careful handling and installation procedures. Requires oil cooling at high rubbing speeds.

B

TABLE IV - Continued

Configuration	Engine Model	Location	Feat
II. Housing Split Line			
Metal-to-metal parallel and piloted flange surfaces	T-56	All horizontal and vertical split lines	Simple assemb
	J65	"	Low cost.
	T-53, T-55	"	
	T-64, T-58, T-75, J-85	"	
	J-52, TF-30	Vertical split lines	
	J-57	Hot section vertical split lines	
	J-75	Hot section vertical split lines	
Hollow metallic O-ring fully confined in a machined groove in one flange face	J-52	Rear compressor housing rear vertical flange to diffuser case front flange	Accommodates from flatnes allelism.
	J-52	Diffuser case rear vertical flange to combustor housing front flange	
	J-75	Front compressor case rear flange to compressor intermediate case front flange	
III. Variable-Geometry Trunnion Seal			
Metal spacers with close fit Teflon flanged bushings on trunnions	J-79	Compressor stator stages No. 1 through No. 6	Low leakag
	T-64, T-58	1GV - 1st through 4th stages	Requires l torque due ient of fr
Flanged bronze bushings on trunnion with spring-loaded face contact	Industrial	Power turbine stator	Compatible antigallin

IV - Continued

ation	Seal Characteristics	
	Features	Limitations
al and verti- nes " " "	Simple assembly. Low cost.	Sensitive to surface irregularities, out-of-flatness, distortion, etc.
it lines vertical split vertical split		
sor housing l flange to e front e rear verti- o combustor t flange ssor case rear mpressor inter- front flange	Accommodates deviation from flatness and parallelism.	Over-temperature causes relaxation of seal. 32 microinch RMS on grooves and flanges. Sensitive to dirt and other foreign material.
tator stages h No. 6	Low leakage.	Teflon limited to 500°F.
rough 4th	Requires low actuation torque due to low coefficient of friction for Teflon.	
e stator	Compatible materials for antigalling, etc.	Temperature-limited materials; water-cooled trunnion.

B

TABLE V. TASK I - SEALS SELECTION

I. ROTATING SEALS

1. Face contact carbon seal with secondary piston ring

2. Axial labyrinth staggered-fin type seal

II. FLANGE SEALS OR SEALING SURFACES

1. Metal-to-metal (horizontal flange)

2. Metal-to-metal with step pilot (vertical flange)

3. Pressurized metal O-ring with soft plating (vertical flange)

4. Metal tubing with soft plating (horizontal flange)

5. Pressure-energized metal V-ring with soft plating (vertical flange)

6. Metal-asbestos braided packing (horizontal flange)

III. VARIABLE-GEOMETRY TRUNNION SEAL

A. Compressor

Teflon bushing and washer

B. Turbine

Compatible metal bushing and trunnion materials

In all labyrinth seal designs, the leakage is controlled primarily by the running clearance. Other factors affecting leakage include the number of restrictions (fins), ratio of fin height to pitch, diameter, pressure ratio, upstream pressure, and temperature.

Labyrinth seals incorporated on the engine models investigated were used as air-to-air and air-to-oil seals. Some models used the noncontact air-to-air combination as interstage seals and to meter compressor discharge bleed for turbine disc cooling. In other applications, "contact" type labyrinth configurations using rub-tolerant honeycomb or silver-plated shrouds were incorporated to minimize leakage from the turbine section and from low-pressure low-temperature air buffer zones for bearing seals which connect to a common overboard-vented cavity. In all of these applications, engine geometry necessitated the use of labyrinth type seals because of the high ΔP or peripheral velocities involved or the inability to provide lubrication or cooling for contact seals. Some engine models, such as the T-58 and TF41, use complex close-clearance multilabyrinth stages as air (gas)-to-bearing sump seals.

The survey indicated that a hypothetical small engine would incorporate labyrinth seals at similar locations. However, application of the multilabyrinth staging for air-to-bearing sump seals would require prohibitively large space requirements for the temperature and pressure differentials estimated for the small engine. In addition, the relatively high air-leakage rates of these labyrinth seals may introduce dirt particles into the bearings and oil system under the severe contamination environments experienced by Army engines (i.e., helicopter applications).

Although many sources of labyrinth seal leakage data are available, the effects of tooth height and pitch combinations for the seal and shroud and very low clearances over a range of pressure ratios are not well defined. Since the major portion of total estimated air leakage overboard and bypassing the combustor occurs past labyrinth seals, it was felt that Task II testing should include a labyrinth seal configuration designed for the small engine.

The characteristics of labyrinth type seals are summarized in Table VI.

2. Carbon Seals

In all cases reviewed, carbon shaft seals were used as air-(gas)-to-oil sump seals. The circumferential and face-type seals make direct contact with a rotating shaft runner, while the controlled gap floating ring seal is considered to be a noncontact type seal.

TABLE VI. CURRENT L

Configuration	Leakage	Sensitivi
A. Flat Plate Shroud 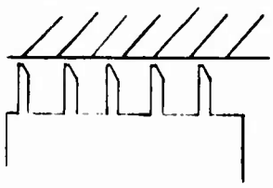	Leakage Coefficient = .003 at .005" steady state operating clearance.	Shroud is intole rotating fin con
B. Honeycomb Shroud 	Leakage Coefficient = .008 at .005" running clearance in a .005" deep rub-in slot.	Leakage varies w and depth of rub a given fin to s clearance.
C. Silver-Plated Shroud 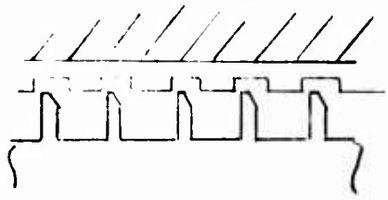	Leakage Coefficient = .002 at .005" running clearance in a .005" deep rub-in slot.	Leakage varies w and depth of rub a given fin to s clearance.
D. Multifinned Shroud 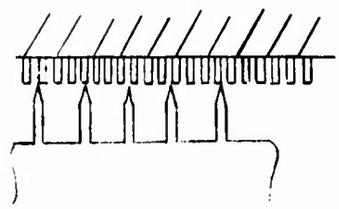	Considered lowest leakage configuration due to the minimizing effect of the finned shroud on effective flow area.	Relative axial s rotating and sta fins.

URRENT LABYRINTH SEALS

ensitivities	Wear	Applicability
s intolerant of fin contact.	Any rotating fin contact with shroud causes fin wear with increased leakage.	Leakage excessive - cannot maintain close enough clearance with allowance for misalignment and transient operation.
aries with length of rub-in slot for in to shroud radial .	Honeycomb abrades with little rotating fin wear.	Leakage through honeycomb cells excessive.
aries with length of rub-in slot for in to shroud radial .	Rubbed-out material builds up on shroud making disassembly difficult. Metal chips generated can contaminate cooling air system.	Unacceptable because of disassembly and contamination problems.
axial spacing of and stationary	Thin fins on shroud peel back upon contact by rotating member.	Considered to be the most applicable configuration. No test data available to substantiate seal efficiency.

B

BLANK PAGE

The carbon element which is the common sealing surface of all configurations is made from powdered carbon and graphite bonded with a hydrocarbon, compacted, and sintered. Graphite as a bearing material has good lubricity but relatively low strength; carbon has higher strength and hardness but is only a fair lubricant. The graphite-carbon combination provides a useful compromise of self-lubrication and relatively high compressive strength. Other properties are low density, brittleness, low tensile strength, resistance to thermal shock, and corrosion. Carbon oxidizes excessively above 600°F and has a coefficient of expansion approximately one-third that of metals used for bearing shafts. Since the material is porous, it can be impregnated with oxidation-resistant coatings or treatments to seal against the entry of air, which at present can increase extended operation up to 800°F. These proprietary surface treatments are apparently relatively thin since most suppliers warn against machining treated surfaces. Impregnation also increases compressive strength and elastic modulus.

A promising development for higher temperature capability is a nearly impervious graphite-glass composition which combines high compressive strength with a high degree of oxidation and chemical resistance.

The best graphite-carbon grade cannot be selected on the basis of operating temperature alone. There are many other dependent variables to consider, such as shaft condition, friction coefficient, load level, shaft speed, and dissipation of heat from the mating surfaces. A major factor in wear rate is the runner surface. This surface must be a hardened, corrosion-resistant steel protected with a highly polished chromium plate. For service above 1000°F, this surface should be Stellite or tungsten carbide.

Oil coking and system contamination from severe operating environments also affect, to varying degrees, the operating capabilities of all seal configurations studied. Coking can affect the radial and axial floating movement of controlled-gap carbon ring and face type seals respectively, while radial movement and pressure balance can be disturbed on the segmented carbon ring design. The effectiveness of highly polished seal surfaces required to maintain a good seal and keep heat generation to a minimum can be severely reduced by introduction of abrasive dirt particles. Since susceptibility to oil coking and foreign particle contamination must be considered, low oil inlet temperature or adequate cooling and efficient oil and coolant air filter systems are desirable.

a. Segmented Carbon Ring

The segmented carbon ring bearing cavity circumferential seal can be considered as a ring manufactured to a bore size coincident with shaft size, which is then segmented and held

around the shaft with a garter spring restraint. As wear occurs, the gaps between segments decrease until eventually the ring is arch bound and is again essentially a bushing with minimum clearance. This seal configuration has favorable characteristics such as low air leakage (0.5 SCFM at 70 psi ΔP and 6-inch diameter), large relative axial displacement capability, small installation envelope, and fail-safe operation (by the retention action of the circumferential spring on a fractured segment).

There are a number of disadvantages to this seal configuration. This seal is expensive because of the many pieces involved and the extensive machining required for pressure balance. In addition, the carbon segments are fragile and require careful handling. Assembly problems also exist in that the force of the circumferential garter spring compresses the seal segments to an I.D. size smaller than the mating shaft or runner. During engine operation, initial friction loading and wear are relatively high due to the action of the circumferential spring loading and unbalanced radial pressures. This condition can be aggravated by the formation of oil coking in the I.D. surface grooves, causing an increase in the radial pressure unbalance. The coked oil will also fill the segment gaps, causing the seal to hang open with increased air leakage.

The allowable ΔP across this seal is approximately 50 psi for the small engine application.

b. Controlled Gap Seal

The controlled gap carbon seal is a continuous carbon ring contained under compression (shrink fit) in a metal ring (Figure 1). This configuration is much less fragile than the segmented design since carbon has high compressive strength. Also, the extensive machining required on the segmented ring for radial pressure balance is not necessary, making the cost of this seal about one-fifth that of the segmented seal.

The disadvantage of this configuration is the higher air leakage associated with the design. Sufficient seal-to-runner clearance has to be allowed to preclude the possibility of the carbon element and backup ring from seizing and spinning with the shaft at some severe transient condition.

Allowable ΔP across this seal is in the 50-psi range for the small engine.

c. Face-Contact Carbon Seals

Face seals offer an attractive package for solution of high-temperature, pressure, and speed conditions. By the nature of

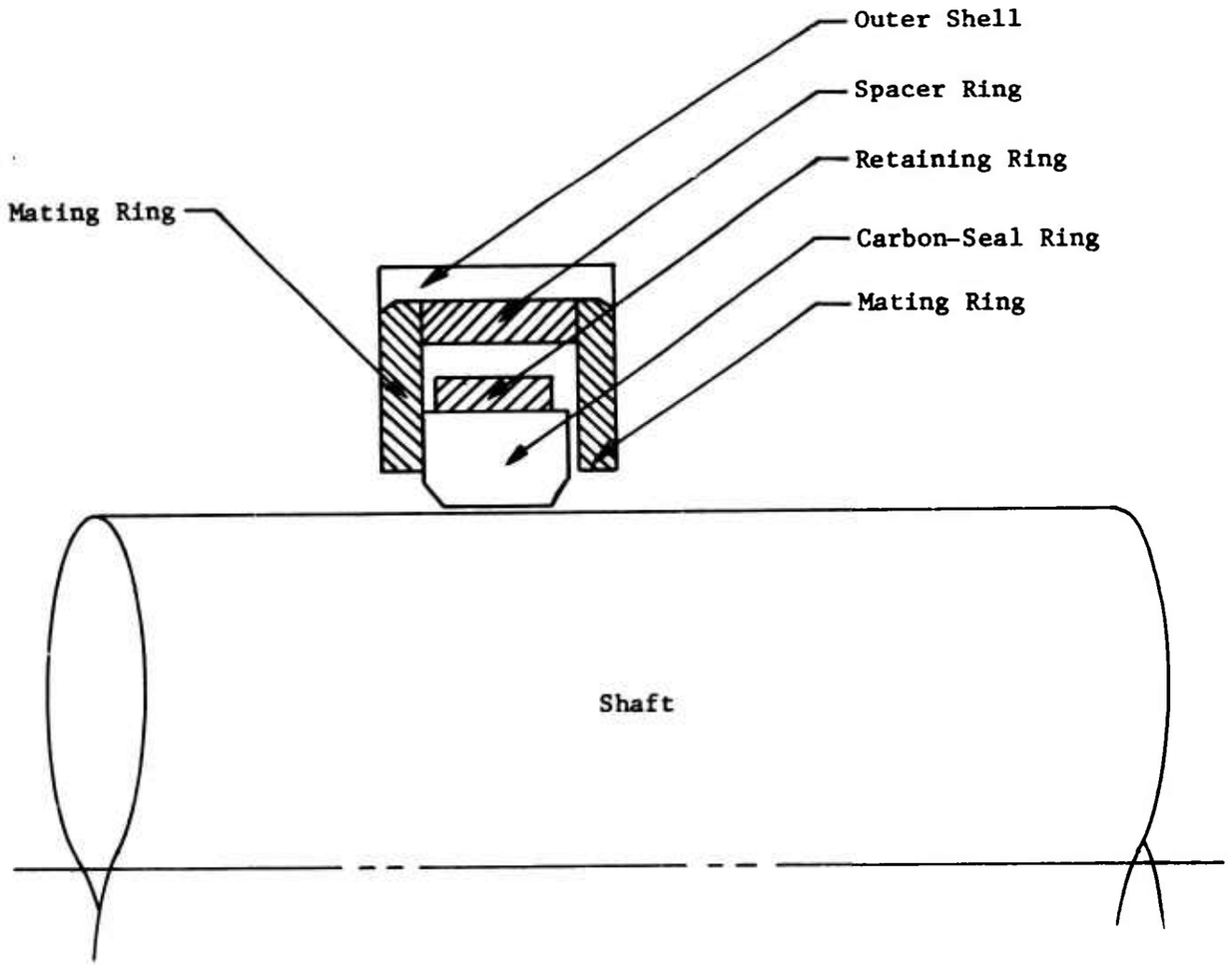

Figure 1. Controlled-Gap Carbon Floating Seal.

the design, a complete spectrum of pressure balancing can be achieved. The seal can be overbalanced, underbalanced, or completely balanced. This results in light face loading generally supplied by either a bellows, coil springs, or wave washers. The result is much lower heat generation at the interface and a less severe heat rejection problem. The seal concept shown in Figure 2 represents a typical face contacting seal of the pressure-balanced type. Secondary sealing is accomplished using a piston ring. Construction of the seal consists of a housing, wave or coil springs to provide axial load, a seal ring carrier, a carbon seal ring, a piston ring, a heat shield, and a shaft mating ring.

Use of a face-type seal at all bearing locations where assembly procedures and clearances will allow appears to have overall advantages over the circumferential seals. Because of the pressure balance possible with a face-type seal design, friction loading is low, and higher pressure ratios across the seal face are possible. This capability would reduce the requirement for venting the air cavity upstream of the seal and thereby also reduce leakage overboard.

Air leakage through the face seal occurs mainly past the piston ring secondary stationary seals. The leakage of this type of seal is low (approximately 1 SCFM at 80 psi on a 2-inch-diameter seal). Oil coking, which may be a serious problem with the segmented seal, does not functionally affect the face seal.

Face seals accumulating 2000 to 4000 hours between overhaul with little increase in seal leakage over this time period have been reported from engine experience. In many cases, the used seal is refaced and reinstalled at overhaul.

The allowable ΔP across this seal is in the 150-psi range for the small engine application.

Characteristics of the carbon-type seals are compared in Table VII.

Split-Line Flange Seals

The primary function of the engine housing split-lines is to facilitate assembly and mechanical joining of dissimilar materials such as between the compressor and combustor housing. Since split-lines present a discontinuity in the engine pressure vessel, they are potential sources of leakage.

All engines surveyed, with the exception of three models at special locations, use bare metal-to-metal flange attachments at all outer housing split-line locations. Many engine models utilize piloted vertical flanges to maintain internal radial clearances. At special locations where high internal pressure levels occur at a flange design offering a poor metal-to-

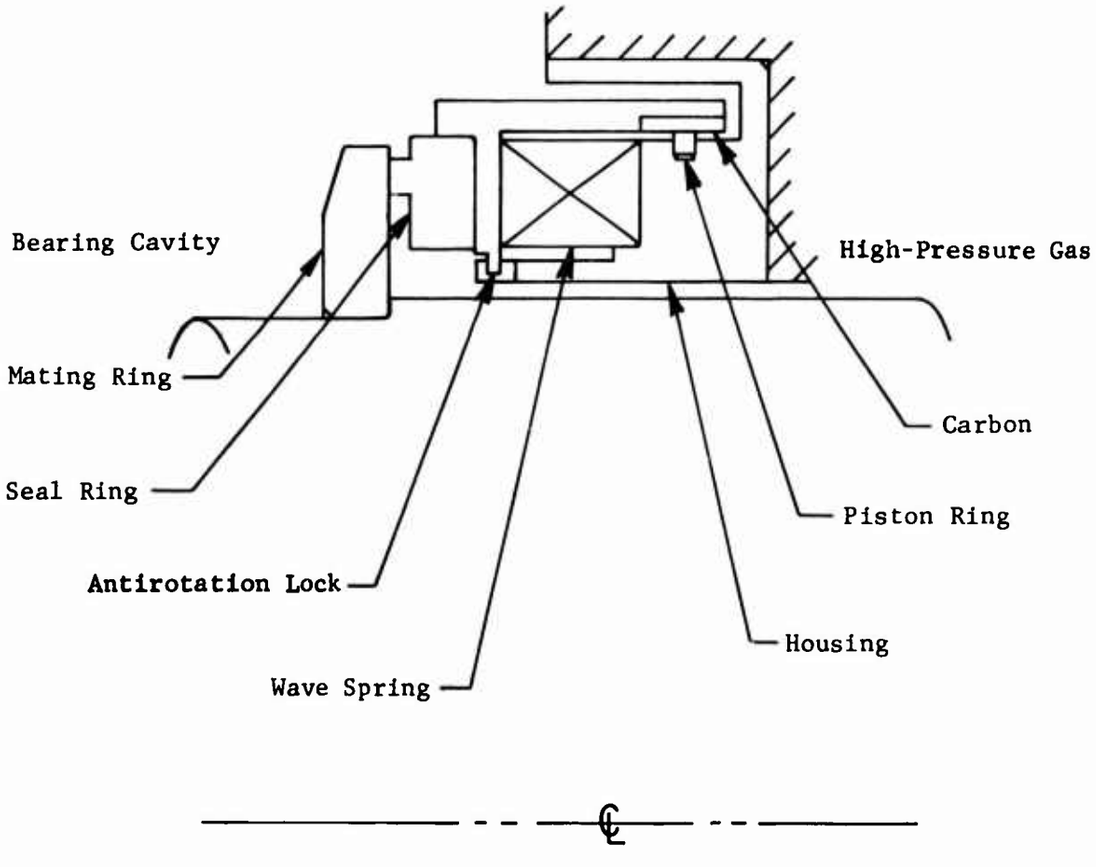

Figure 2. Face-Contact Carbon Seal With Piston Ring as Secondary Seal.

TABLE VII. CARBON SEALS

Configuration	Air Leakage	Friction Losses	Handling and Assy Problems	Sensitivities	Relative Cost	Design Limitations
A. Controlled Gap	Highest	Lowest when gap is maintained.	Lowest	Moderate number	Lowest	ΔP = 50 psi @ 330 fps and 800°F air temperature. Difficult to maintain gap under all operating conditions.
B. Segmented Ring	Lowest initially but approaches controlled gap leakage with wear.	Highest loading and contact area due to spring force and radial pressure unbalance.	Highest - Carbon segments are fragile and present interference fit at assembly	Highest number	Highest	ΔP = 50 psi @ 330 fps and 800°F air temperature.
C. Face Seal with Piston Ring Secondary	Usually maintains low leakage thru overhaul life.	Low face loading due to pressure balance capability.	High - Mainly seal alignment at assembly.	Lowest number	High	ΔP = 150 psi @ 400 fps and 800°F air temperature.

metal sealing arrangement, a hollow metallic O-ring fully confined in a groove is used.

Since these sealing configurations are so exclusively used and could be applicable to a small engine, a comparative test of these configurations was warranted in Task III. Alternate flange sealing arrangements will also be evaluated.

The critical engine sections are considered to be the combustion chamber housing flanges and turbine nozzle support and rotor shroud flanges. These sections are most susceptible to distortion from high operating temperature with high resultant leakage because of high Δ P and large perimeter. The centrifugal compressor exit housing flange diameter is equivalent to the size of a straight axial compressor gas turbine engine with approximately 10 times the airflow. Therefore, a given leakage gap at this location will have a disproportionate effect on the small engine as compared to the larger engine. Flange leakage even at those locations which are more representative of the small engine inlet size of 6 inches diameter for 4.5 pounds per second engine airflow will still be more than three times larger for given pressure compared to the J-85 engine with an 18-inch-diameter inlet and 44 pounds per second airflow, and more than five times larger when compared to the J-52 with a 30-inch-diameter inlet and 150 pounds per second airflow. Therefore, minimization of flange leakage paths becomes more critical as engine size decreases.

For these areas, seals should be capable of conforming to surface irregularities and accommodating considerable deviation from seal surface flatness and parallelism, high temperature and Δ P operation, small size, and relatively low bolt loading requirements. Two seal designs meeting the above specifications are: (1) gas-filled high-temperature alloy tubing with silver or nickel plating and (2) light cross-section V-shaped pressure-actuated high-temperature alloy gasket with silver or nickel plating. These configurations are expensive but may be necessary for a satisfactory seal in those areas which experience the most severe operating conditions. Both of these configurations require less than 400 pounds force per circumferential inch to seal properly, are available in small sizes, have a 1500°F temperature and a 1000-psi pressure capability, and use of soft plating to conform to surface irregularities. Typical materials for metallic O-rings and pressure-actuated metal gaskets ("V" groove) are presented in Table VIII.

Table IX summarizes the design and operating characteristics of the flange seals discussed.

Variable Geometry Vane Trunnion Seals

The variable area requirement of compressor and power turbine stator vanes is generally accomplished by extending the shank of the stator vane in the form of a trunnion through a bushing located in a support housing (Figure 3). The actuating and synchronizing mechanisms are attached to the shank outside the housing.

TABLE VIII. FLANGE SEALS - TYPICAL MATERIALS

A. BASE MATERIALS

	Operating Temperature (°F)
Beryllium-Copper	200
Aluminum	400
17-4PH	900
18-8	900
A-286	1500
Inconel X	1600
René 41	1800
Haynes 25	1800
Hastelloy	2000
Tantalum 90%/10%	2500

B. PLATING MATERIALS

Indium	300
Kel-F	350
Teflon	450
Silver	1650
Copper	1800
Gold	1850
Nickel (Soft)	2500

TABLE IX. FLANGE SEALS

Configuration	Wear	Leakage	Limitations	Sensitivities	Relative Cost
A. Metal to Metal 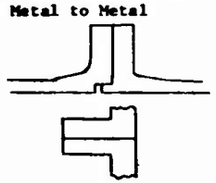	Mating surfaces distort during engine operation.	Can be excessive on a small engine at high ΔP.	Machining tolerances	Surface imperfect. Mating surface alignment bolt spacing.	Least expensive
B. Metal O-Ring 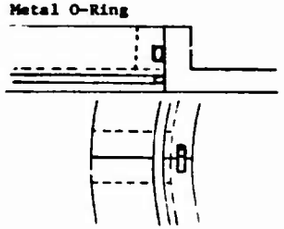	Not reusable after compression.	Reduced leakage by accommodating some deviation from flatness and parallel.	1200°F 1000 psi	Requires 16-microinch surface finish on sealing surfaces. Tool marks concentric with ring.	A + approx. $15 per joint.
C. Metal O-Ring Same as (B) except pressure filled and soft metal plating.	Not reusable after compression.	Soft plating improves sealing ability. Pressurization provides 100% increase in O-Ring resilience at 1000°F.	1500°F 1000 psi Deflection - .004 Warpage - .001 Flatness - .001 TIR	Requires 32-microinch surface finish on sealing surfaces. Tool marks concentric with ring.	A + approx. $25 per joint.
D. Pressure-actuated metal gasket, soft metal plating. 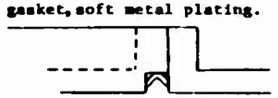	Can be reused 3 to 4 times if handled properly.	Reduces leakage to a minimum by conforming to surface irregularities.	1500°F Deflection - .005 Warpage - .002 Flatness - .002 TIR	Same as (C).	A + approx. $60 per joint.

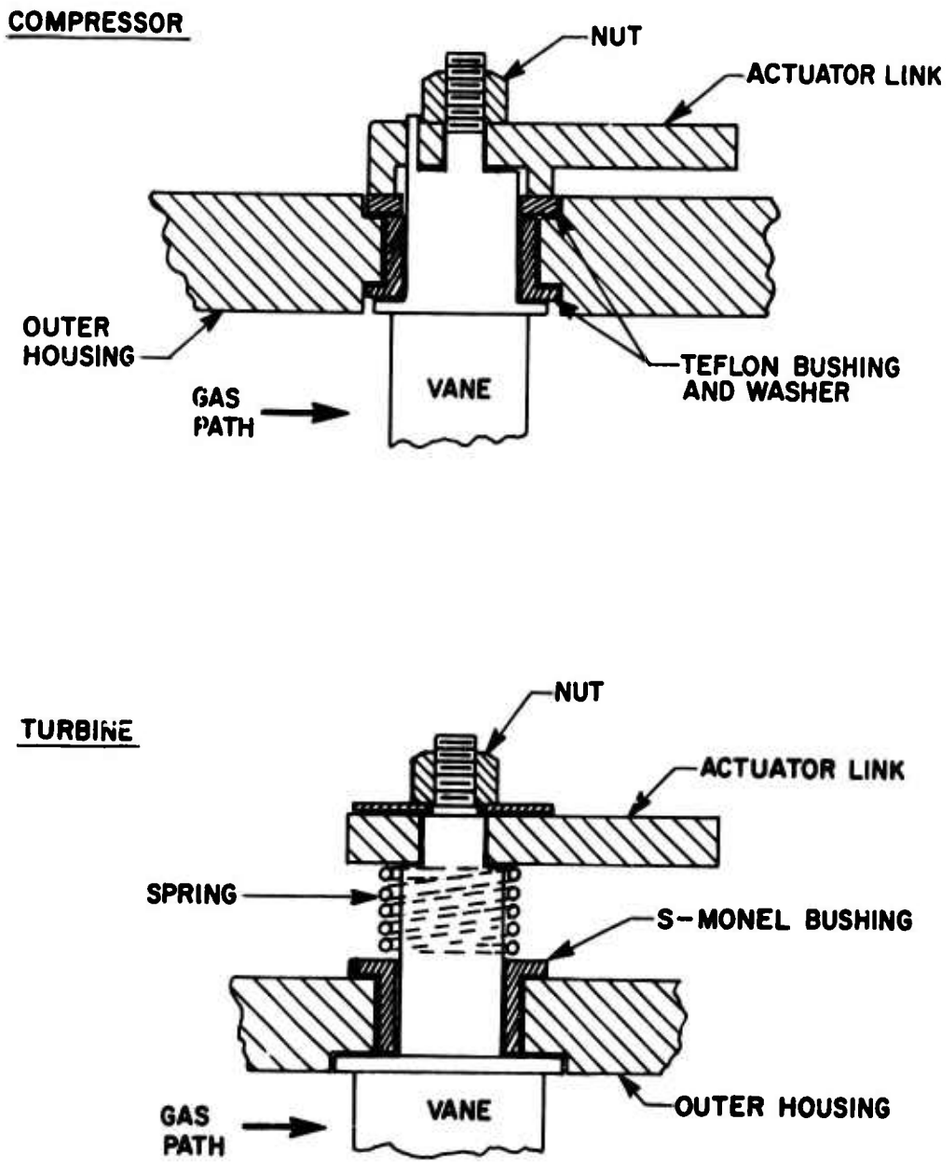

Figure 3 . Variable-Geometry Trunnion Seals.

Of the engines surveyed, only three incorporated variable-geometry vanes. These three engines have variable-geometry compressor vanes in the early stages where operating temperatures are below 500°F and Teflon bushings can be used. The close-fitting bushing, coupled with the low actuation torque required due to the Teflon, results in an excellent seal.

At the present time there is one industrial power turbine production model which has a variable-geometry turbine. However, anticipating the requirement, several experimental engines have tested variable-geometry turbine configurations.

The trunnion and bushing assemblies are sources of air/gas leakage due to clearances, wear, and deflection between the two components. One of the prime factors concerning wear between the trunnion and bushings in a high-temperature environment is material compatibility. The materials of the trunnions and bushings must be selected to prevent galling, scoring, and other surface deterioration during cyclic operation. Compatible materials for the turbine vane trunnion and bushing for wear and gall resistance are presented in Table X.

Engine Leakage Estimates

Typical small engine operating conditions were established in order to estimate leakages at typical seal locations and to serve as a guide in determining test parameters for the seal configurations selected for testing in Tasks II, III, and IV. Estimated state conditions at all sections incorporating rotating and static seals in a small gas turbine engine of 16:1 compressor pressure ratio, 2315°F T.I.T., and 4.5 pounds per second airflow are shown in Figure 4 . The locations of various rotating and static seals and typical air/gas leakage paths in a small gas turbine engine are illustrated in Figure 5.

Leakages were estimated for the various sealing configurations associated with the hypothetical engine (See Appendix). Each seal was identified as to type, location, and approximate size. Typical fits and clearances were assumed for each seal, and the engine state conditions of temperature and pressure at the particular seal location were applied. The results of this analysis are summarized in Tables XI and XII. From this data it should be noted that 40 percent of the total overboard leakage is from the turbine bearing cooling cavity at Station 4a (a labyrinth seal) and 28 percent is flange leakage at the compressor discharge.

The importance of sealing in a small gas turbine is indicated in Table XIII, which compares leakage as a percentage of engine airflow for a small and large engine. The small engine flanges and labyrinth seals result in a 2-percent leakage; in a larger engine similar seals have only a 0.3-percent leakage. In comparing engines, the leakage by a labyrinth or circumferential flange seal for a given clearance is proportional to the diameter. Since main airflow is proportional to the diameter squared, the small engine leakage as a percentage of airflow becomes substantial and therefore produces a larger effect on engine performance.

ROTATING SEALS (TASK II)

Test Rig

An existing rotating test rig was used to test both the labyrinth seal and the carbon-face seal. Drawings representing the labyrinth seal and carbon-face seal installed in the rotating rig test head are shown in Figures 6 and 7. The basic arrangement of the test rig and associated test equipment and instrumentation is presented schematically in Figure 8 . The prime mover is a 75-hp dynamometer coupled to a speed increaser. The output shaft of the speed increaser is coupled to the shaft of the test head and is capable of driving the test head shaft to speeds approaching 20,000 rpm. End play of the test head shaft is eliminated with a matched set of angular contact bearings. The end cover on the test head contains electric heaters capable of heating the rig cavity to 800°F at low airflows. The rig cavity contains pressure and temperature probes upstream and downstream of the seal. Filtered shop air or bottled gas is fed into the test head cavity through a port in the end cover. From there it flows across the seal and is vented to atmosphere.

A view of the test rig and the test head cavity with the rotating component of the labyrinth seal installed on the shaft is shown in Figure 9. Various adapters and spacers for the shaft and housing were modified as required to accomplish the installation and alignment in the test head cavity of the labyrinth seal and carbon-face seal. The end cover containing electric heaters, air supply porting, and instrumentation is shown installed on the test head in Figure 10.

Labyrinth Seal

A labyrinth seal with multifinned shroud, suitable for installation in the previously described rotating test rig, was designed and fabricated for Task II testing. Detail drawings of the rotating and stationary components are shown in Figures 11 and 12, and an enlarged and detailed description of the finning arrangement is shown in Figure 13.

The detail drawings show a radial clearance of 0.00075 to 0.00025 inch for the labyrinth seal. However, the initial installed dimensions were measured at several I.D. and O.D. locations and indicated a radial clearance ranging from 0.0006 inch loose to 0.0004 inch interference. These measured dimensions took into account both the actual I.D. and O.D. of the mating fins plus some O.D. growth of the rotating component due to a planned shrink fit on the rig shaft. The shrink fit was desirable from the standpoint of assuring concentricity with the rig shaft for the first series of tests in the aligned condition. The labyrinth seal clearance approaching a slight interference fit was also a desirable condition since it was loose enough to allow assembly of the components yet small enough to assure a slight rub of the fins, which is typical of actual labyrinth seal operating conditions.

TABLE X. VARIABLE GEOMETRY TURBINE SEAL MATERIALS

Trunnion	Bushing
Nitrided A286	75% Ni-25% Moly (Powder)
Nitrided A286	S-Monel
René 41	S-Monel, A 286
Coated A286	A 286, René 41
Coated René 41	A 286, René 41
A 286	NM100
A 286, René 41	Clevite 300 (Powder)
A 286, René 41	Stellite 25

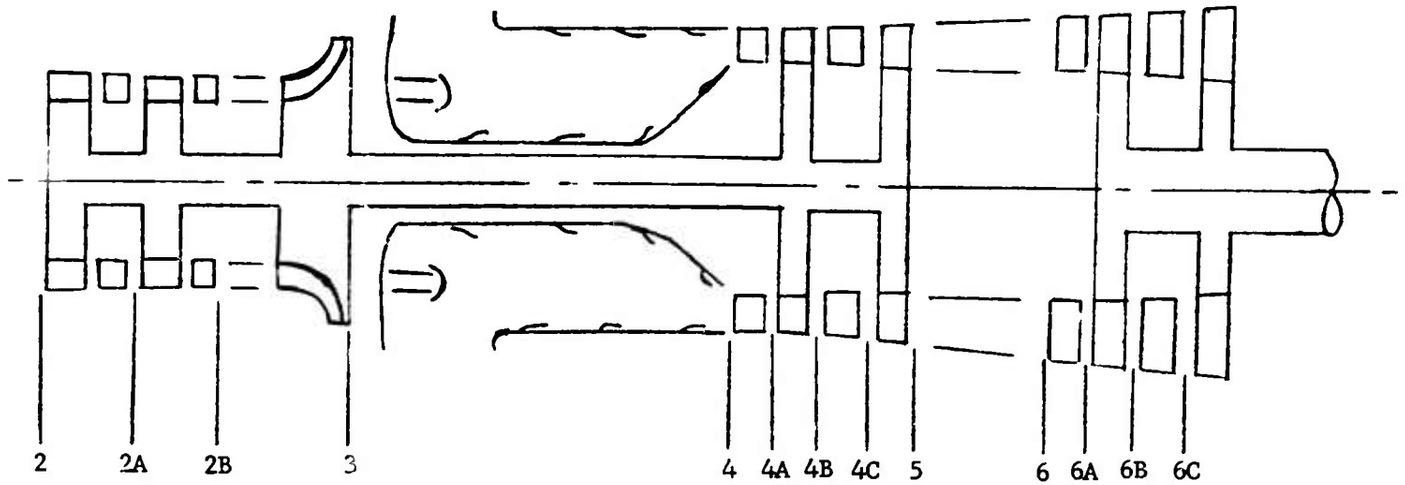

Engine Station	2A	2B	3	4	4A	4B	4C	5/6	6A	6B	6C
Total Pressure, psia	39.9	58.6	234	222	222	99.7	99.7	54.0	54.0	26.2	26.2
Static Pressure, psia	31.5	51.6	226	217.5	119	84.0	53.4	31.0	29.0	22.1	14.7
Total Temperature, ^{o}F	250	350	794	2315	2243	1845	1820	1600	1572	1290	1280

Figure 4. Task I - USAAMRDL Engine Internal Conditions.

BLANK PAGE

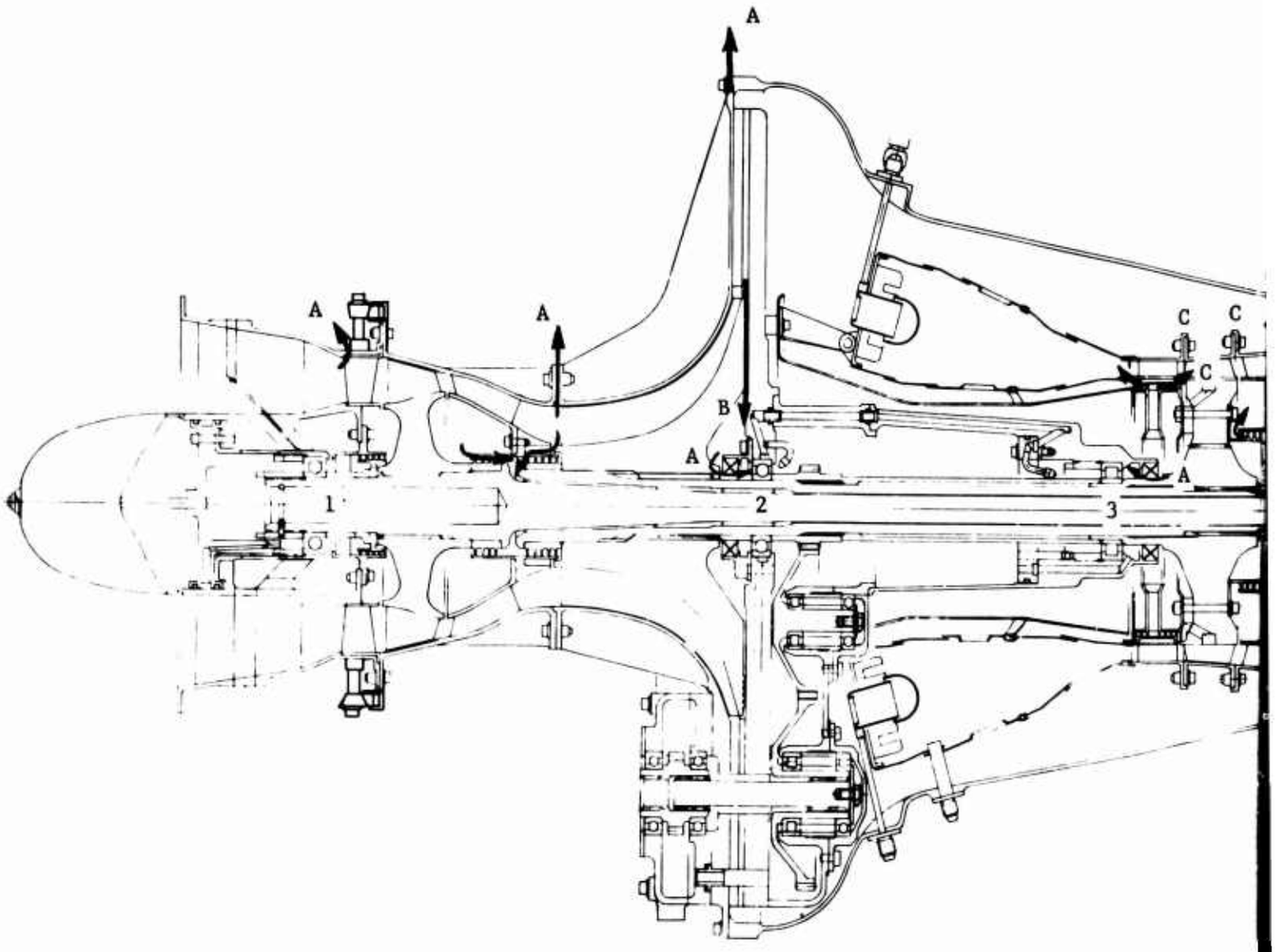

Figure 5. Typical Small Gas Turbine Engine Showing Air/Gas Leakage Paths.

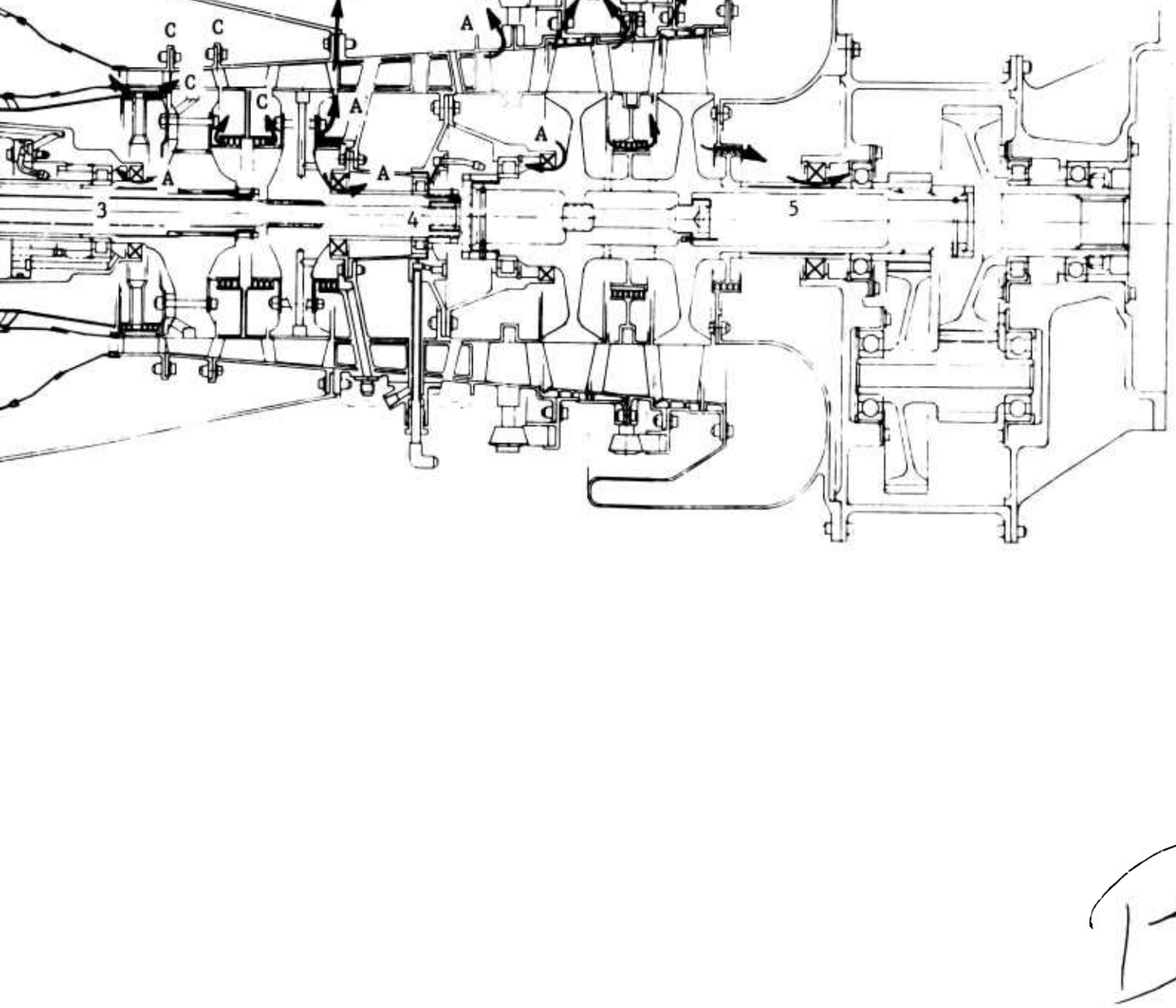

B

TABLE XI. TASK I - ESTIMATE OF SEAL LEAKAGES

Engine Section	Type Seal	Assumptions
Station 2 -Compressor Inlet		
a. Axial compressor front hsg flange to axial compressor rear hsg flange.	a. Metal-to-metal piloted flange surfaces.	a. Flange distortion, c flatness, etc., will an avg. 0.0005" leak between bolt centers lent to a leakage sc the total flange len
b. Second axial compressor stage variable vane trunnion.	b. Flanged sleeve with Teflon bushing inserts	b. Assume 39 vanes with #3 fit 0.0005" - 0.0 diametral loose (sam
c. Interaxial compressor stage labyrinth seal.	c. Four axial fin labyrinth seals - close spaced thin-finned shroud.	c. 0.005" - 0.007" radi assembly clearance, 0.003" running clear assume flat plate sl
Station 2A - Axial Compressor		
a. Axial compressor rear hsg. flange to centrifugal compressor hsg front flange.	a. Same as Station (1) a.	a. Same as Station (2)
b. Axial to centrifugal compressor interstage labyrinth seal.	b. Same as Station (1) c.	b. Same as Station (2)
Station 3 - Centrifugal Compressor		
a. Centrifugal compressor hsg rear flange to combustor hsg front flange.	a. Same as Station (1) a.	a. Same as Station (2)
b. Centrifugal compressor outlet circumferential fin labyrinth seal.	b. Five circumferential lab fins - flat plate grooved to simulate rub-in	b. 0.005" - 0.010" as-sembly and running clearance held by b bearing.
c. Number 2 bearing coolant su ply cavity labyrinth seal.	c. Four axial finned labyrinth seal - close spaced thin-finned shroud.	c. Same as Station (2)
d. Carbon ring bearing seal.	d. Controlled gap single piece carbon ring.	d. Radial clearance = (same as T-53)
e. Carbon face type bearing seal.	e. Face type carbon seal with piston ring secondary.	e. Allowable leakage = @ 80 psi Δ P

MATE OF SEAL LEAKAGES OF USAAMRDL ENGINE

Assumptions		Estimated State Condition Temp (°F)	Δ P (psig)	Estimated Leakage (See Appendix)
Flange distortion, out-of flatness, etc., will cause an avg. 0.0005" leakage gap between bolt centers equivalent to a leakage source 40% the total flange length.	a.	250	17	a. 0.002 lb/sec overboard before 2nd compressor axial stage.
Assume 39 vanes with class #3 fit 0.0005" - 0.0015" diametral loose (same as T-64)	b.	250	13	b. 0.0004 lb/sec overboard before 2nd compressor axial stage.
0.005" - 0.007" radial assembly clearance, 0.001" - 0.003" running clearance, assume flat plate shroud.	c.	250	8.0	c. 0.0052 lb/sec circulation downstream to upstream of vanes.
Same as Station (2) a.	a.	350	37	a. 0.0024 lb/sec overboard before centrifugal compressor.
Same as Station (2) c.	b.	350	12	b. 0.0053 lb/sec circulation downstream to upstream of 2nd stage axial compres. stators.
Same as Station (2) a.	a.	794	211	a. 0.028 lb/sec overboard before combustor.
.005" - 0.010" assembly and running axial clearance held by ball bearing.	b.	794	206	b. 0.098 lb/sec overboard can be dumped in at 1st stage power turbine rotor shroud. 0.066 lb/sec vent to power turbine to cool stator shrouds and trunnions.
Same as Station (2) c.	c.	300	11.5	c. 0.0055 lb/sec overboard before centrifugal compressor.
Radial clearance = 0.0013" (same as T-53)	d.	800	50	d. 0.0024 lb/sec overboard
Allowable leakage = 1 SCFM @ 80 psi Δ P	e.	800	135	e. 0.0014 lb/sec overboard

TABLE XI - Contin

Engine Section	Type Seal	Assump
Station 4A - 1st Stage Turbine		
a. 1st-stage turbine coolant axial labyrinth seal.	a. Four axial fin labyrinth seal - close spaced thin finned shroud.	a. Same as S b. Same as S
b. Number 3 bearing coolant supply cavity labyrinth seal.	b. Same as a.	c. Radial cl
c. Carbon ring bearing seal.	c. Controlled gap single-piece carbon ring.	d. Allowable @ 80 psi
d. Carbon face-type bearing seal.	d. Face type carbon seal with piston ring secondary.	e. Same as S
e. Turbine stator support rear flange to 1st-stage turbine rotor shroud front flange.	e. Same as Station (2) a.	
Station 4B - 2nd Stage Turbine Stator		
a. 1st-stage turbine rotor shroud rear flange to 2nd-stage stator vane support front flange.	a. Same as Station (2) a. b. Same as Station (4A) a.	a. Same as St b. Same as St
b. 2nd-stage turbine stator coolant axial fin labyrinth.		
Station 4C - 2nd Stage Turbine Rotor		
a. 2nd-stage turbine rotor coolant axial fin labyrinth.	a. Same as Station (4A) a.	a. Same as S

I - Continued

Assumptions	Estimated State Condition Temp °F	Δ P (psig)	Estimated Leakage (See Appendix)
Same as Station (2) c.	800	110	a. 0 07 lb/sec bypass combustor and 1st turb. stator. In at 1st T/R.
Same as Station (2) c.	800	210	b. 0.04 lb/sec overboard before combustor.
Radial clearance 0.0013".			
Allowable leakage = 1 CFM @ 80 psi Δ P	400	35	c. 0.0022 lb/sec overboard before combustor.
Same as Station (2) a.	400	35	d. 0.0005 lb/sec overboard
	800	110	e. 0.011 lb/sec bypass combustor in at 1st T/R
ame as Station (2) a.	- a. Same as Station 4A e.		a. 0.011 lb/sec bypass combustor in at 1st T/R
ame as Station (2) c.	b. 500	26	b. 0.016 lb/sec bypass combustor in at 2nd T/R
ame as Station (2) c.	a. 900	57	a. 0.021 lb/sec bypass combustor in at 2nd T/R.

B

TABLE XI - Continued

Engine Section	Type Seal	Assumptions	Est
Station (5) - 2nd Stage Turbine			
a. 2nd-Stage T/R shroud rear flange to combustor outer hsg. rear flange	a. Same as Station (2) a.	a. Same as Station (2) a.	a.
b. Combustor outer hsg. rear flange to power turbine transition duct front flange	b. Same as Station (2) a.	b. Same as Station (2) a.	b.
c. 2nd-stage T/R rear axial labyrinth fin gas seal	c. Same as Station (4A)a.	c. Same as Station (2) c.	c.
d. Number 4 bearing coolant supply cavity labyrinth seal	d. Same as Station (4A)a.	d. Same as Station (2) c.	d.
e. Carbon ring bearing seal	e. Same as Station (4A)c.	e. Same as Station (4A)c.	e.
Station (6) - Power Turbine			
a. Variable turbine nozzle trunnion seals	a. Close fit metal bushing	a. Class #2 Fit (0.001-0.003) Loose diametral clearance	a.
b. Carbon ring bearing seal	b. Same as Station (4A)c.	b. Same as Station (4A)c.	b.
Station (6A) - 1st Stage Power Turbine			
a. 1st-stage power turbine stator support rear flange to 1st-stage T/R shroud front flange	a. Same as Station (2) a.	a. Same as Station (2) a.	a.
Station (6B)			
a. Interstage power turbine labyrinth seal	a. Seven fin axial labyrinth fin seal with thin-finned multi-finned shroud	a. Same as Station (2) c.	a.
b. 2nd-stage power turbine stator nozzle trunnion	b. Close fit metal bushing	b. Same as Station (6) a.	b.

ABLE XI - Continued

ıs		Estimated State Condition Temp °F	Estimated State Condition ΔP (psig)	Estimated Leakage (See Appendix)
.on (2) a.	a.	790	170	a. 0.012 lb/sec bypass combustor, in at power turbine 1st stg.
.on (2) a.	b.	1600	36	b. 0.0021 lb/sec overboard before power turbine
.on (2) c.	c.	1600	31	c. 0.0144 lb/sec overboard before power turbine
ion (2) c.	d.	400	30	d. 0.009 lb/sec overboard before centrifugal compressor
ion (4A)c.	e.	350	16	e. 0.0013 lb/sec overboard before combustor
(0.001-0.003) :al clearance	a.	1570	25	a. 0.0013 lb/sec overboard before 1st-stage power turbine
ion (4A)c.	b.	700	50	b. 0.0026 lb/sec overboard
ion (2) a.	a.	1572	14	a. 0.0013 lb/sec overboard before 1st-stage power turbine
ion (2) c.	a.	1290	7.2	a. 0.003 lb/sec bypasses 2nd-stage power turbine stator
ion (6) a.	b.	1290	3.7	b. 0.0008 lb/sec bypasses 2nd-stage power T/R

B

BLANK PAGE

TABLE XII. TASK I - USAAMRDL SIZE ENGINE AIR/GAS SEAL LEAKAGE ESTIMATES

	Station	Overboard		By-Pass Combustor	
		lb/sec	%	lb/sec	%
I Rotating Seals					
	3	0.0024		-	
	4	0.0022		-	
	4A	0.04		0.070	
	4B	-		0.016	
	4C	-		0.021	
	5	0.0144		-	
	6	0.0026		-	
Total		0.0616	1.36	0.107	2.4
II. Flanges					
	2A	0.002		-	
	2B	0.0024		-	
	3	0.028		-	
	4A	-		0.011	
	4B	-		0.011	
	5	0.0021		0.012	
	6A	0.0013		-	
Total		0.0358	0.8	0.034	0.75
III. Vane Trunnions					
	2A	0.0004		-	
	6	0.0013		-	
	6B	0.0008		-	
Total		0.0025	0.056	-	
Summation		0.0999	2.216	0.141	3.15

TABLE XIII. LEAKAGE ESTIMATES COMPARISON, SMALL VERSUS LARGE ENGINE

	Small Engine (800 SHP Size)		Large Engine (J52 Size)	
	$\frac{W_{Leak}}{W_{Inlet}}$ Overboard (%)	$\frac{W_{Leak}}{W_{Inlet}}$ By-Pass Combustor (%)	$\frac{W_{Leak}}{W_{Inlet}}$ Overboard (%)	$\frac{W_{Leak}}{W_{Inlet}}$ By-Pass Combustor (%)
A. Metal-to-Metal Flange	0.80	0.75	0.08	0.14
B. Rotating Labyrinth	1.20	2.30	0.22	0.45
C. Controlled-Gap Carbon	0.20	-	0.020	-
D. Carbon Face	0.06	-	0.006	-
E. Segmented Carbon	0.03	-	0.003	-
F. Variable Compressor	0.03	-	-	-
G. Variable Nozzle	0.05	-	-	-

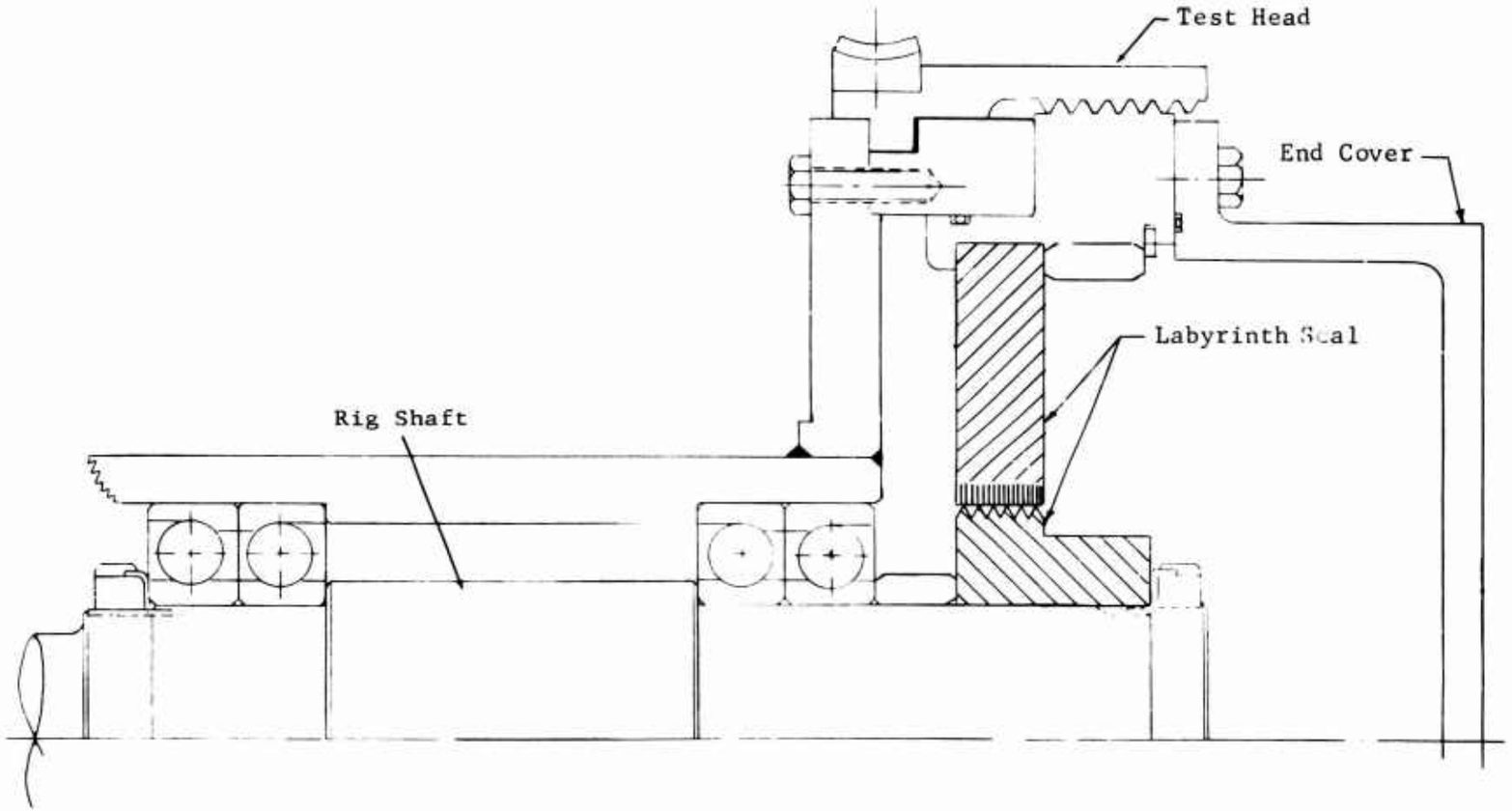

Figure 6. Rotating Seal Rig Test Head With Labyrinth Seal Installed.

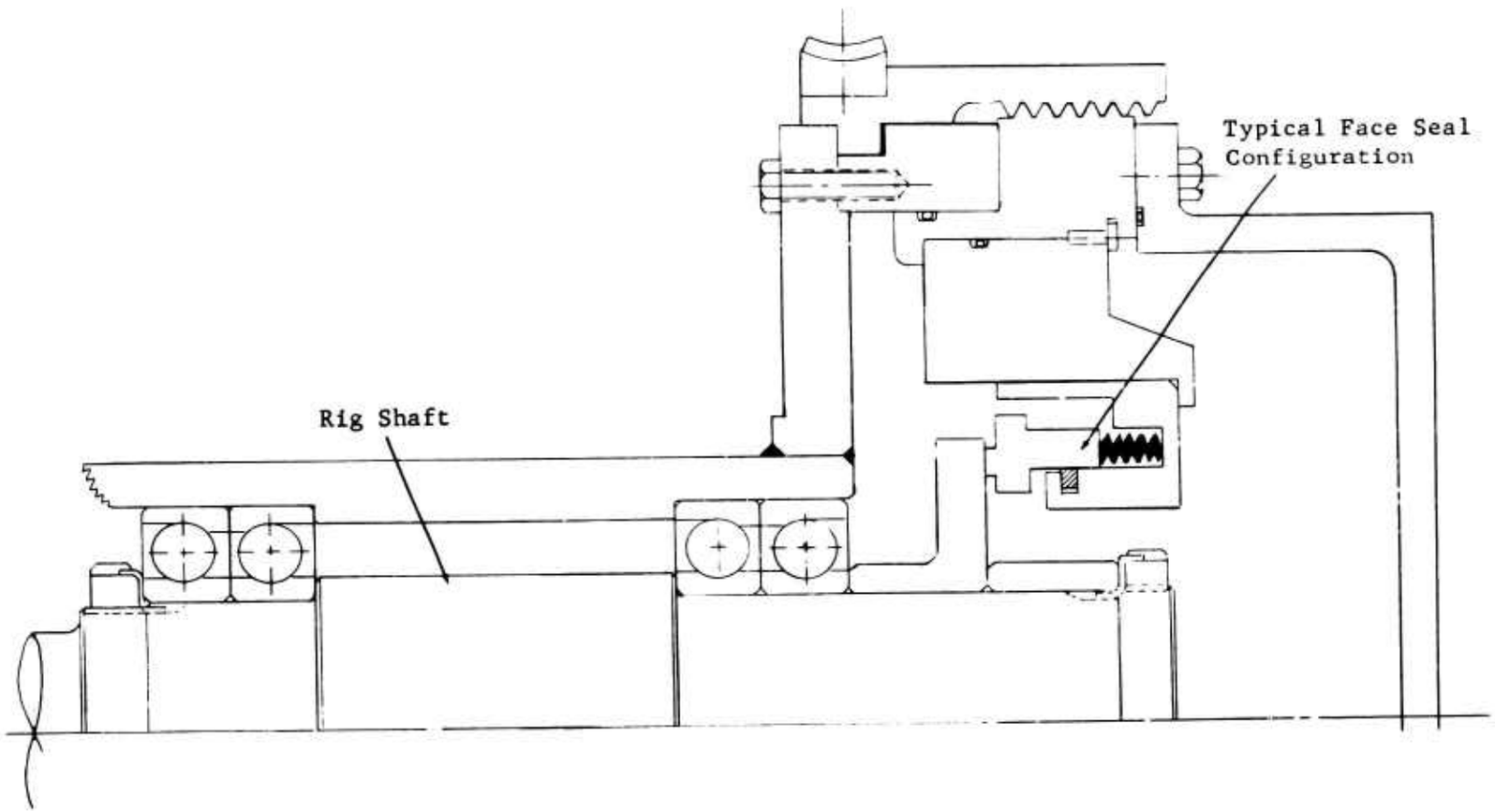

Figure 7 . Rotating Seal Rig Test Head With Carbon-Face Seal Installed.

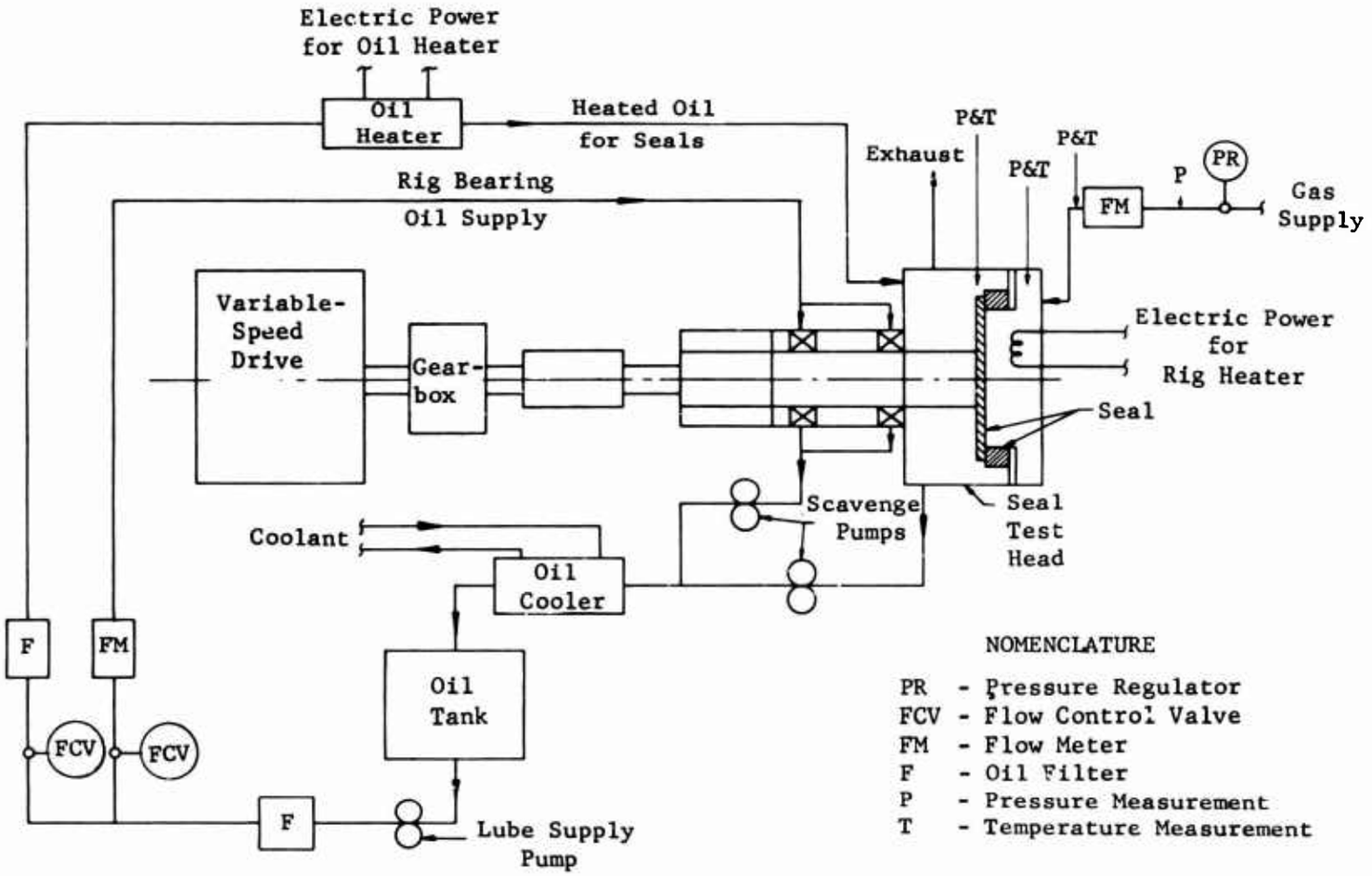

Figure 8. Schematic of Rotating Rig.

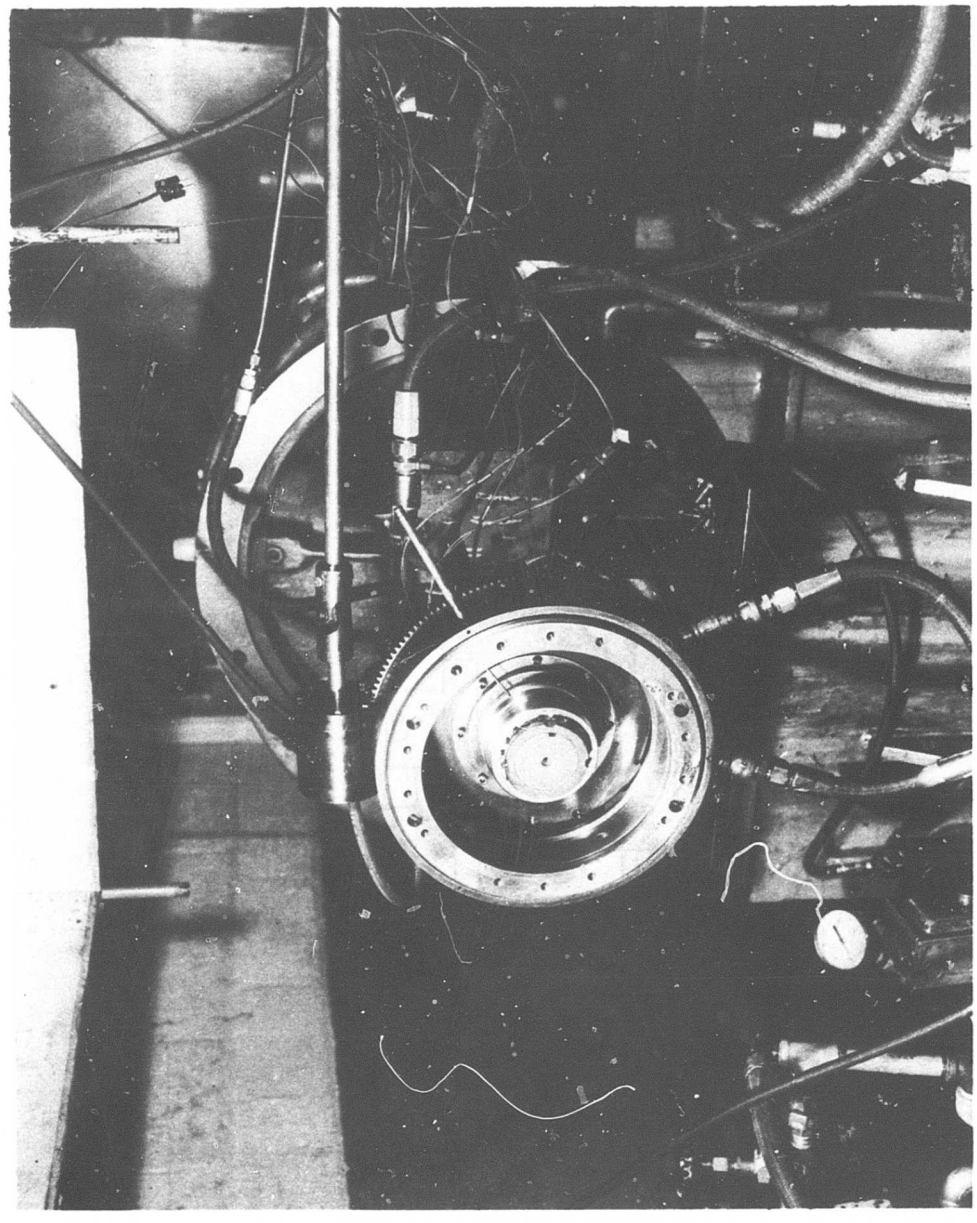

Figure 9. Rotating Seal Test Rig - Test Head Cavity.

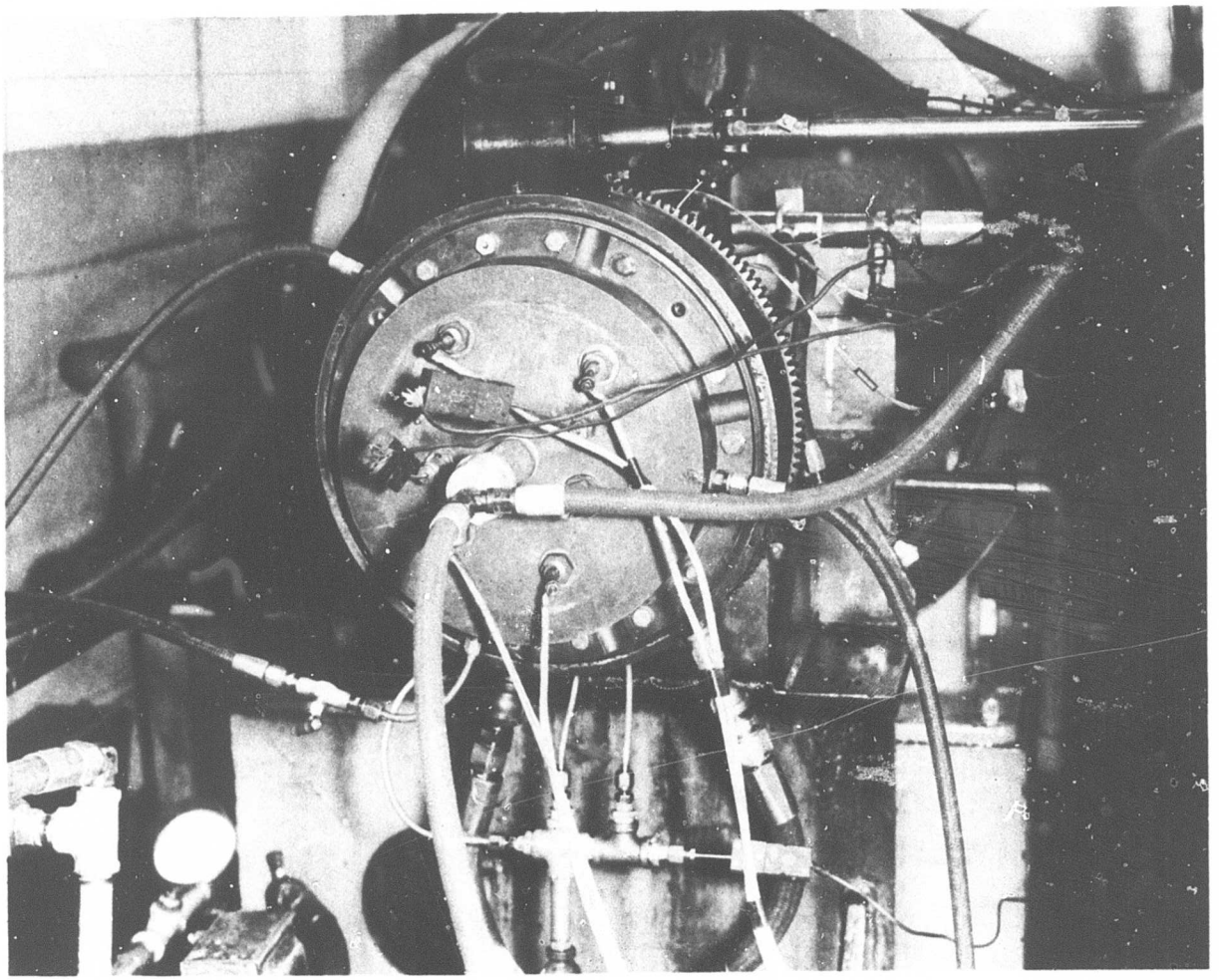

Figure 10. Rotating Seal Test Rig - Test Head End Cover Installed.

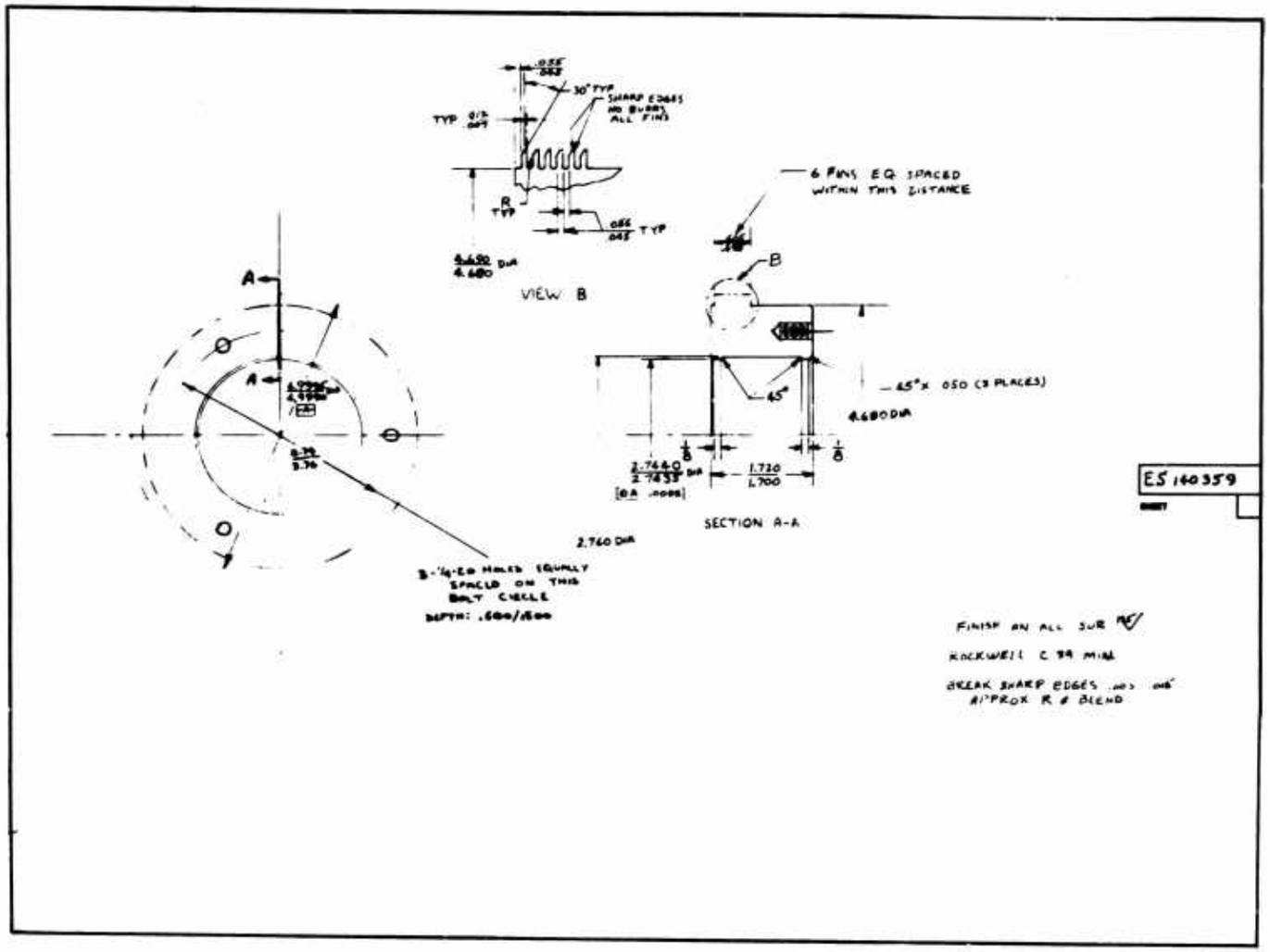

Figure 11. Labyrinth Seal Rotating Component - Detail Drawing.

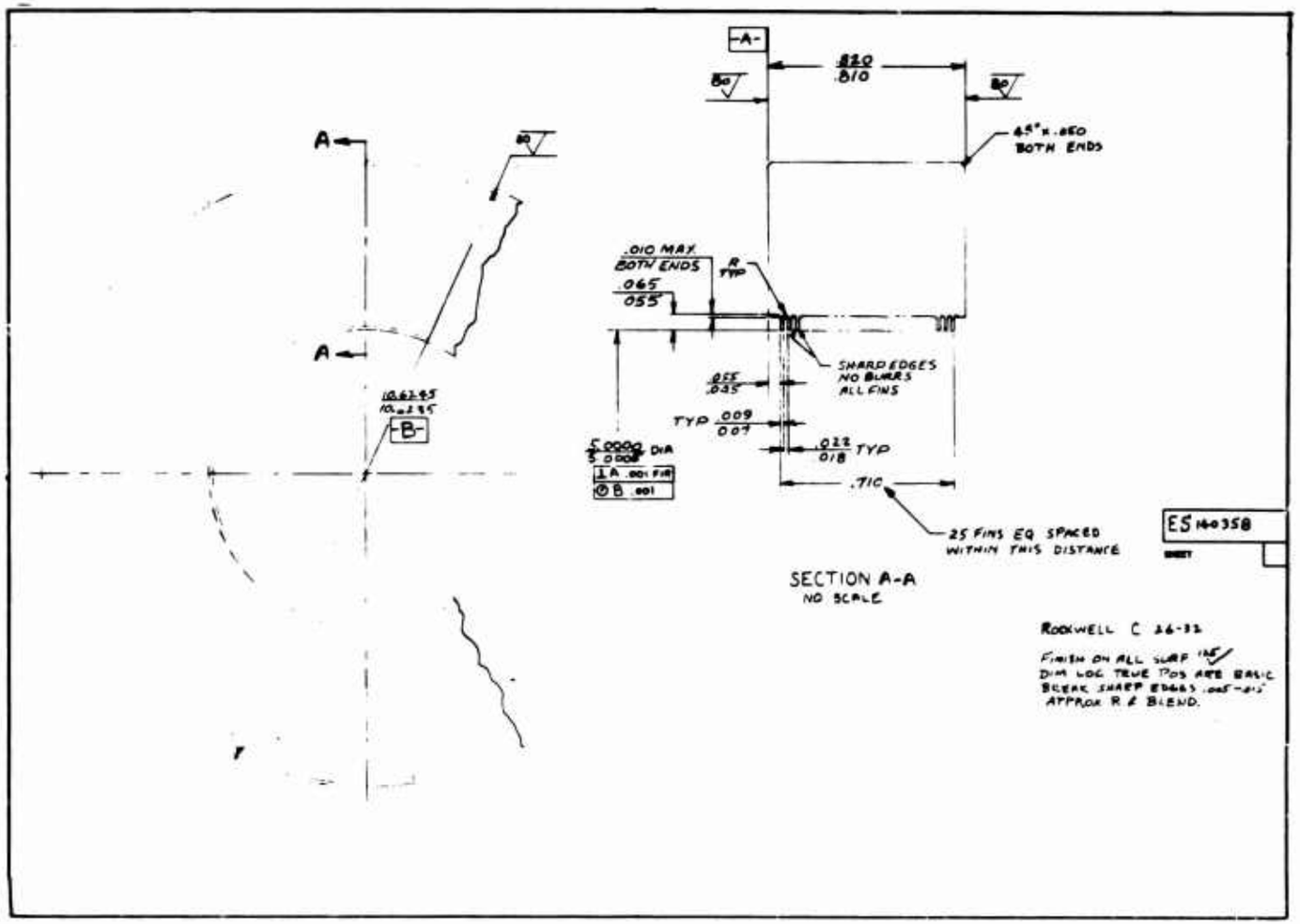

Figure 12. Labyrinth Seal Stationary Component - Detail Drawing.

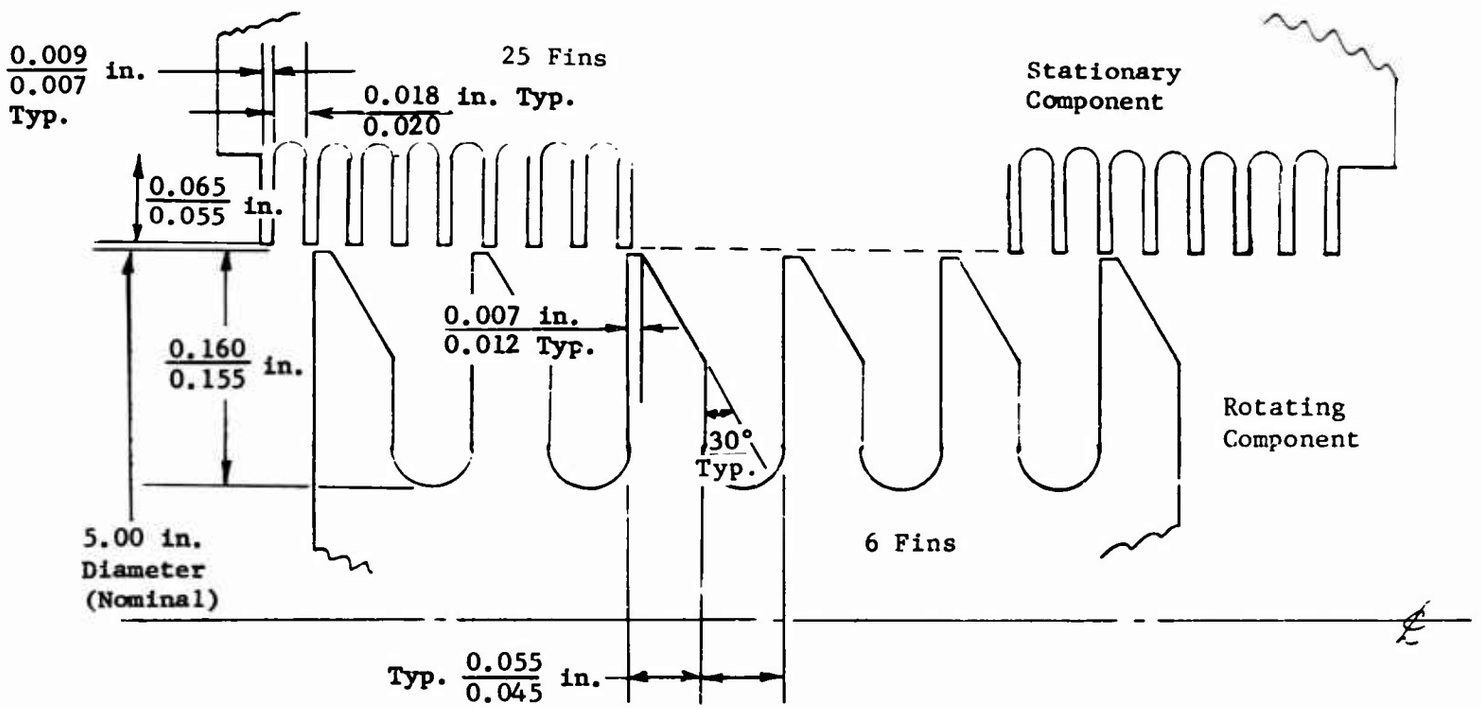

Installed Radial Clearance (Nominal) 0.0001 in.

Figure 13. Labyrinth Seal Arrangement.

The material used for the rotating component was Inconel 718 (AMS 5662); for the stationary component, it was 431 stainless steel (AMS 5628). A photograph of the rotating and stationary seal components prior to testing is shown in Figure 14. Close-up views of the fins on the rotating and stationary components prior to testing are shown in Figures 15 and 16.

Labyrinth Seal Test Program

Testing of the labyrinth seal in the rotating test rig consisted of operating the seal at various conditions of pressure, temperature, speed and alignment while measuring gas leakage at the various conditions. The test conditions at which the labyrinth seal was evaluated are summarized in Table XIV, and the instrumentation used is listed in Table XV. The seal was pressurized with bottled nitrogen gas and leakage flows were measured with a Fischer-Porter Flowrator. Gas specific gravity corrections were made using standard Fischer-Porter correction curves.

Initially, the seal was installed in an aligned condition and subjected to a room temperature run-in for approximately 2 hours at speeds up to 18,400 rpm which simulated surface velocities of small engines. The aligned condition consisted of a full indicator reading runout of 0.0009 inch measured on the O.D. of the rotating component.

A static calibration was then conducted at room temperature, without shaft rotation and with pressure applied to 200 psig in 50-psig increments, while measuring leakage. This was followed by a dynamic calibration with leakages measured at room temperature and 250°F, at incremental shaft speeds of up to 18,400 rpm, and at pressures up to 200 psig in 50-psig increments.

Cyclic testing was then conducted, consisting of applying to the seal 50 consecutive operating cycles of temperature, pressure, and shaft speed. An operating cycle consisted of increasing the shaft speed from zero to 18,400 rpm and the pressure from zero to 200 psig over a period of 1 to 2 minutes. Temperature of 250°F was also applied; approximately 10 minutes was required to stabilize at 250°F. Upon obtaining stable conditions, pressure and shaft speed were rapidly reduced to zero to simulate engine shutdown, and the rig was allowed to cool to room temperature. Achieving room temperature concluded an operating cycle. The conditions were repeated until 50 cycles were obtained.

After completing the static and dynamic calibrations and cyclic testing, the same labyrinth seal hardware was subjected to two misalignment tests. Prior to each misalignment test, the seal was again subjected to a 2-hour run-in period before obtaining leakage data. Misalignment was achieved by machining the I.D. of the rotating component to a larger diameter to create a degree of looseness in its fit on the rig shaft. The rotating component was then installed on the shaft and shimmed between its I.D. and the shaft O.D. to achieve a radially offset or eccentric condition. For the first misalignment test, the runout of the rotating component measured on its O.D. was a full indicator reading of 0.0015 inch. For the second misalignment test this runout was 0.0023 inch.

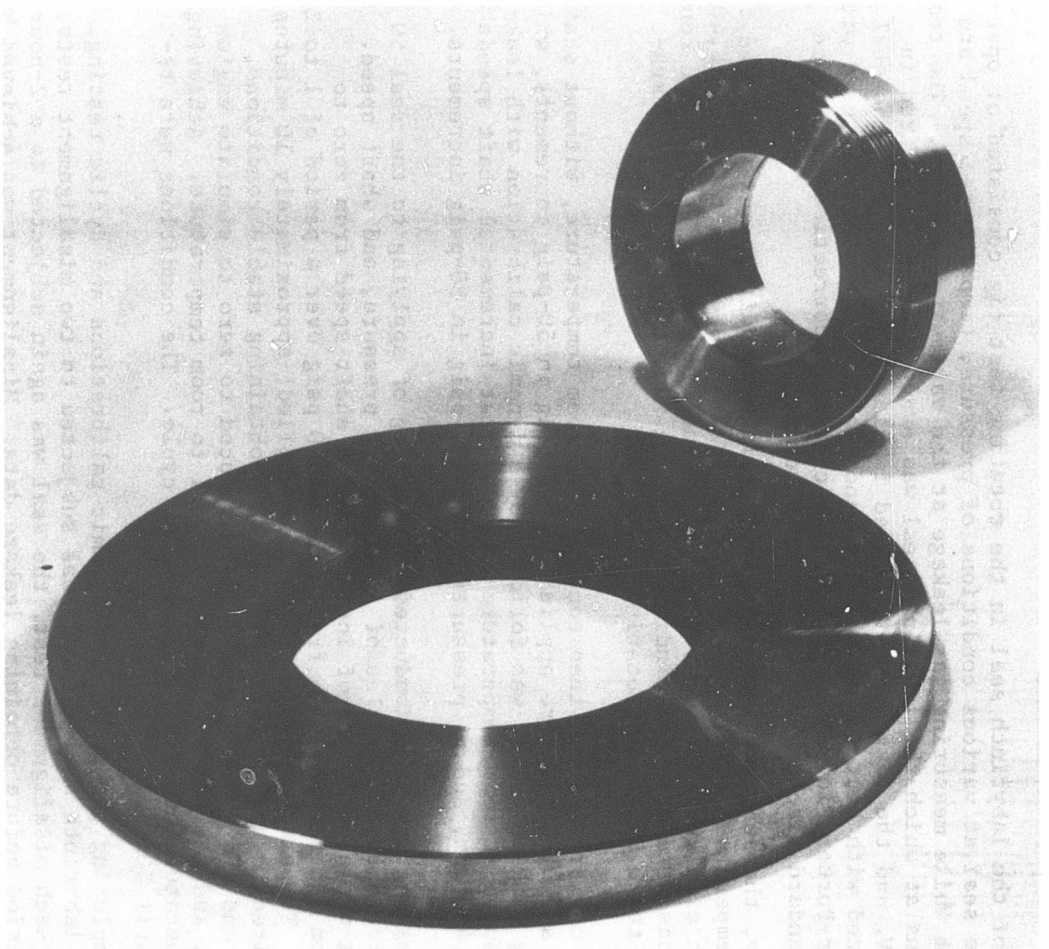

Figure 14. Labyrinth Seal Components.

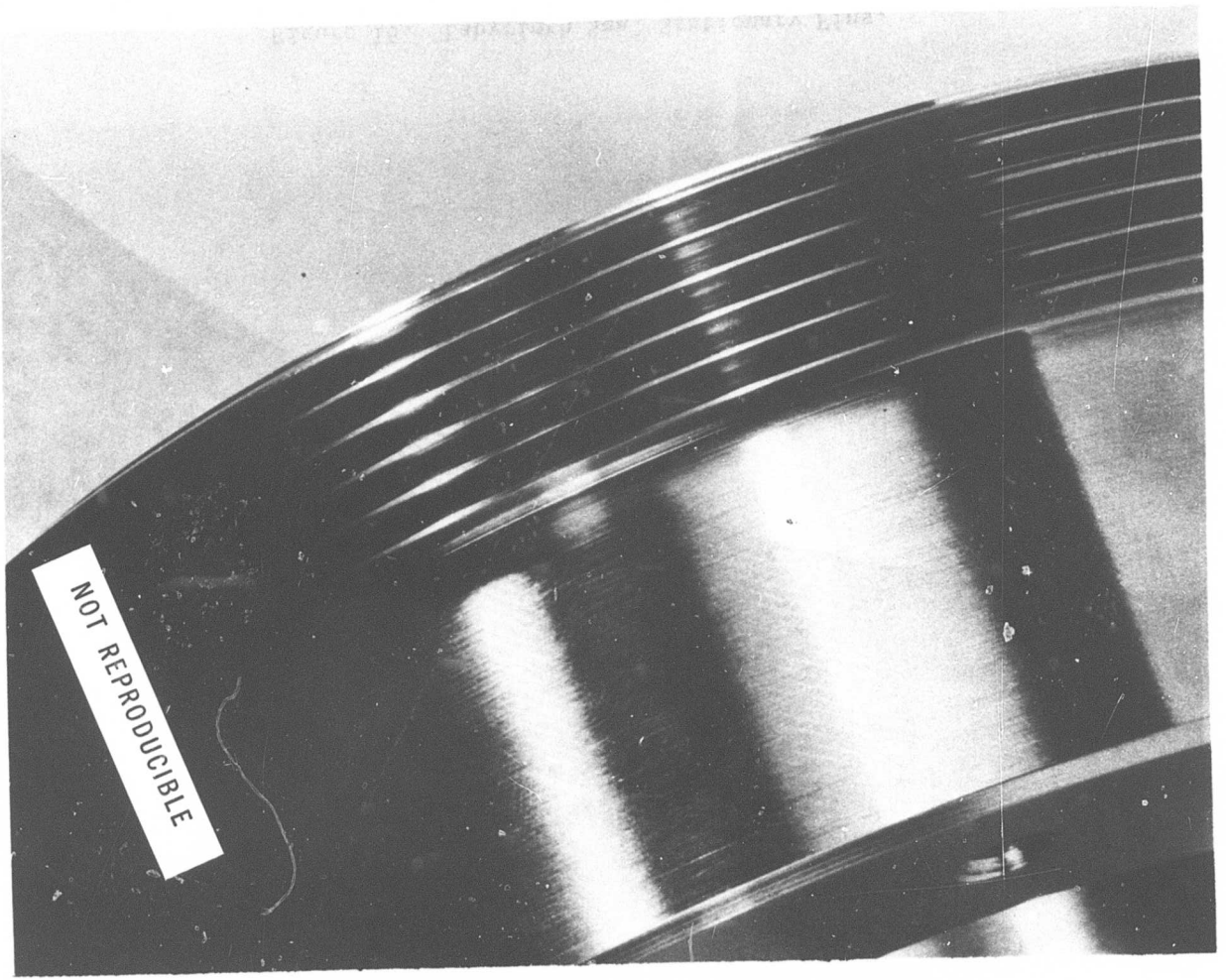

Figure 15. Labyrinth Seal Rotating Fins.

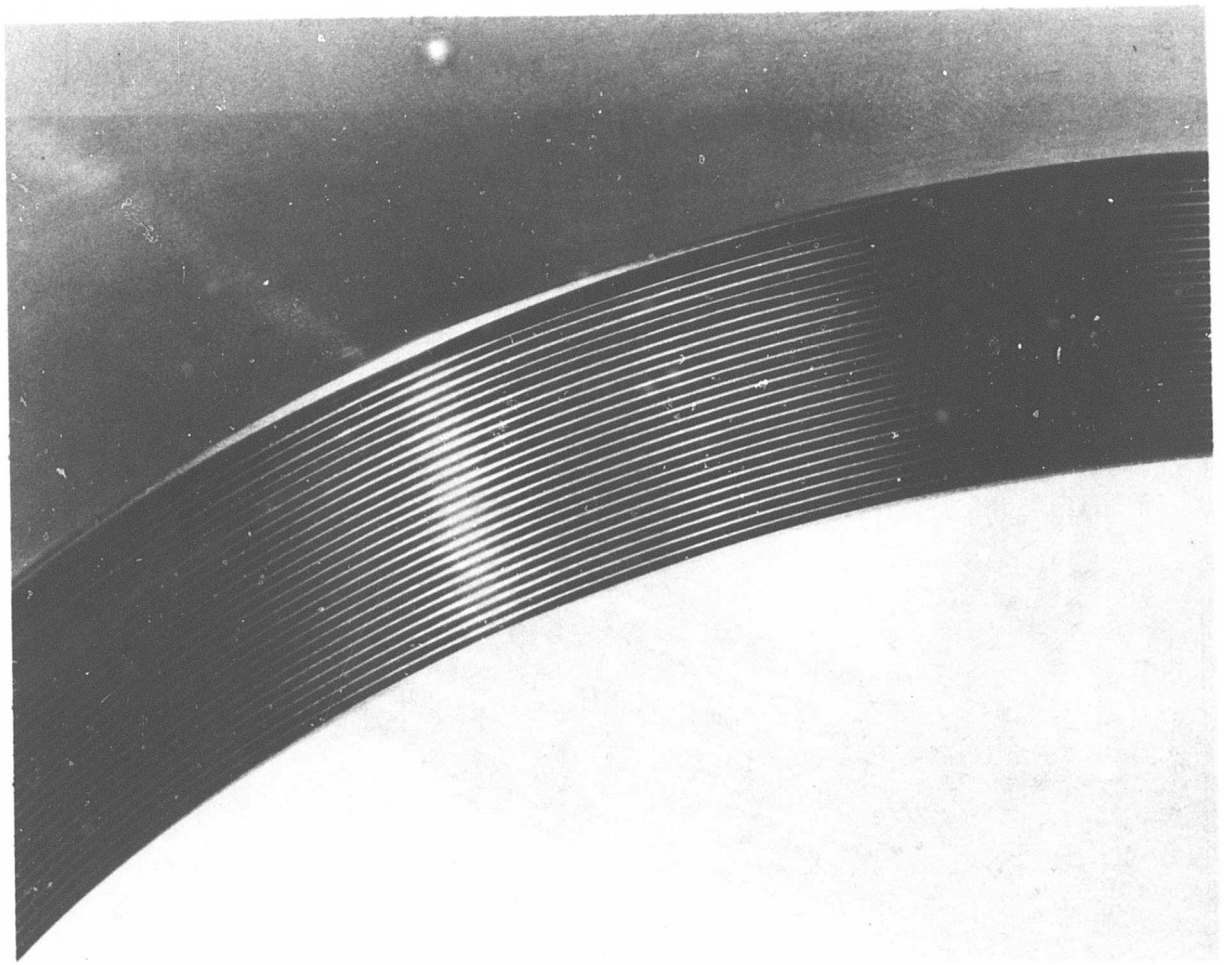

Figure 16. Labyrinth Seal Stationary Fins.

TABLE XIV . LABYRINTH SEAL TEST CONDITIONS

Test Category	Pressure (psig)	Temperature (°F)	Shaft Speed (rpm)
A. Static Calibration	50 to 200	Room Temp	-
B. Dynamic Calibration	50 to 200	Room Temp	4,500
	50 to 200	Room Temp	9,000
	50 to 200	Room Temp	13,500
	50 to 200	Room Temp	18,400
	50 to 200	Room Temp	18,400
	50 to 200	250	18,400
	50 to 200	250	13,500
	50 to 200	250	9,000
	50 to 200	Room Temp	9,000
	50 to 200	Room Temp	4,500
	50 to 200	Room Temp	-
C. Cyclic (50 Cycles)	200	250	18,400
D. First Misalignment	50 to 200	Room Temp	-
	50 to 200	250	-
	50 to 200	Room Temp	4,500
	50 to 200	Room Temp	9,000
	50 to 200	Room Temp	13,500
	50 to 200	Room Temp	10,000
	50 to 200	250	10,000
	50 to 200	Room Temp	-
E. Second Misalignment	50 to 200	Room Temp	-
	50 to 200	250	-
	50 to 200	250	3,500
	50 to 200	250	5,000
	50 to 200	250	7,500
	50 to 200	250	10,000
	50 to 200	250	14,700
	50 to 200	250	10,000
	50 to 200	Room Temp	-

TABLF XV. LABYRINTH SEAL TEST INSTRUMENTATION

Parameter	Location	Instrumentation	Range	Units
Gas Pressure	Upstream of Flowmeter	Gage	0-300	psig
Gas Pressure	Downstream of Flowmeter	Gage	0-300	psig
Gas Pressure	Upstream of Seal	Gage	0-250	psig
Gas Pressure	Downstream of Seal	Gage	0-10	psig
Gas Temp.	Downstream of Flowmeter	I-C Thermocouple	60-90	°F
Gas Temp.	Upstream of Seal	I-C Thermocouple	R.T.-200	°F
Gas Temp.	Downstream of Seal	I-C Thermocouple	R.T.-300	°F
Shaft Speed	Test Head Shaft	Tachometer	0-20,000	rpm
Gas Flow (Leakage)	Gas Pressurizing Line	Fischer-Porter Flowrator Model 6311-A3592 (two in parallel when required)	.004-.019 air at 14.7 psia and 60°F	lb/sec

Labyrinth Seal Test Results

The basic leakage characteristics of the labyrinth seal as affected by air temperature and wearing of the fins are displayed in Figure 17, which shows plots of air leakage across the seal versus upstream air pressure for three different test conditions at a constant shaft speed. The upstream air pressure is also the pressure differential across the seal, since all testing was conducted with the downstream side of the seal vented to atmosphere. The lower two of the three curves are the test results on the labyrinth seal in the aligned condition, before the 50-cycle test but after run-in. These curves display the effect of air temperature, with the lowermost curve being at the higher temperature and therefore at the lower leakage rate (mass flow) due to the reduction in air density and/or reduced clearances at increased temperature. The third and uppermost curve was obtained after the 50-cycle test. This curve shows an increase in leakage due to wearing of the fins as a result of the simulated engine operating cycles.

Labyrinth seal leakage associated with wearing of the fins due to misalignment is shown in Figure 18. These curves compare air leakage versus air pressure for the labyrinth seal in the aligned condition and in the maximum misaligned condition tested. The curve plotted for the aligned condition is based on test results obtained prior to the 50-cycle test. Since the seal in the misaligned condition was not subjected to the 50-cycle test, the curves shown are for comparable conditions of wear.

The results of the test simulating 50 engine operating cycles are shown in Figure 19, which is a plot of air leakage versus operating cycles for various air pressures. It appears that wearing of the fins occurred for the first 5 to 10 cycles, resulting in an increase in air leakage. The leakage is essentially unchanged for the remainder of the 50 cycles, indicating that no additional wear occurred during this period.

The results of the misalignment tests appear in Figures 20 and 21, which show air leakage over a range of pressures at room temperature and at 250°F for the aligned and the two misaligned conditions. As shown, the runout for the aligned condition was 0.0009 inch (F.I.R.), which was the minimum radial runout attainable in the test rig. At the same pressure, the characteristically lower leakage at increased temperature is again evident in these curves.

Curves of air leakage versus shaft speed at different pressures are shown in Figure 22. The decrease in leakage with increasing shaft speed is attributable to a reduction in clearance between the fins. It is estimated that a reduction in clearance of 0.0003 inch is sufficient to cause the approximately 30-percent decrease in leakage between zero speed and maximum speed shown. The reduction in clearance is due to radial growth of the rotating component as a result of centrifugal forces and/or an increase in temperature of the rotating component due to heat input from the test rig bearings. A temperature differential of as little as 20°F is sufficient to cause the indicated reduction in clearance.

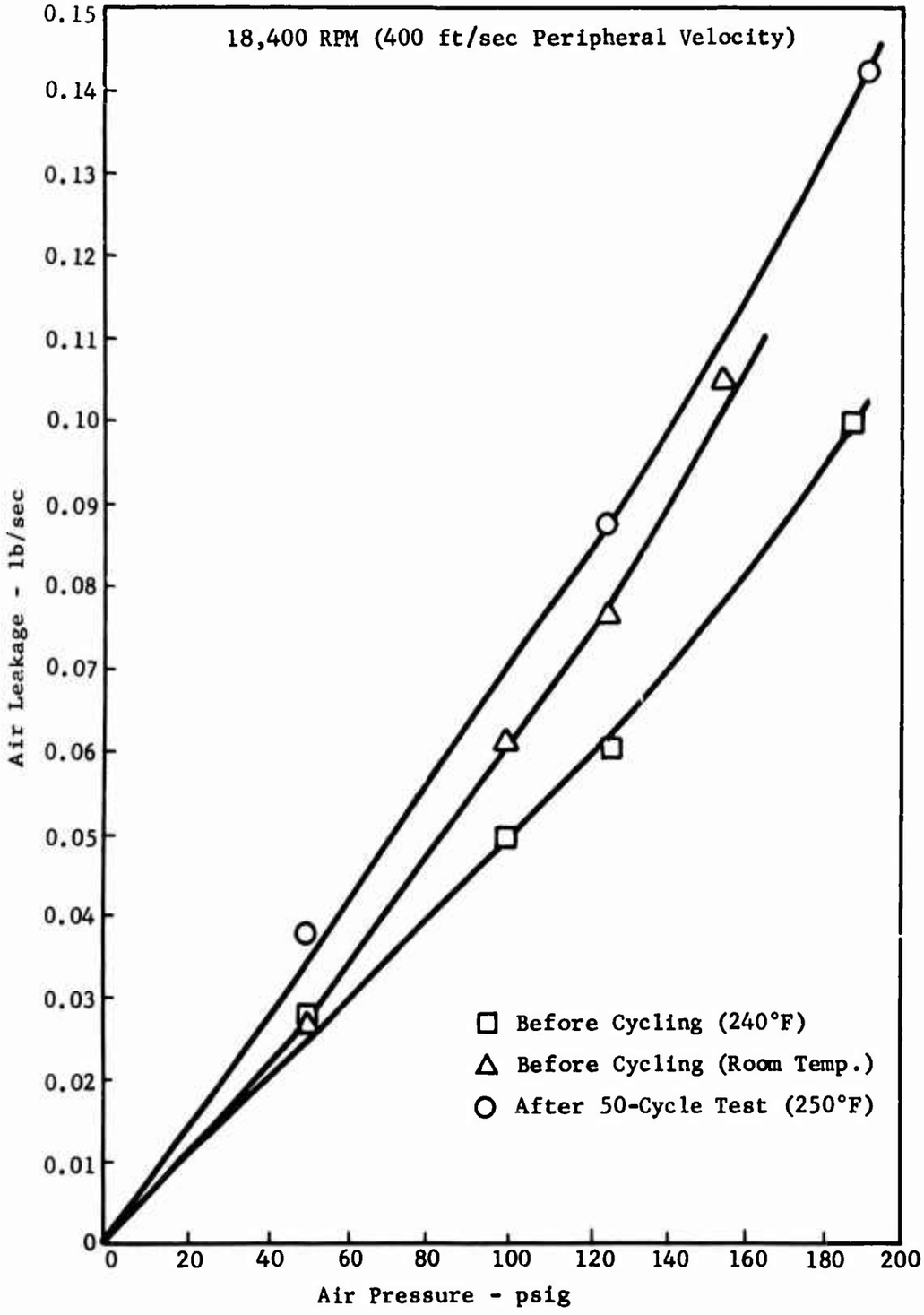

Figure 17. Labyrinth Seal Leakage Versus Air Pressure.

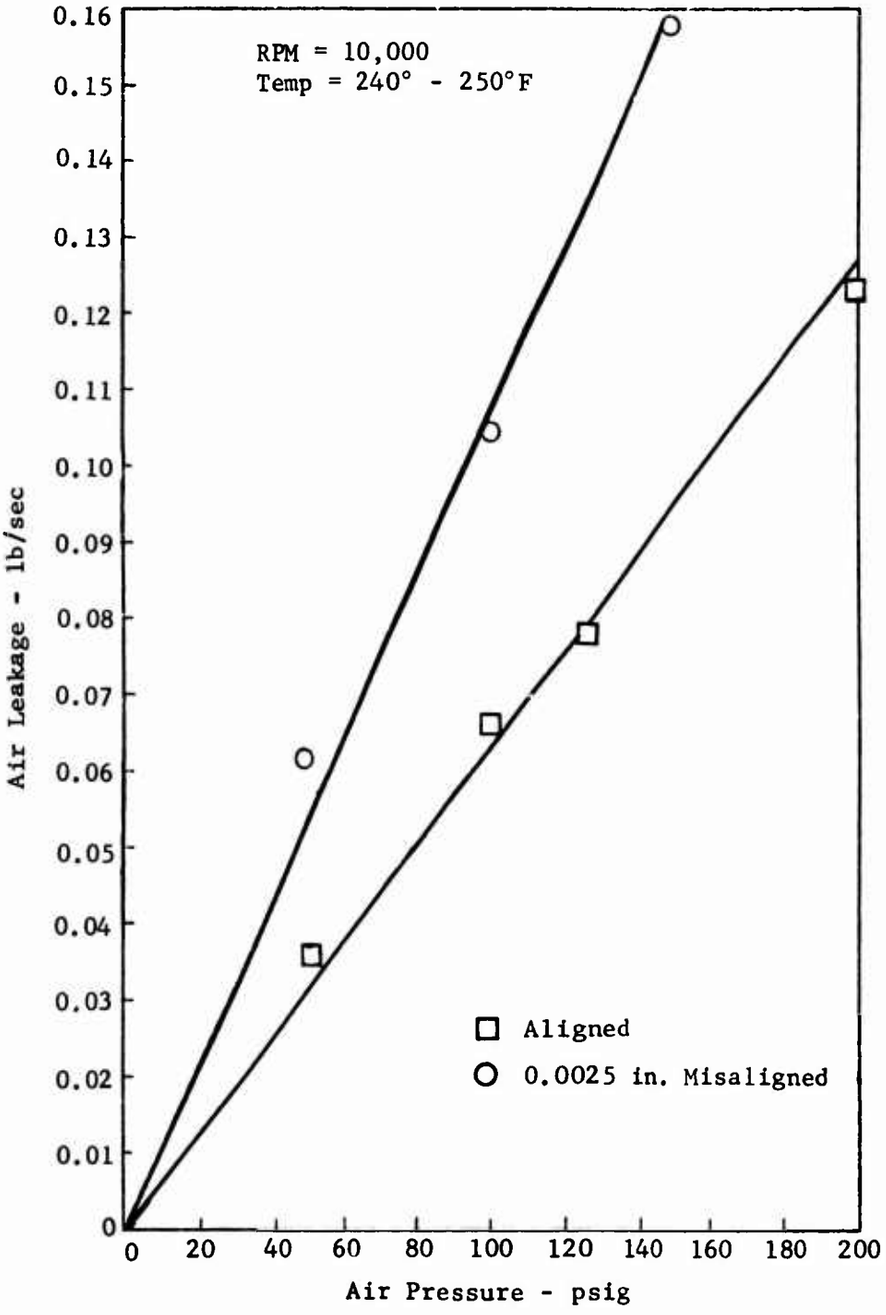

Figure 18. Labyrinth Seal Leakage Versus Air Pressure for Two Alignment Conditions.

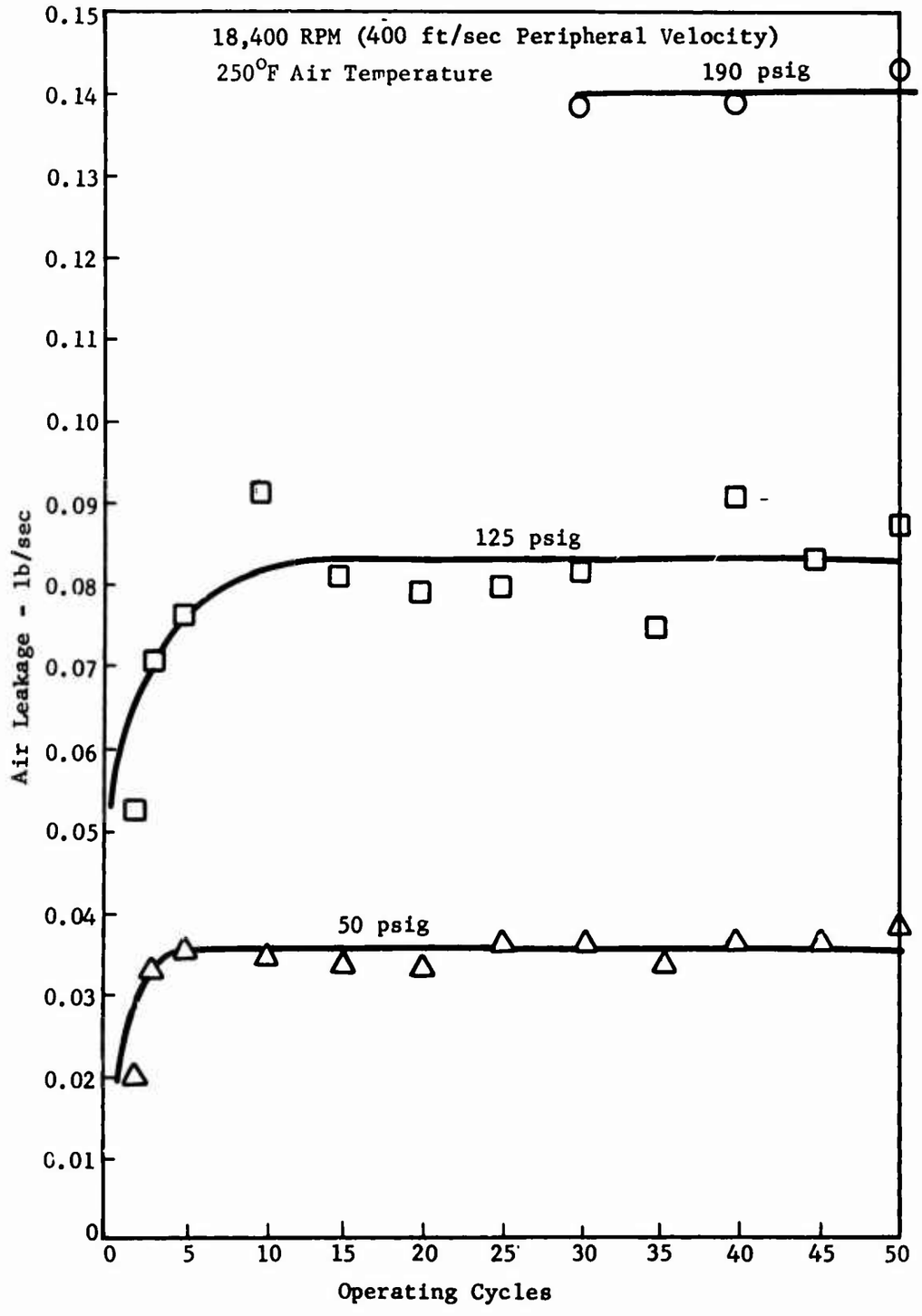

Figure 19. Labyrinth Seal Leakage Versus Operating Cycles.

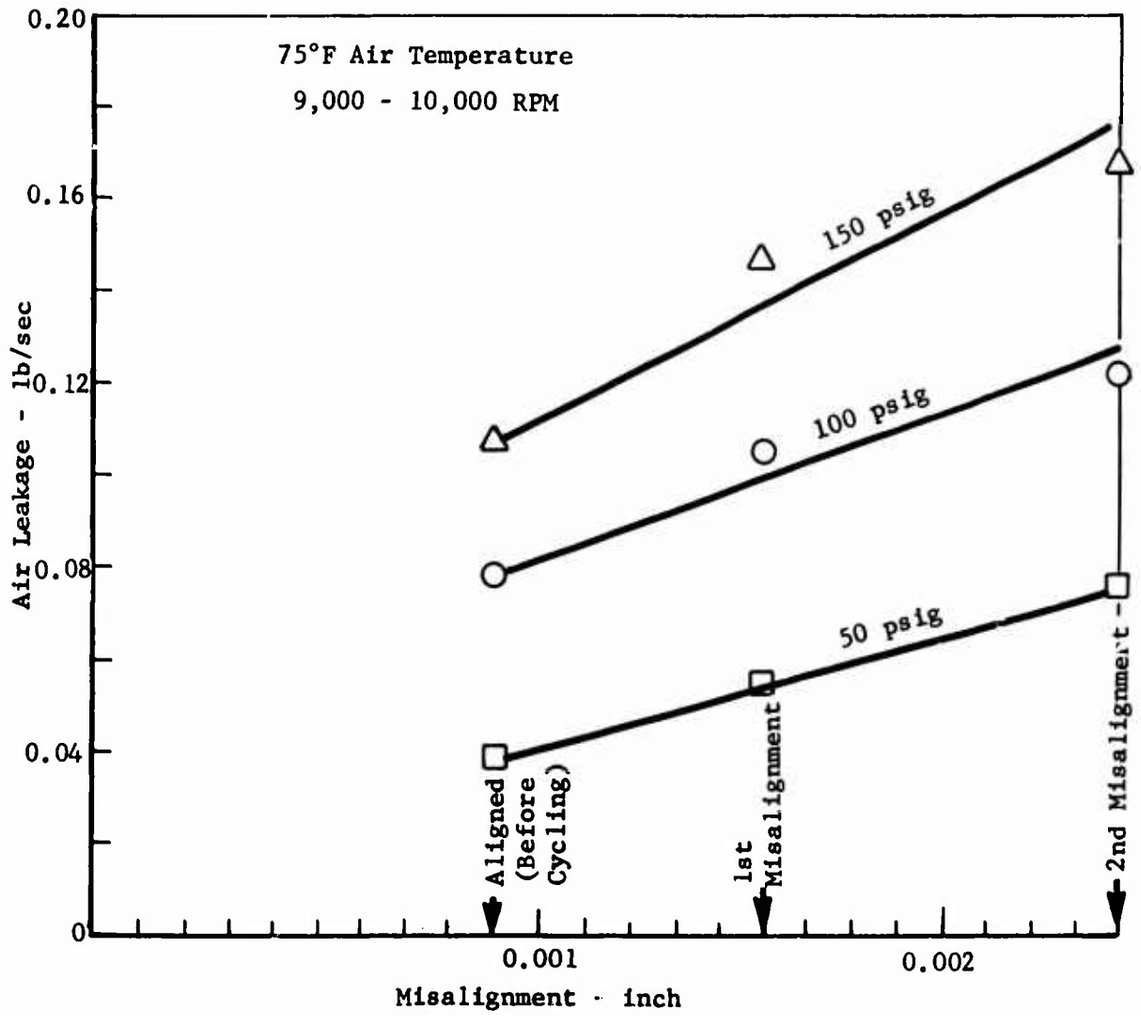

Figure 20. Labyrinth Seal Leakage Verus Misalignment.

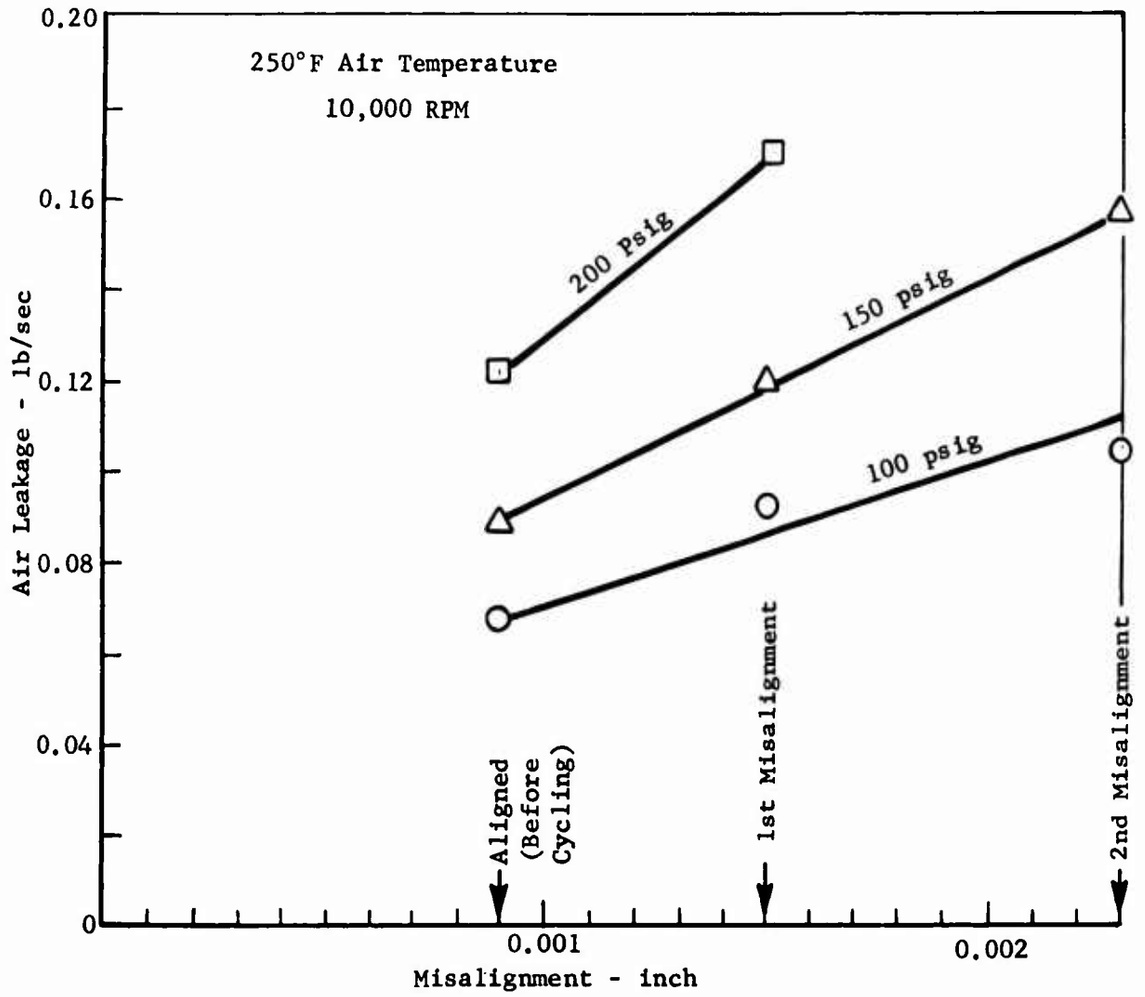

Figure 21. Labyrinth Seal Leakage Versus Misalignment.

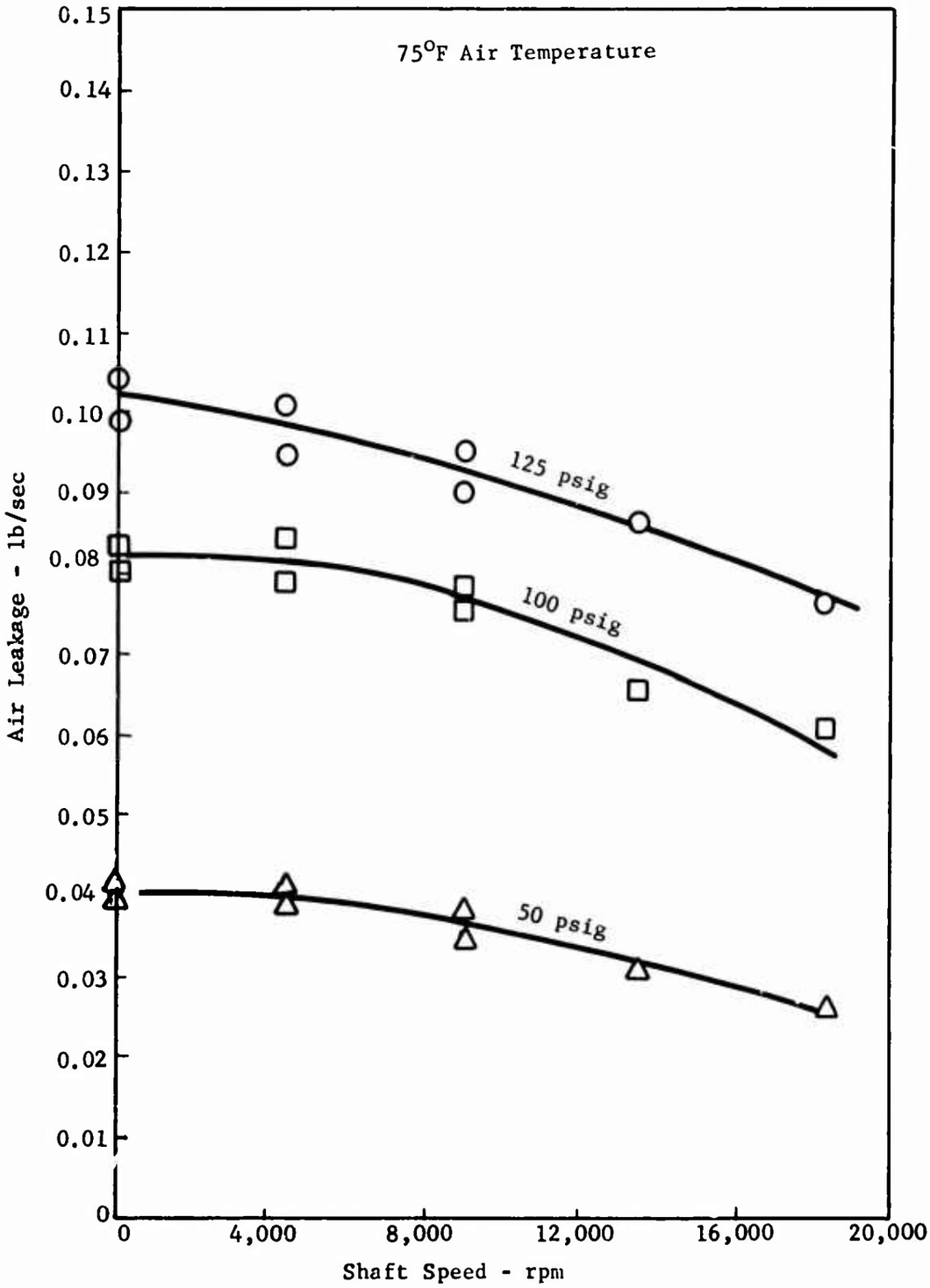

Figure 22. Labyrinth Seal Leakage Versus Shaft Speed.

Measurements taken on the labyrinth seal components after completion of all testing in the aligned condition indicated no significant change in O.D. of the rotating component and therefore no measurable wear, although there was visual evidence of rubbing on the fins. At some locations on the rotating component, the O.D. was larger than the pretest condition by as much as 0.001 inch; at these locations, visual inspection indicated what appeared to be pickup of material from the stationary fins.

The stationary fins displayed highly localized and distinct regions of wear associated with the six fins on the rotating component. Figure 23 is a photograph of the stationary fins after all testing in the aligned condition, with six points of wear clearly visible. The I.D. of the unworn fins was unchanged after testing, and the depth of wear (radial) on the worn fins measured with a dial indicator was found to be 0.001 to 0.002 inch.

After completion of both misalignment tests, the rotating component displayed a considerable amount of fin wear, with the O.D. measuring 4.993 to 4.994 inches or 0.005 to 0.006 inch less (diametral) than the pretest condition. The rotating fins after misalignment testing are shown in Figure 24.

The stationary fins displayed a wear depth of 0.002 to 0.005 inch (radial) after misalignment testing, with a less distinct wear pattern as shown in Figure 25. The I.D. of the unworn fins measured the same as the pretest condition.

Carbon-Face Seal

A carbon-face seal manufactured by the Koppers Company, Inc., Baltimore, Maryland was procured for Task II testing. A drawing of the seal is shown in Figure 26. It has a face diameter of 4.64 inches and is designed for operation at a pressure differential of 75 psig, an air temperature of 800°F, and a rubbing velocity of 400 feet per second. Attempts were made to procure a face seal suitable for operation at 150 psi, 800°F, and 400 feet per second, which would more nearly simulate conditions in an advanced, small gas turbine engine. However, seal designs operating at these conditions are available only in various stages of development, and these advanced seals were not considered appropriate for Task II testing.

The face seal selected for testing is normally produced in quantity for 25-psig operation. However, the seal supplied for this program had a change in the geometry of the carbon face which provided an operating capability of up to 75 psig. The sealing surface materials consist of Union Carbide Grade CJP carbon rubbing against chromium-plated steel (AMS 6322). The secondary seal piston ring is also Grade CJP carbon.

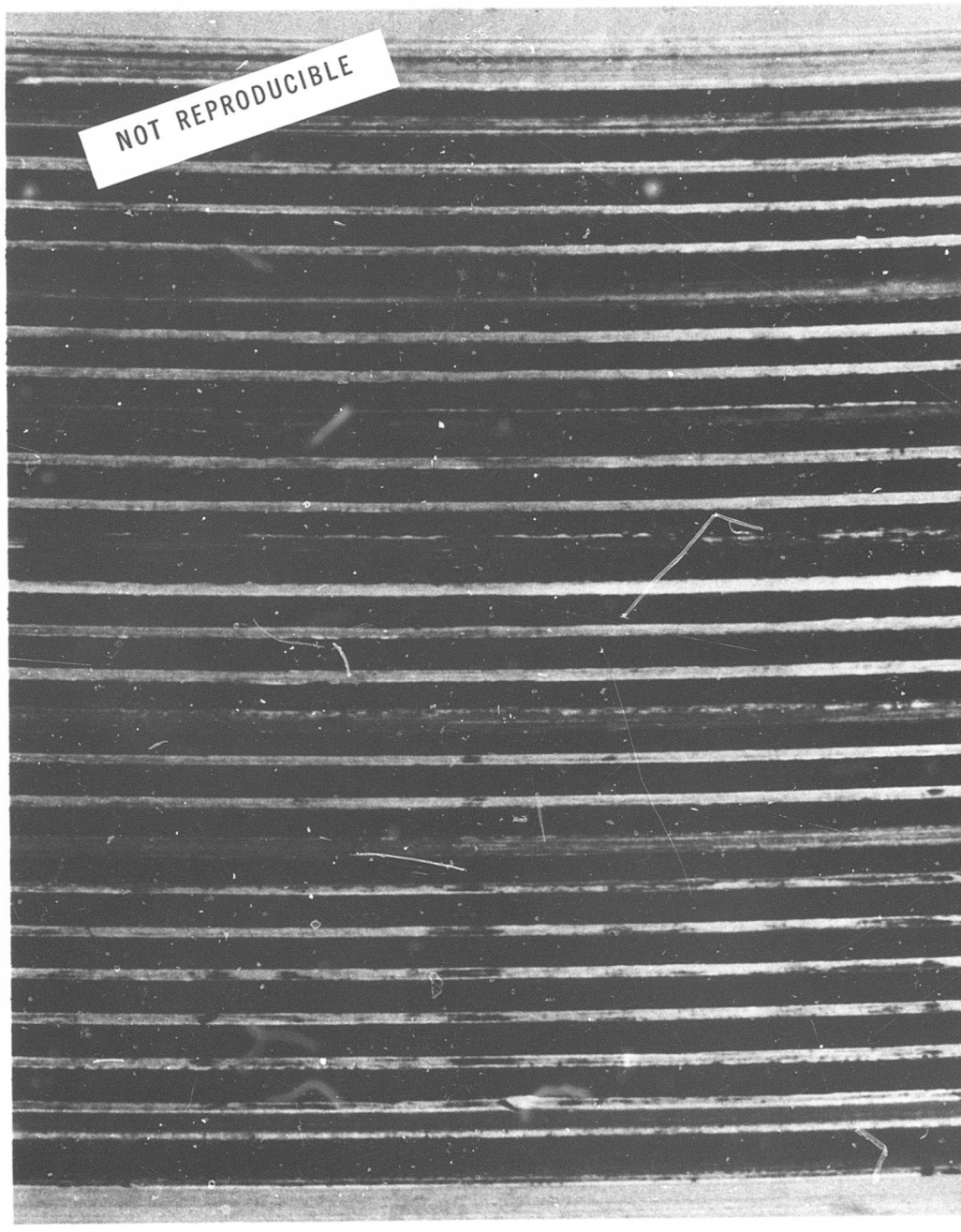

Figure 23. Labyrinth Seal Stationary Component After Aligned Testing.

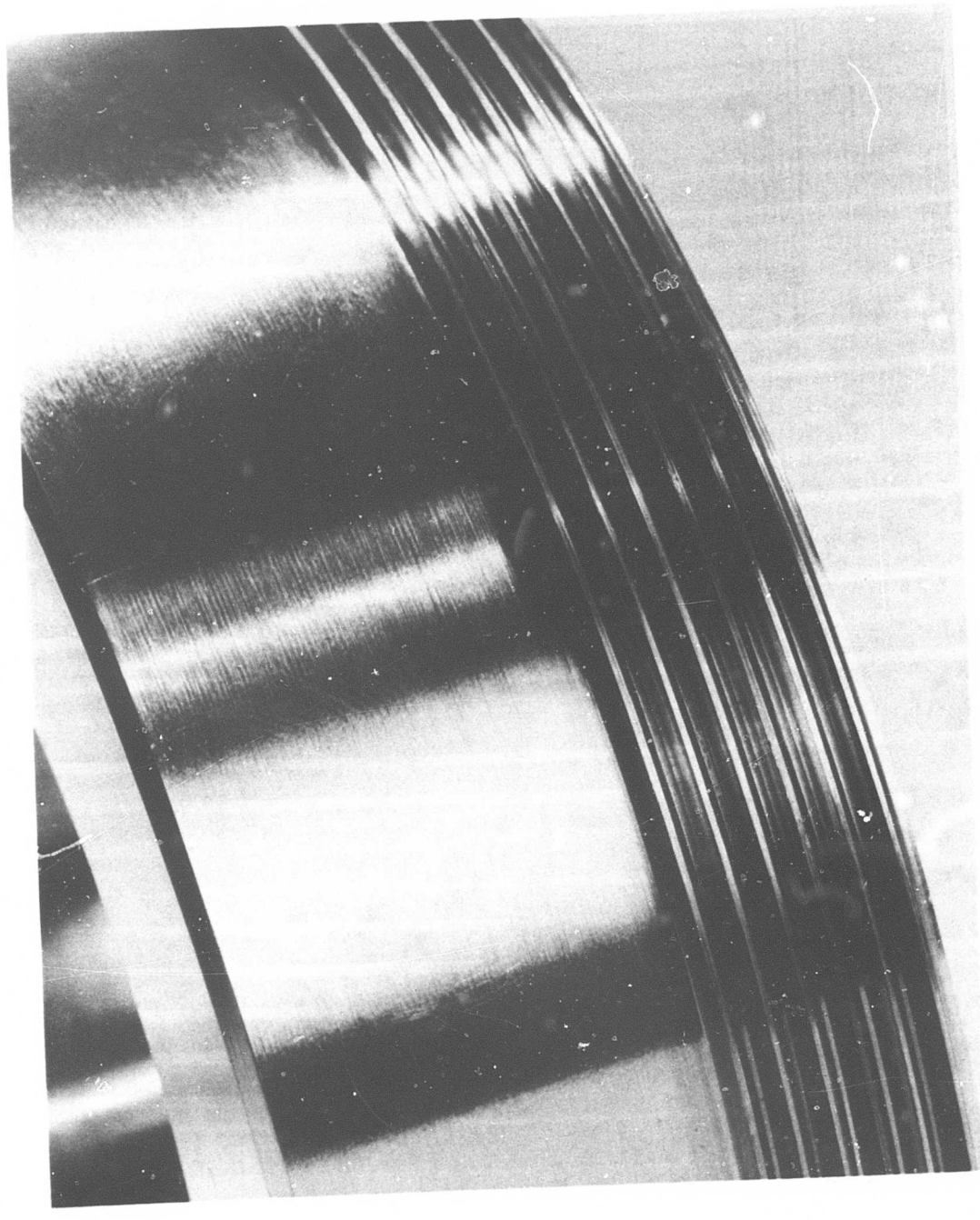

Figure 24. Labyrinth Seal Rotating Component After Testing.

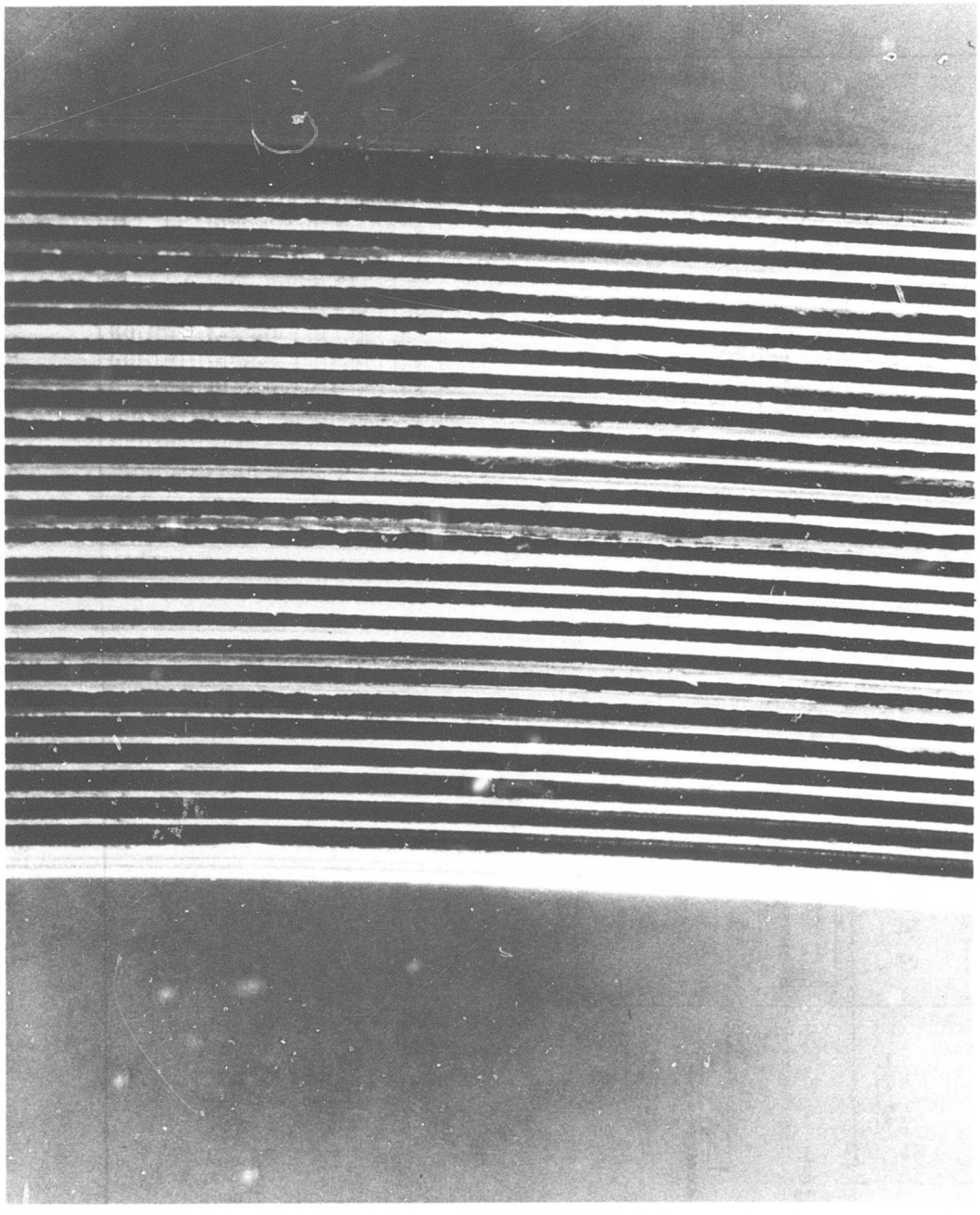

Figure 25. Labyrinth Seal Stationary Component After Misalignment Testing.

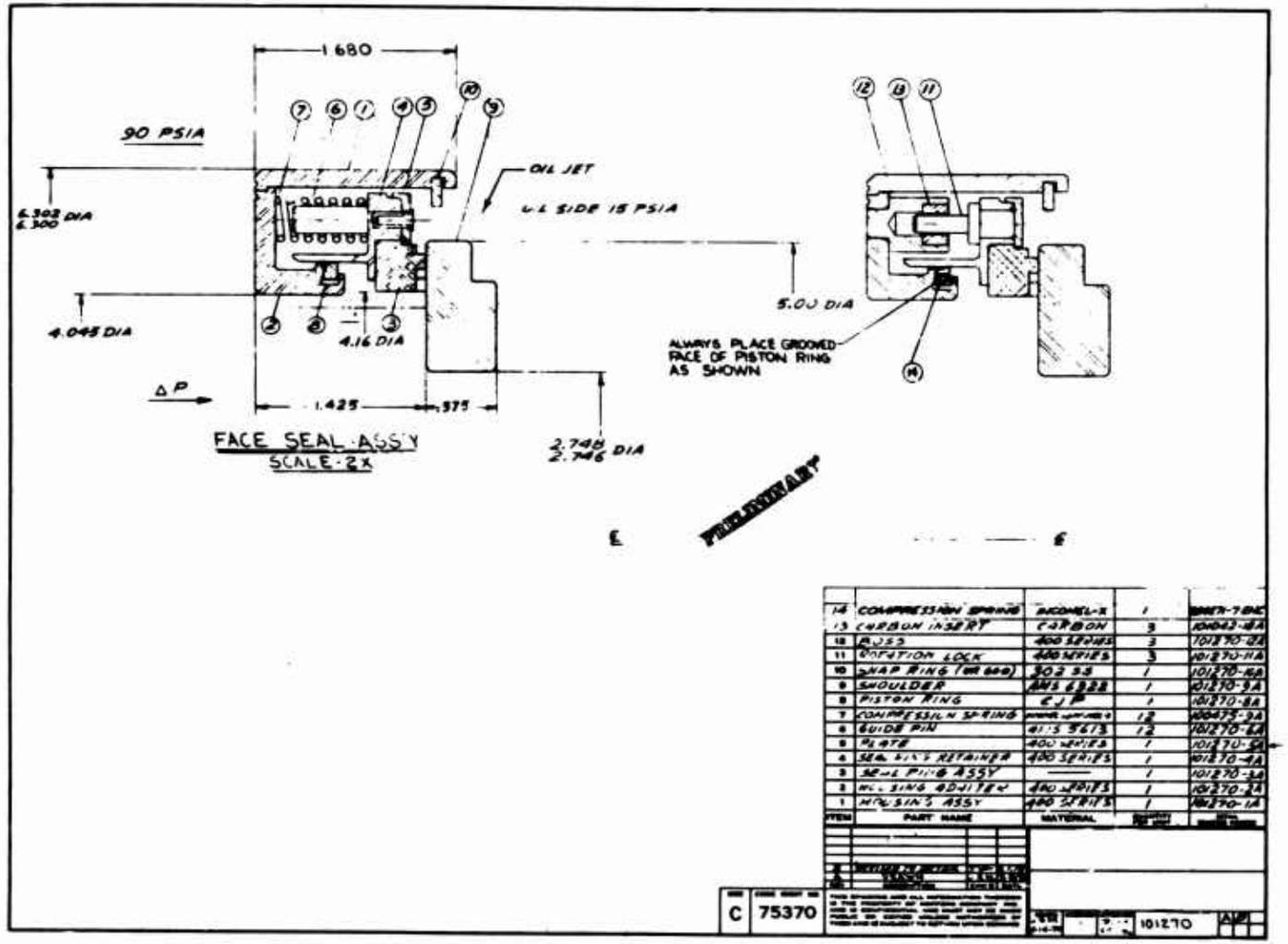

Figure 26. Carbon-Face Seal - Assembly Drawing.

The carbon-face seal assembly and the rotating component are shown in Figure 27. A closer view of the face seal assembly is shown in Figure 28, and the rubbing surfaces of both the stationary and the rotating members are shown in Figure 29.

Carbon-Face Seal Test Program

Testing of the carbon-face seal in the rotating test rig consisted of operating the seal at various conditions of pressure, temperature, speed, and alignment while measuring gas leakage at the various conditions. The seal was pressurized with filtered shop air, and leakage flows were measured with a flowmeter manufactured by the Cox Instrument Company. The test conditions at which the carbon-face seal was evaluated are summarized in Table XVI, and the instrumentation used is listed in Table XVII. All testing of the carbon-face seal was limited to a maximum shaft speed of 15,800 rpm (rubbing velocity of 320 feet per second for the face seal) and a maximum temperature of 500°F to minimize overheating of the test rig bearings.

Initially, the seal was installed in an aligned condition and subjected to a room temperature run-in for approximately 2 hours at speeds up to 15,800 rpm. The aligned condition consisted of a full indicator reading runout of 0.0003 inch measured on the sealing face and near the O.D. of the rotating component.

A static calibration was then conducted, at room temperature, without shaft rotation and with pressure applied to 75 psig in 25 psig increments, while measuring leakage. This was followed by a dynamic calibration with leakages measured at room temperature and 500°F, at incremental shaft speeds up to 15,800 rpm, and at pressures up to 75 psig in 25 psig increments.

Cyclic testing was then conducted, consisting of applying to the seal 50 consecutive operating cycles of temperature, pressure, and shaft speed. An operating cycle consisted of increasing the shaft speed from zero to 15,800 rpm and the pressure from zero to 75 psig over a period of 1 to 2 minutes. Temperature to 500°F was also applied; approximately 20 minutes was required to stabilize at 500°F. Upon obtaining stable conditions, pressure and shaft speed were rapidly reduced to zero to simulate engine shutdown, and the rig was allowed to cool to room temperature. Achieving room temperature concluded an operating cycle. The conditions were repeated until 50 cycles were obtained.

After completing the static and dynamic calibrations and cyclic testing, the same face seal hardware was subjected to two misalignment tests. Prior to each misalignment test, the seal was again subjected to a 2-hour run-in period before obtaining leakage data. Misalignment was achieved by shimming the rotating component fore and aft such that the plane of its sealing surface was no longer normal to the centerline of the shaft. The runout of the rotating component was then measured on its sealing surface near the outer edge. For the first misalignment test the runout was measured at a full indicator reading of 0.0014 inch. For the second misalignment test this runout was 0.0032 inch.

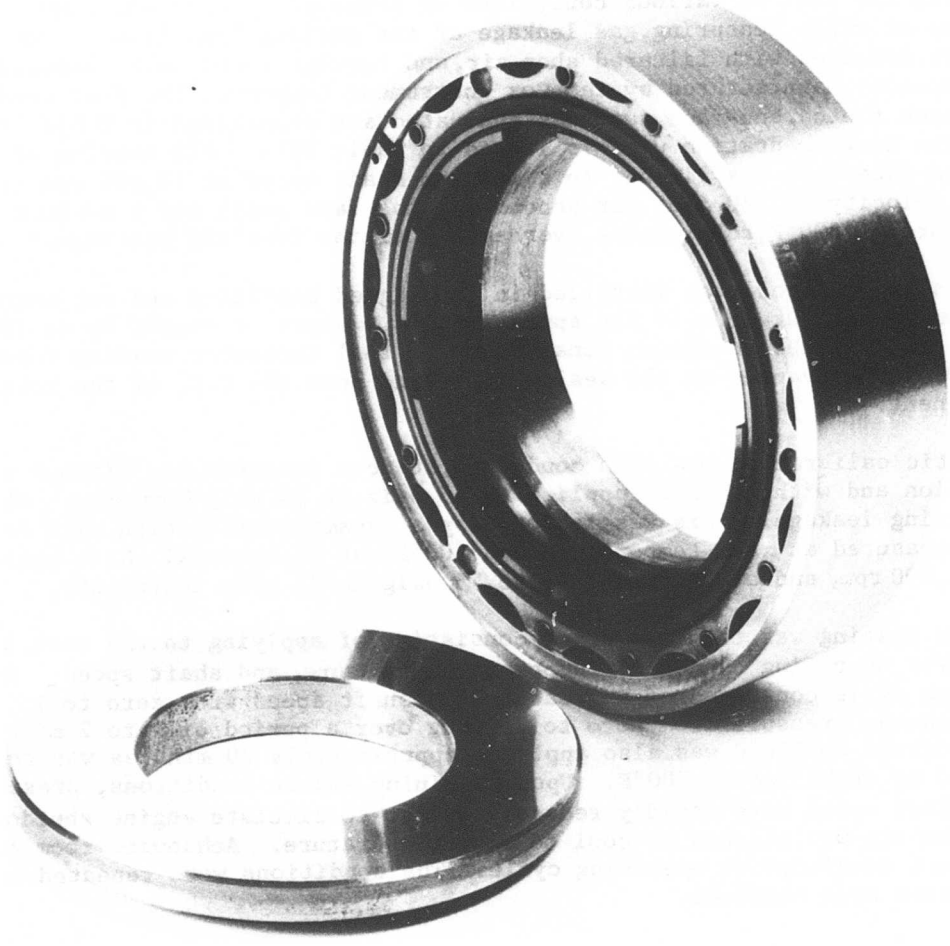

Figure 27. Carbon-Face Seal Components.

Figure 28. Carbon-Face Seal Assembly.

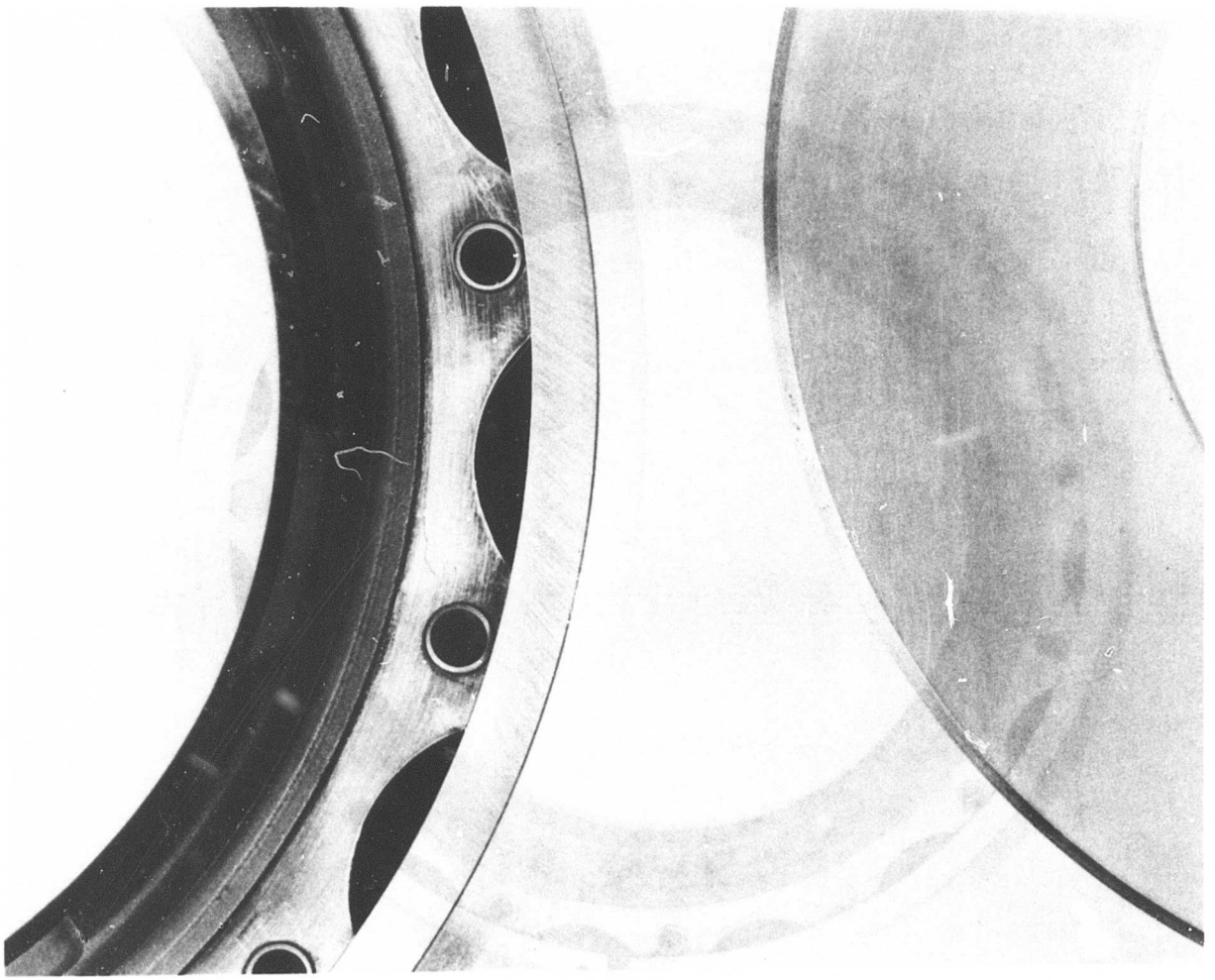

Figure 29. Carbon-Face Seal Rubbing Surface.

TABLE XVI . CARBON-FACE SEAL TEST CONDITIONS

Test Category	Pressure (psig)	Temperature (°F)	Shaft Speed (rpm)
A. Static Calibration	25 to 75	Room Temp	-
B. Dynamic Calibration	25 to 75	Room Temp	5,000
	25 to 75	Room Temp	10,000
	25 to 75	Room Temp	15,800
	25 to 75	500	15,800
	25 to 75	Room Temp	-
C. Cyclic (50 Cycles)	75	500	15,800
D. First Misalignment	25 to 75	Room Temp	-
	25 to 75	Room Temp	5,000
	25 to 75	Room Temp	10,000
	25 to 75	Room Temp	15,000
	25 to 75	500	15,800
	25 to 75	Room Temp	-
E. Second Misalignment	25 to 75	Room Temp	-
	25 to 75	Room Temp	5,000
	25 to 75	Room Temp	10,000
	25 to 75	Room Temp	15,800
	25 to 75	500	15,800
	25 to 75	Room Temp	-

TABLE XVII. CARBON-FACE SEAL TEST INSTRUMENTATION

Parameter	Location	Instrumentation	Range	Units
Gas Pressure	Upstream of Flowmeter	Gage	0-150	psig
Gas Pressure	Downstream of Flowmeter	Gage	0-150	psig
Gas Pressure	Upstream of Seal	Gage	0-100	psig
Gas Pressure	Downstream of Seal	Gage	0-10	psig
Gas Temp.	Downstream of Flowmeter	I-C Thermocouple	60-90	°F
Gas Temp.	Upstream of Seal	I-C Thermocouple	R.T.-600	°F
Gas Temp.	Downstream of Seal	I-C Thermocouple	R.T.-600	°F
Shaft Speed	Test Head Shaft	Tachometer	0-20,000	rpm
Gas Flow (Leakage)	Gas Pressurizing Line	Cox Flowmeter Model 120-281	0.00045-0.045 nitrogen at 250 psig and 70°F	lb/sec

Carbon-Face Seal Test Results

The basic leakage characteristics of the carbon-face seal as affected by alignment of the rotating component, air temperature, and 50 simulated engine operating cycles are displayed in Figure 30, which shows plots of air leakage across the seal versus upstream air pressure for various test conditions at a constant shaft speed. The upstream air pressure is also the pressure differential across the seal, since all testing was conducted with the downstream side of the seal vented to atmosphere. The lower group of curves are the test results on the face seal in the aligned condition, before and after the 50-cycle test, and at room temperature and 500°F. A slight decrease in leakage at increased temperature is evident, and a further decrease in leakage after the 50-cycle test is also evident. The uppermost pair of curves represent the maximum misaligned condition tested and display the increased leakage associated with the misalignment; and they also indicate a reduction in leakage at increased air temperature.

The results of the test simulating 50 engine operating cycles are shown in Figure 31, which is a plot of air leakage versus operating cycles for different pressures. The seal shows distinct improvement in sealing characteristics with the accumulation of operating cycles, the cause of the polishing of the rubbing surfaces and the resultant improvement in mate-up of these surfaces. The lower pressures indicate that optimum mate-up of the sealing surfaces occurred early in the 50-cycle test. However, the highest pressure indicates a continuous improvement in sealing characteristics throughout the test, with minimum leakage capability yet to be achieved but approaching a constant value of less than two-thirds of the initial leakage.

The results of the misalignment tests are presented in Figure 32, which shows curves of air leakage at several temperature and pressure conditions versus the full indicator reading runout measured on the sealing face near the O.D. of the rotating component for the aligned and the two misaligned conditions. The dashed portions of the two uppermost curves are extrapolations from slightly lower pressures to the 75-psig pressure level taken from air leakage versus air pressure curves presented earlier for the maximum misalignment condition.

The effect of shaft speed on seal leakage at three different pressures is shown in Figure 33. The dynamics of the mating surfaces tend to cause an increase in leakage with an increase in shaft speed.

Views of the rubbing surfaces on the carbon-face seal rotating and stationary components after completion of all testing are shown in Figures 34 and 35. Both surfaces were in excellent condition after testing, showing a high polish and no visible evidence of scoring.

The surface finish condition of both rubbing surfaces was determined on a Taylor-Hobson Talysurf Model No. 3 surface-finish measuring instrument, with results in the form of representative sections of strip chart presented in Figures 36 and 37. On the rotating component, the pretest and posttest surface conditions are graphically displayed by tracing the probe of the measuring instrument in a single sweep across an untouched or "as is"

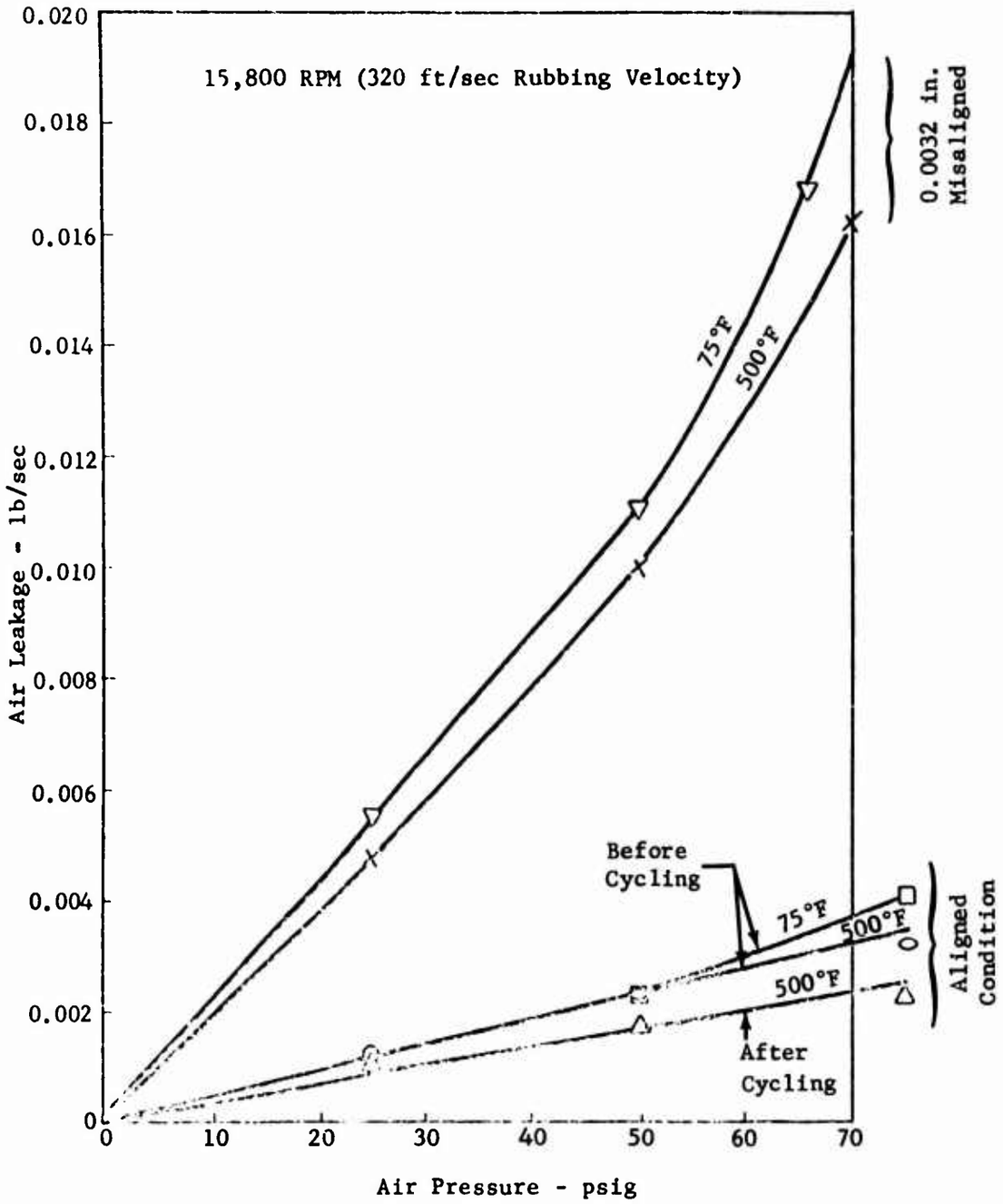

Figure 30. Carbon-Face Seal Leakage Versus Air Pressure.

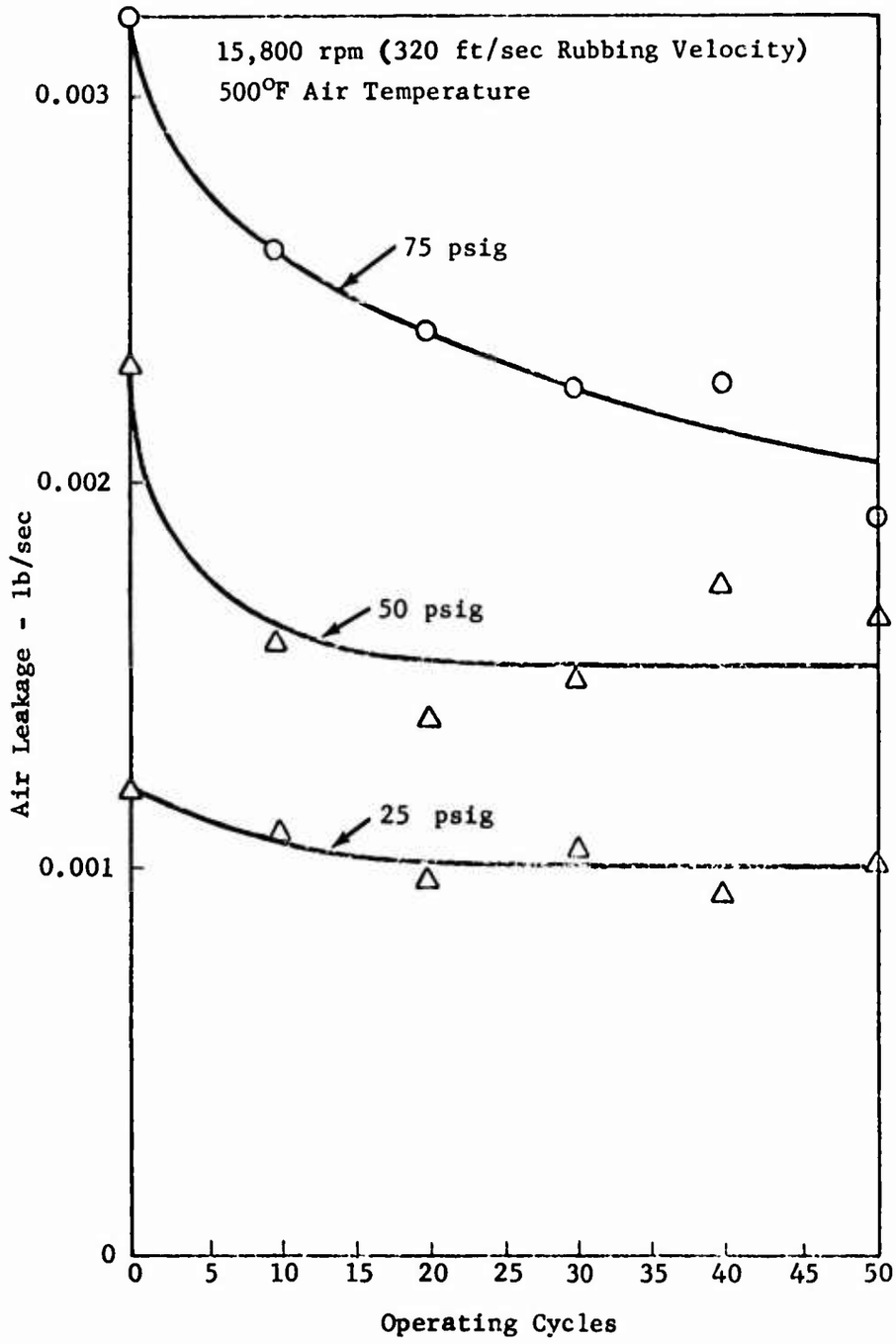

Figure 31. Carbon-Face Seal Leakage Versus Operating Cycles.

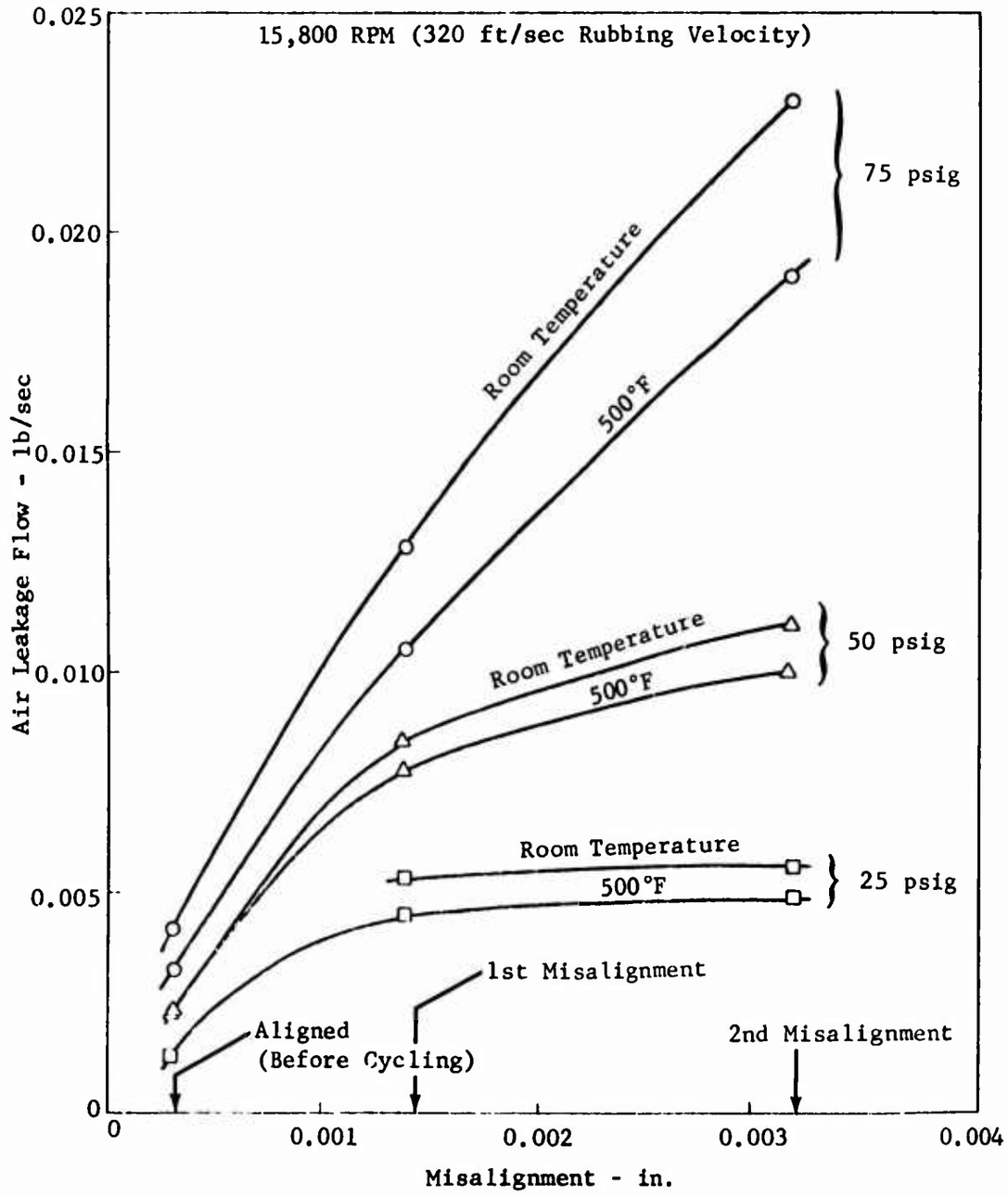

Figure 32. Carbon-Face Seal Leakage Versus Misalignment.

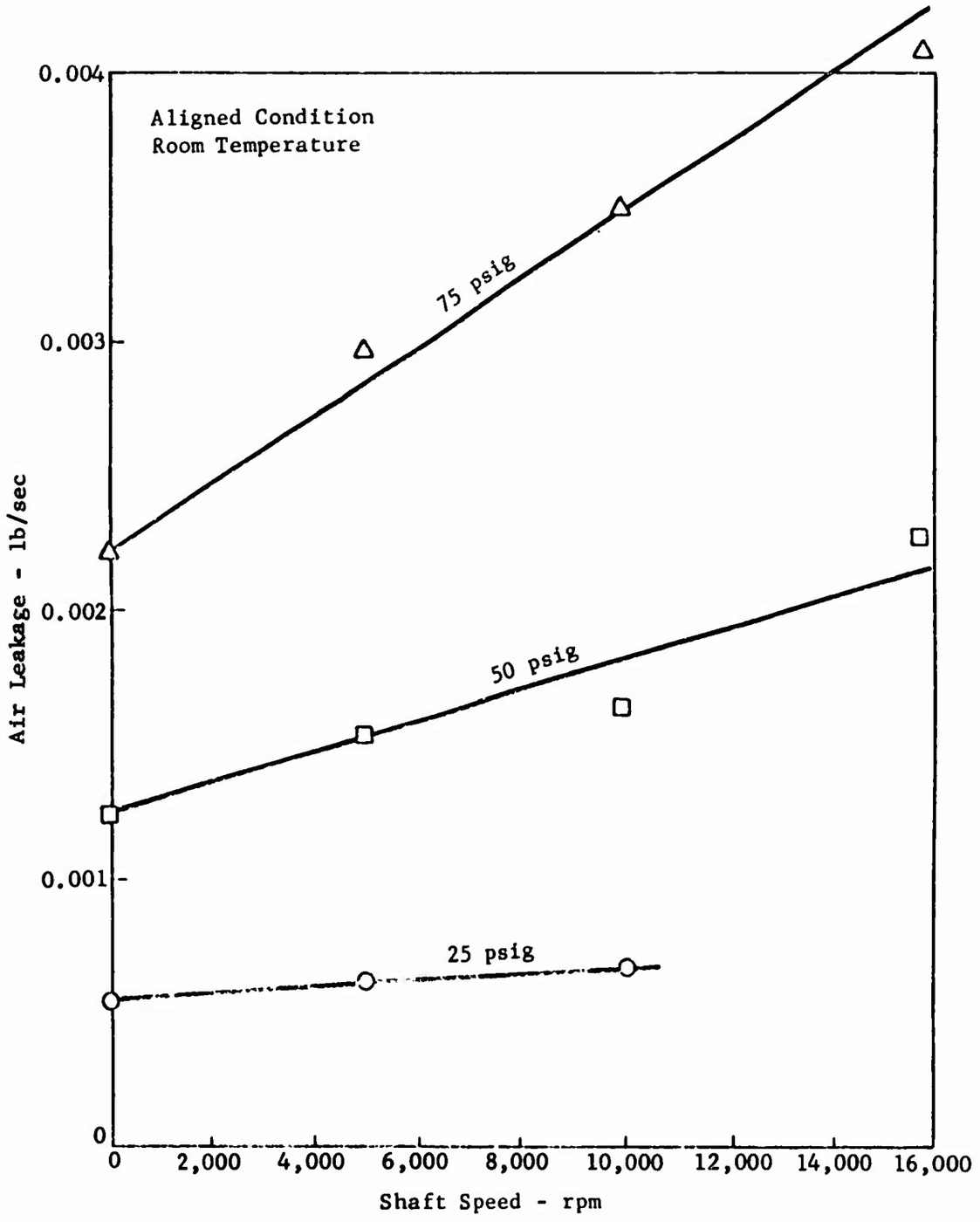

Figure 33. Carbon-Face Seal Leakage Versus Shaft Speed.

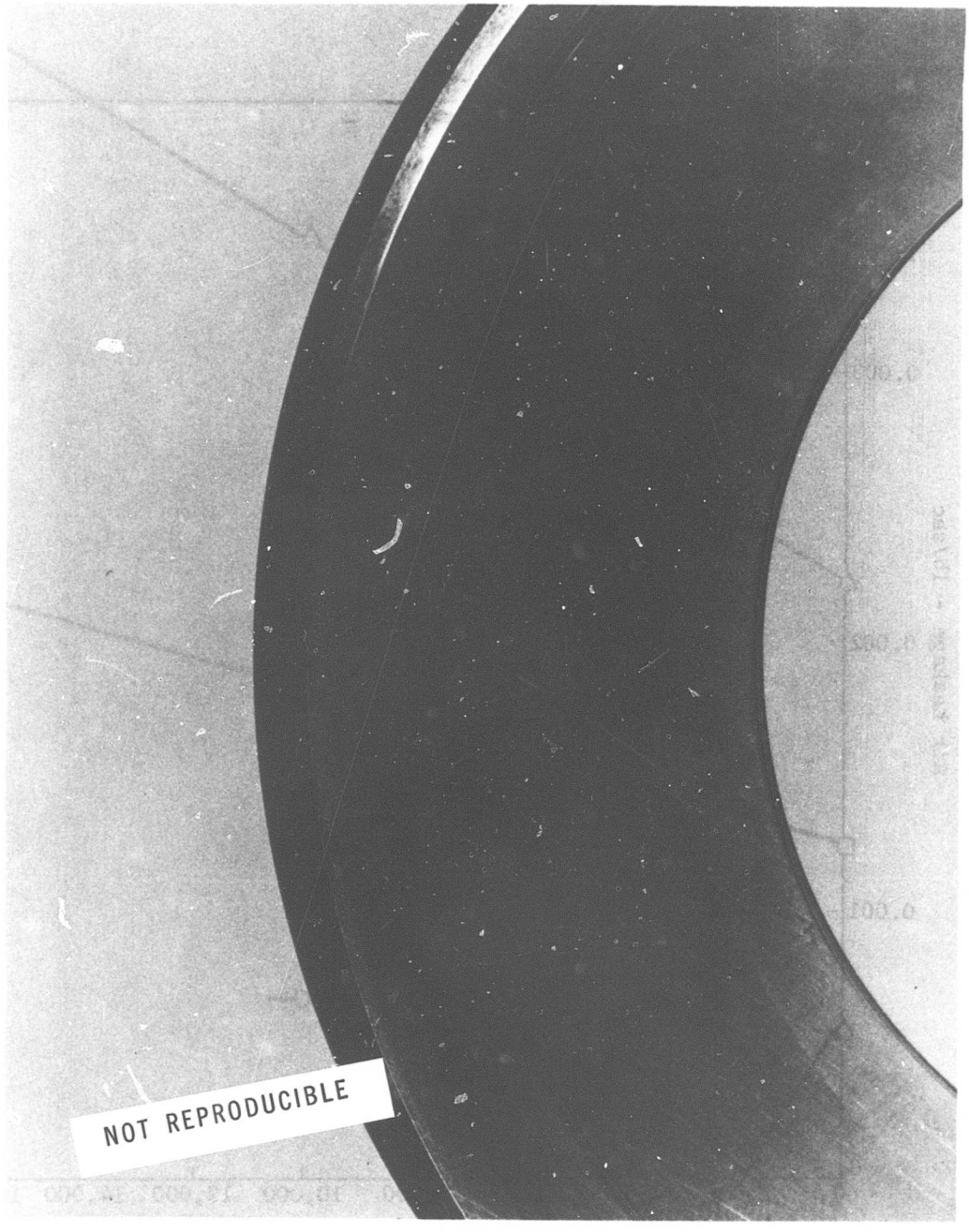

Figure 34. Carbon-Face Seal Rotating Component After Testing.

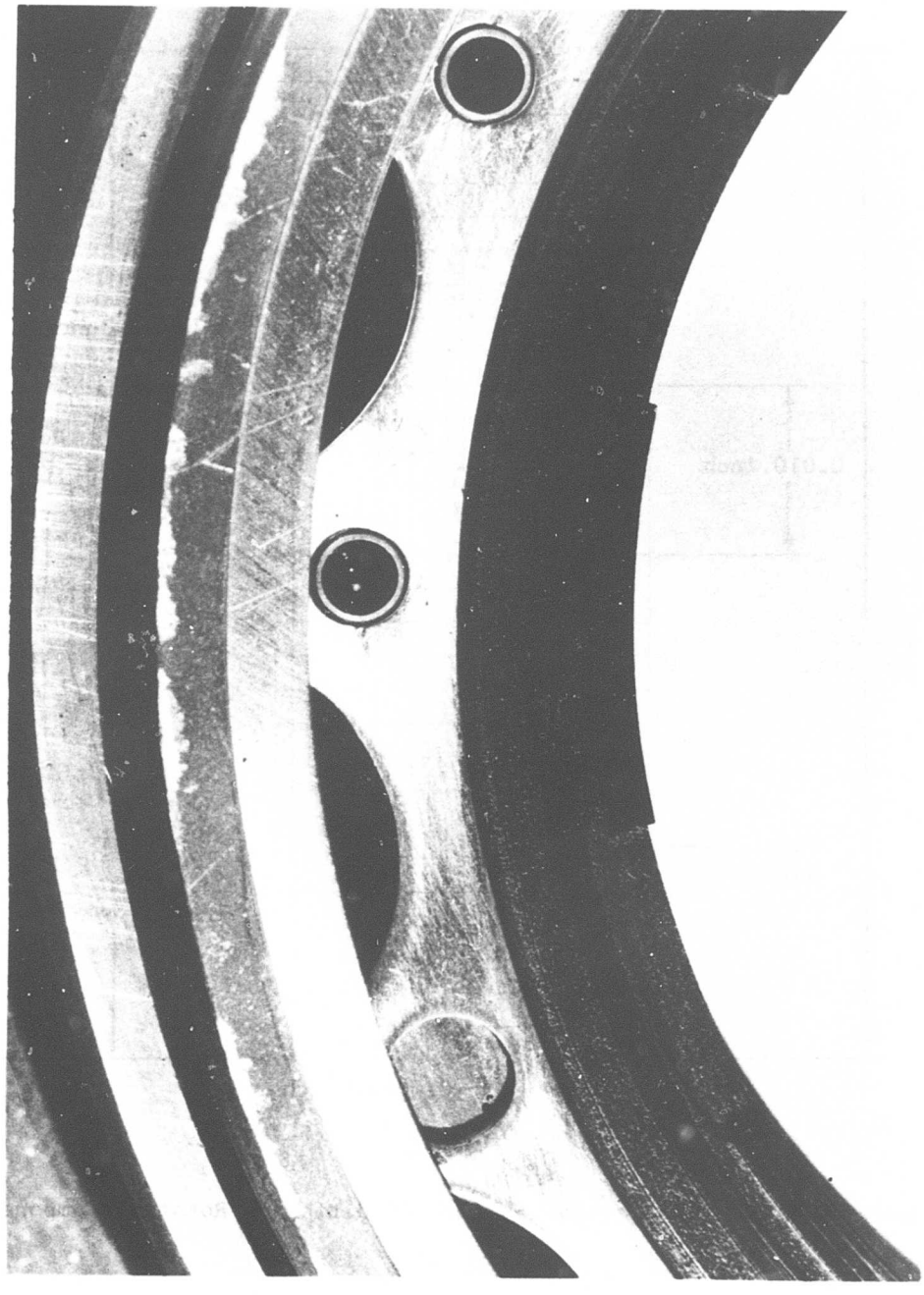

Figure 35. Carbon-Face Seal Stationary Component After Testing.

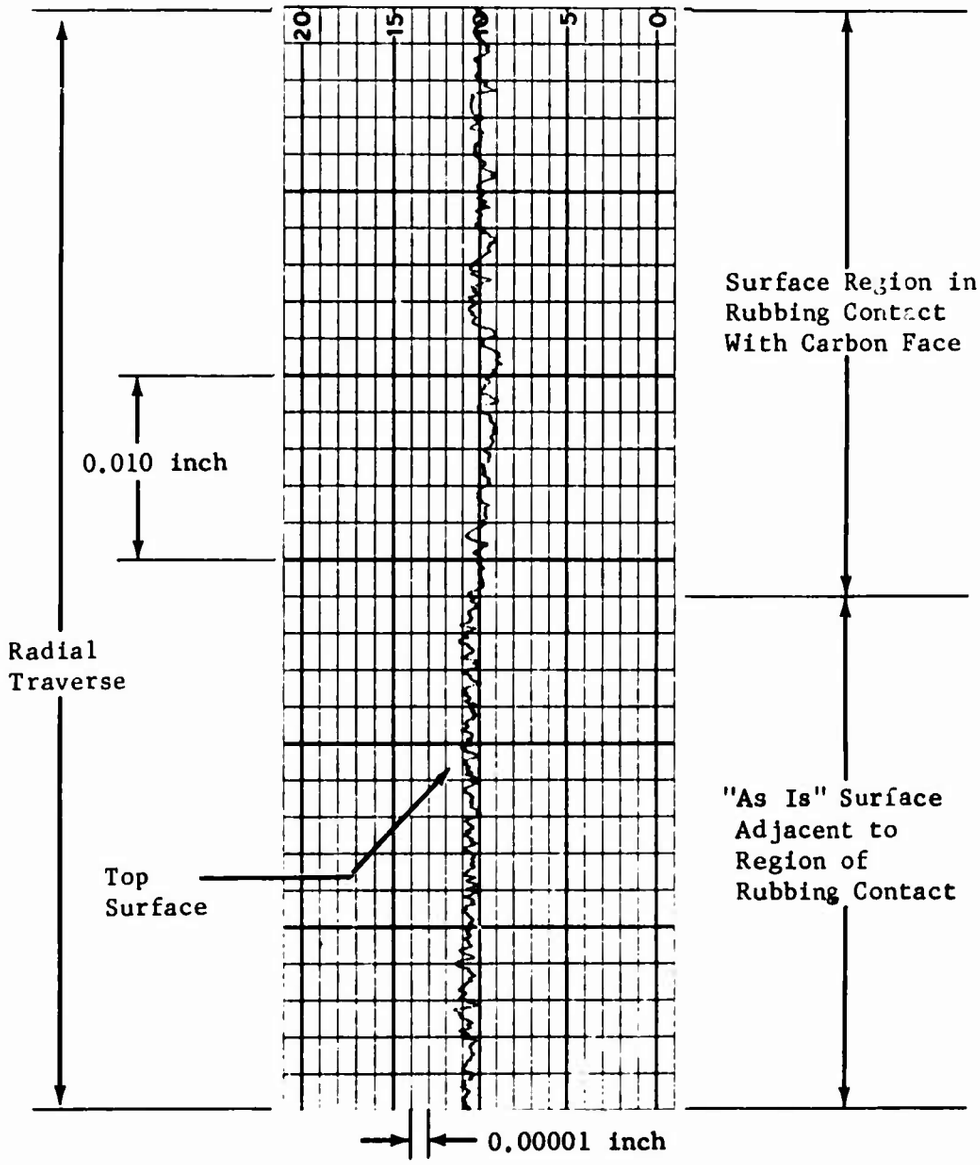

Figure 36. Carbon-Face Seal Surface Condition of Rotating Component.

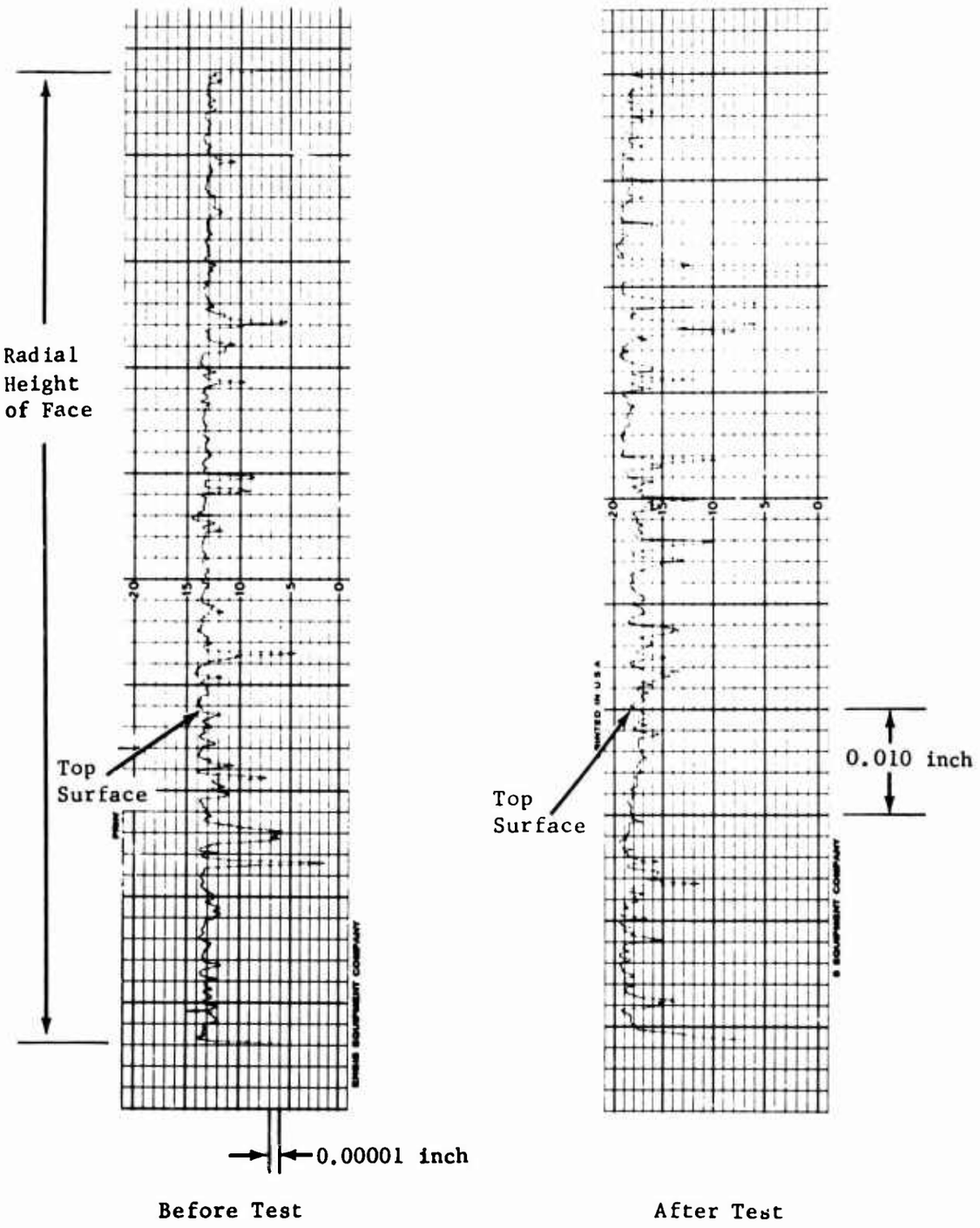

Figure 37. Carbon-Face Seal Surface Condition of Carbon Element (Stationary Component).

portion of the rubbing surface and into the region that was in rubbing contact with the carbon element throughout the testing. In this manner both the "before test" and the "after test" conditions may be displayed and compared on a single chart. The surface finish shows an insignificant change in the region of rubbing with peak-to-peak roughness at a maximum of about 15 microinches, while the roughness in the "as is" region is a peak-to-peak value of about 10 microinches.

The condition of the rubbing surface on the carbon element is displayed in two separate charts obtained before and after testing. In the pretest condition, the typical surface finish is about 10 microinches (peak-to-peak) with occasional deviations up to 120 microinches in depth, which appear to be the result of the surface finishing process. In the post-test condition, surface roughness has increased to about 20 to 30 microinches (peak-to-peak) with deviations as high as 200 microinches, which may not necessarily be the result of testing but a product of the surface finishing process during manufacture of the unit.

The spring rate of the internal spring mechanism in the stationary component was measured at 0.066 inch per pound both before and after testing, indicating that the spring was not affected by the test conditions imposed upon the carbon-face seal assembly.

CASE SPLIT-LINES (TASK III)

Test Rig

The leakage characteristics of typical engine case flanges using five different sealing methods were evaluated in a cylindrical pressure vessel which was designed and fabricated for this program. A drawing of the pressure vessel test rig is shown in Figure 38. The pressure vessel consists of a cylindrical center section that is split into two half-sections and two cylindrical end sections which attach at each end of the center section.

A view of the split center section is shown in Figure 39, a view of one of the two identical end sections is shown in Figure 40, and the complete assembly is shown in Figure 41. The pressure vessel is a flightweight design with Inconel 718 used in the end sections to simulate a combustor inlet housing or compressor rear bearing support and a 410 stainless steel split center section to simulate the compressor housing.

The five basic sealing configurations tested in the pressure vessel test rig were: (1) metal-to-metal flanges, (2) pressurized metal O-rings, (3) pressure energized metal V-rings, (4) metal-asbestos braided packing, and (5) nonpressurized metal tubing. The metal tube (similar to the metal O-ring in material, cross section, and method of application) and the braided packing were used in the straight split-lines of the pressure vessel center sections. The O-ring and V-ring were used in the circular flange split-lines. The various sealing configurations are shown in detail in the drawing of the pressure vessel test rig. The following is a description of the sealing configurations tested:

1. Metal-to-Metal Flanges - No packing or gasketing of any kind was used between the contacting surfaces of mating flanges. This configuration was tested in both the circular (vertical) and straight (horizontal) flanges, and the dimensions of these flanges are shown in detail in the drawing of the pressure vessel.

2. Metal O-Ring - These seals (Part Number U-6312-12250-PFA) were manufactured by United Aircraft Products, Inc., Dayton, Ohio. Detail information is listed below:

O.D.	12-1/4 inches nominal
I.D.	12-1/16 inches nominal
Tube O.D.	0.096/0.086 inch
Tube Wall	0.012 inch
Tube Material	Inconel-X
Silver Plating	0.002/0.001 inch thick
Type	Pressure Filled
Groove Size	0.069/0.065 inch deep (open at I.D.)

3. Metal V-Ring - These seals (Part Number 8813-2001-1225) were manufactured by Parker Seal Company, Culver City, California. Detail information is listed below:

O.D.	12-1/4 inches nominal
I.D.	12-1/16 inches nominal
Free Height	0.092/0.089 inch
Material	Inconel-X
Silver Plating	0.002/0.001 inch thick
Groove Size	0.078/0.076 inch deep (open at I.D.)

4. Braided Packing - This is a flexible braiding of metal wire and asbestos having a square cross section and manufactured by Raybestos-Manhattan, Inc., Passaic, New Jersey, Part Number R/M 303. Detail information is listed below:

Material	Inconel wire and asbestos
Cross Section (nominal)	1/8 x 1/8 inch
Groove Size	0.094/0.090 inch deep x 0.14/0.13 inch wide

5. Metal Tubing - This configuration consisted of a straight length of metal tubing cut to a length equal to the length of the flange with the ends of the tubing remaining open. Detail information is listed below.

Material	Inconel-X
Tube O.D.	0.095/0.086 inch
Tube Wall	0.014/0.012 inch
Silver Plating	0.002/0.001 inch
Groove Size	0.069/0.065 inch deep x 0.116/0.114 inch wide

The various sealing configurations were tested in the pressure vessel test by a series of reworks to the pressure vessel. The initial test configuration consisted of metal-to-metal flanges at both the straight (horizontal) and circular (vertical) split-lines. Upon completion of testing on this configuration, the pressure vessel was reworked to accept the metal O-rings in the circular flanges and the metal tubing in the straight flanges. After completing the same series of tests on these configurations, the pressure vessel was again reworked in order to accept the metal V-rings in the circular flanges and the braided packing in the straight flanges. The pressure vessel was again subjected to the series of tests which completed the leakage evaluation on the various sealing configurations.

BLANK PAGE

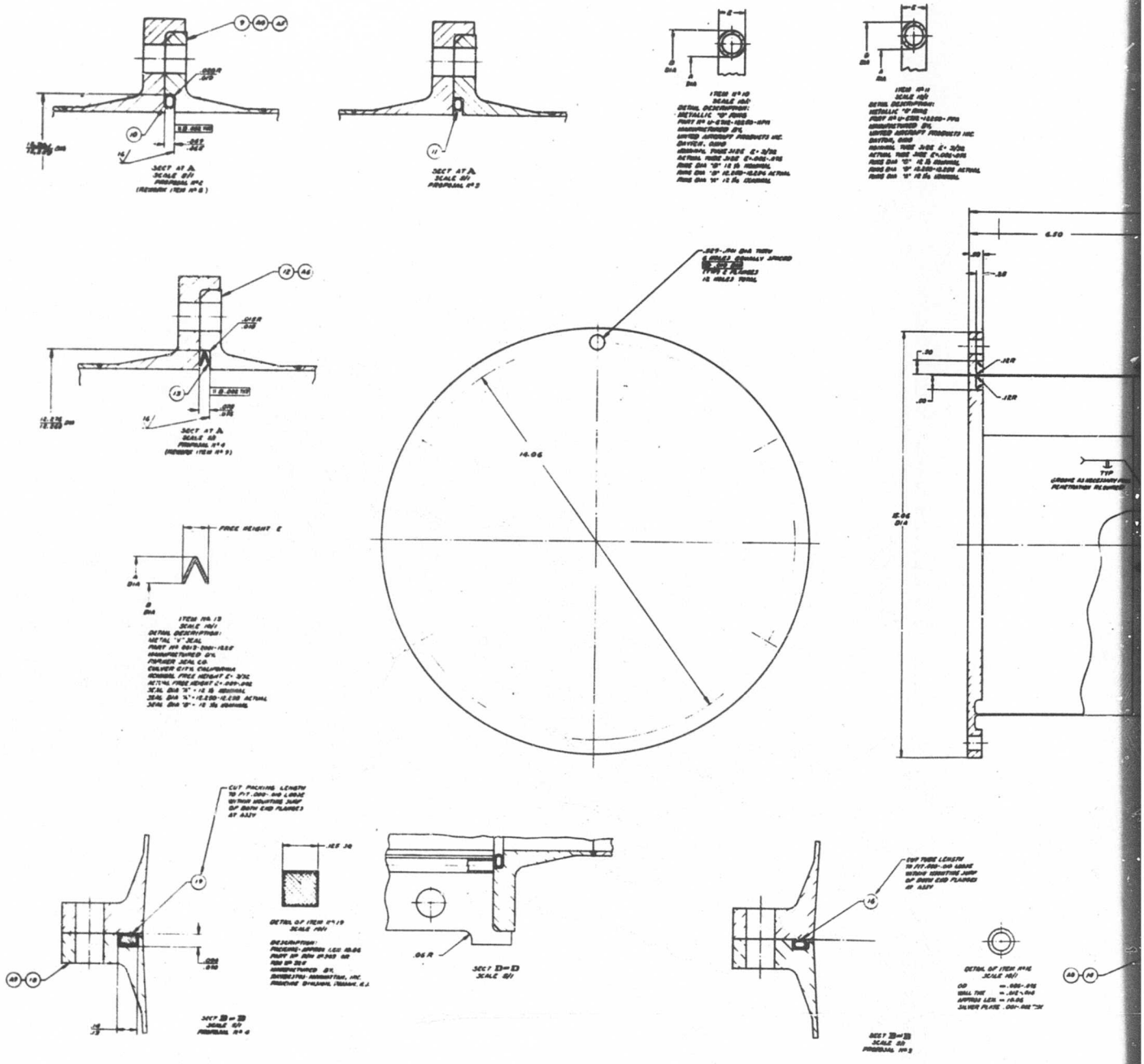

Figure 38. Pressure Vessel Test Rig.

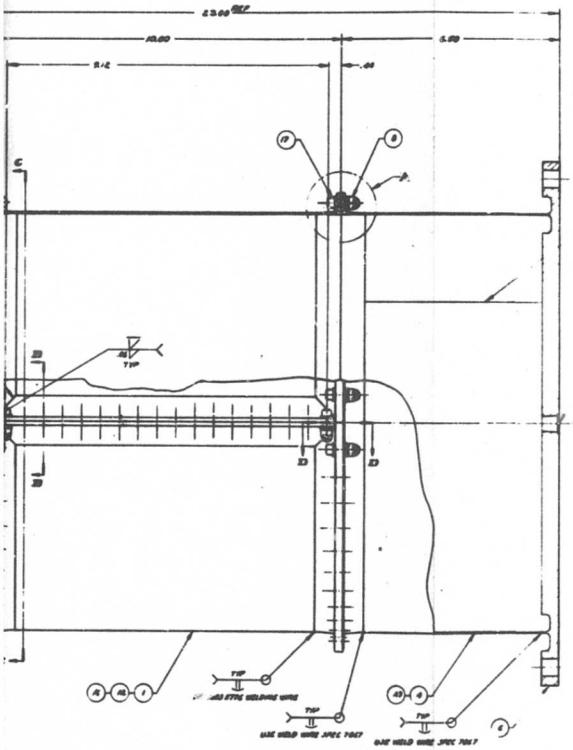

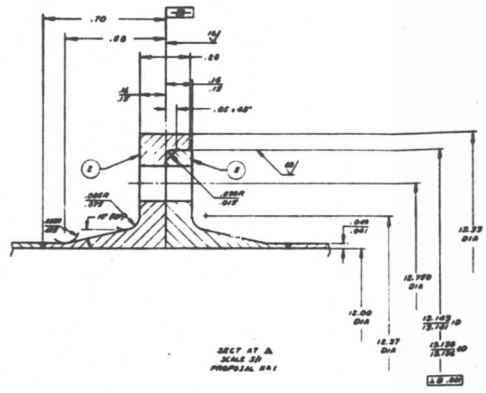

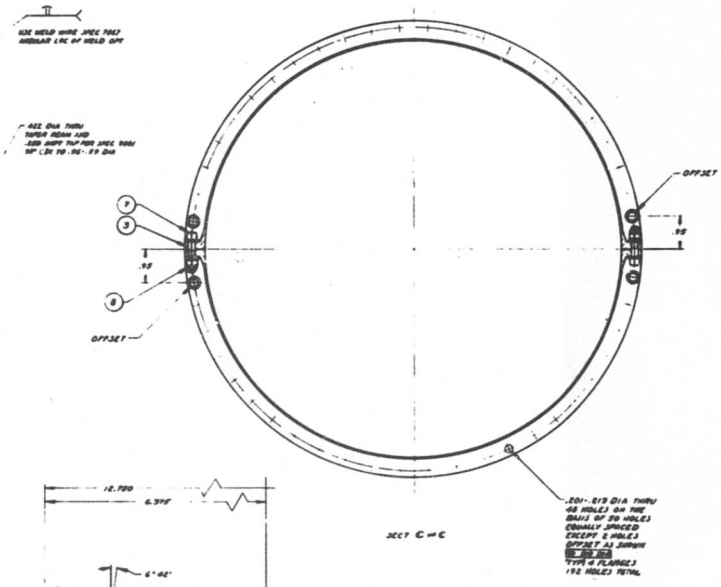

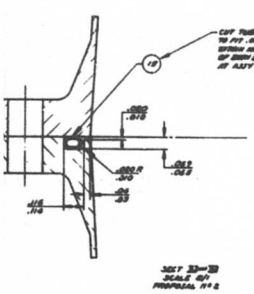

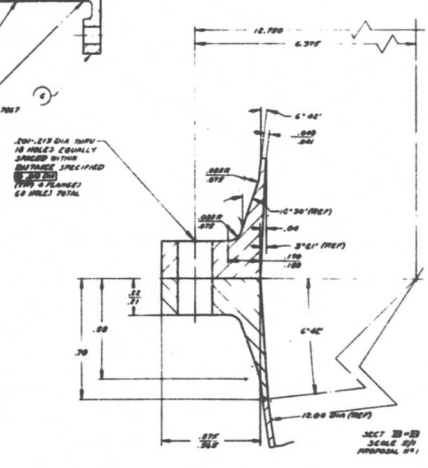

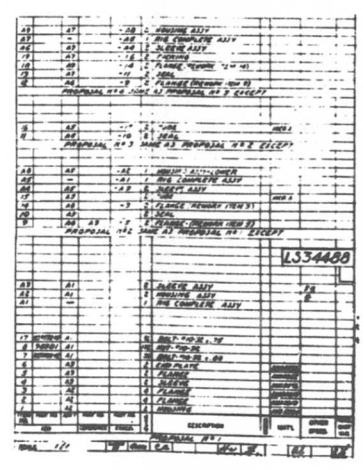

BLANK PAGE

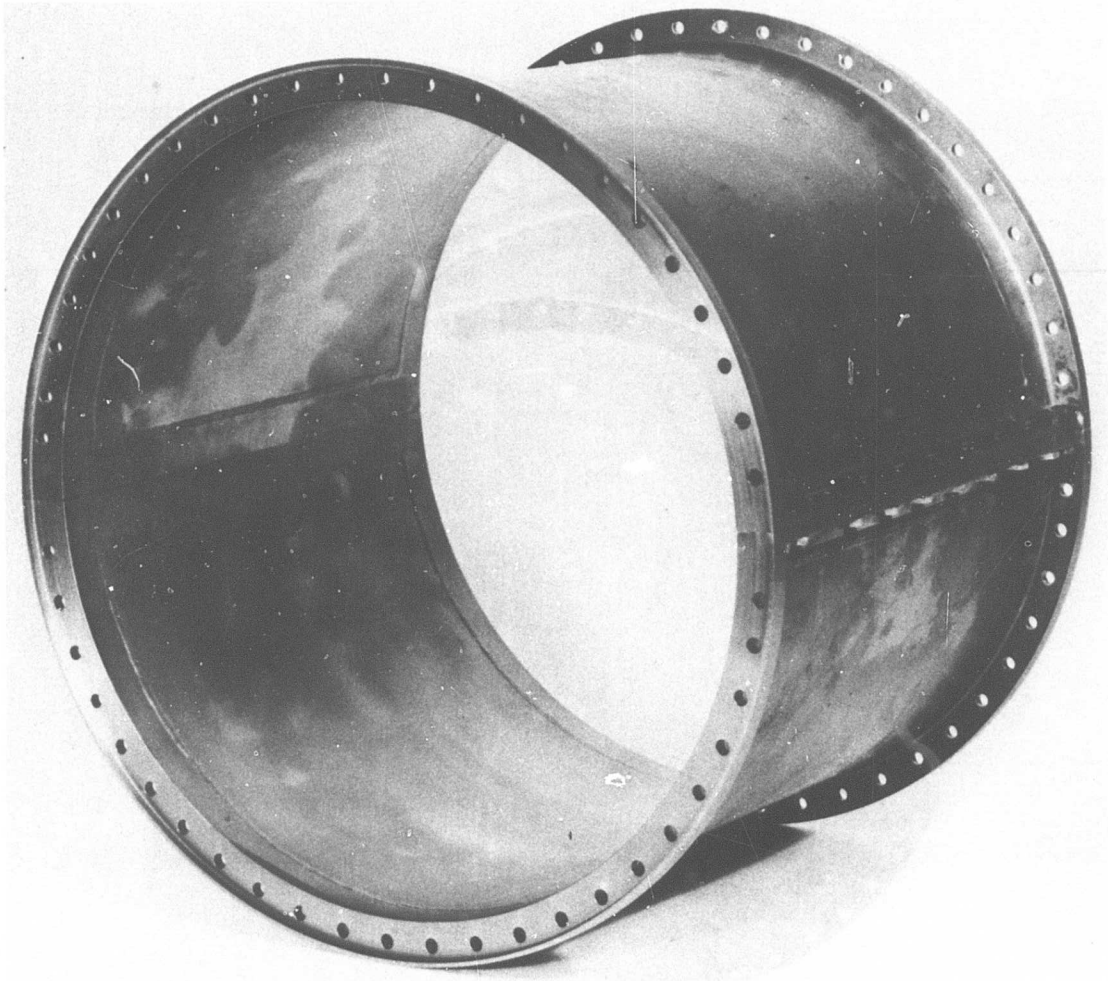

Figure 39. Pressure Vessel Test Rig - Center Section.

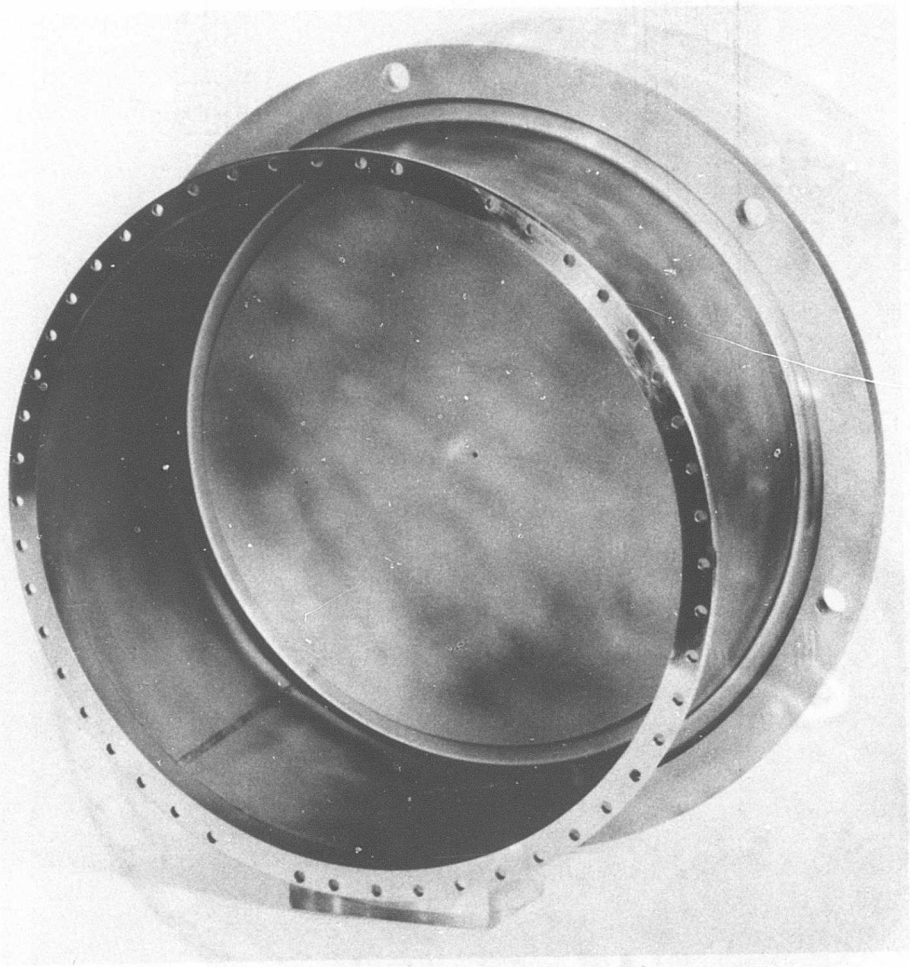

Figure 40. Pressure Vessel Test Rig - End Section.

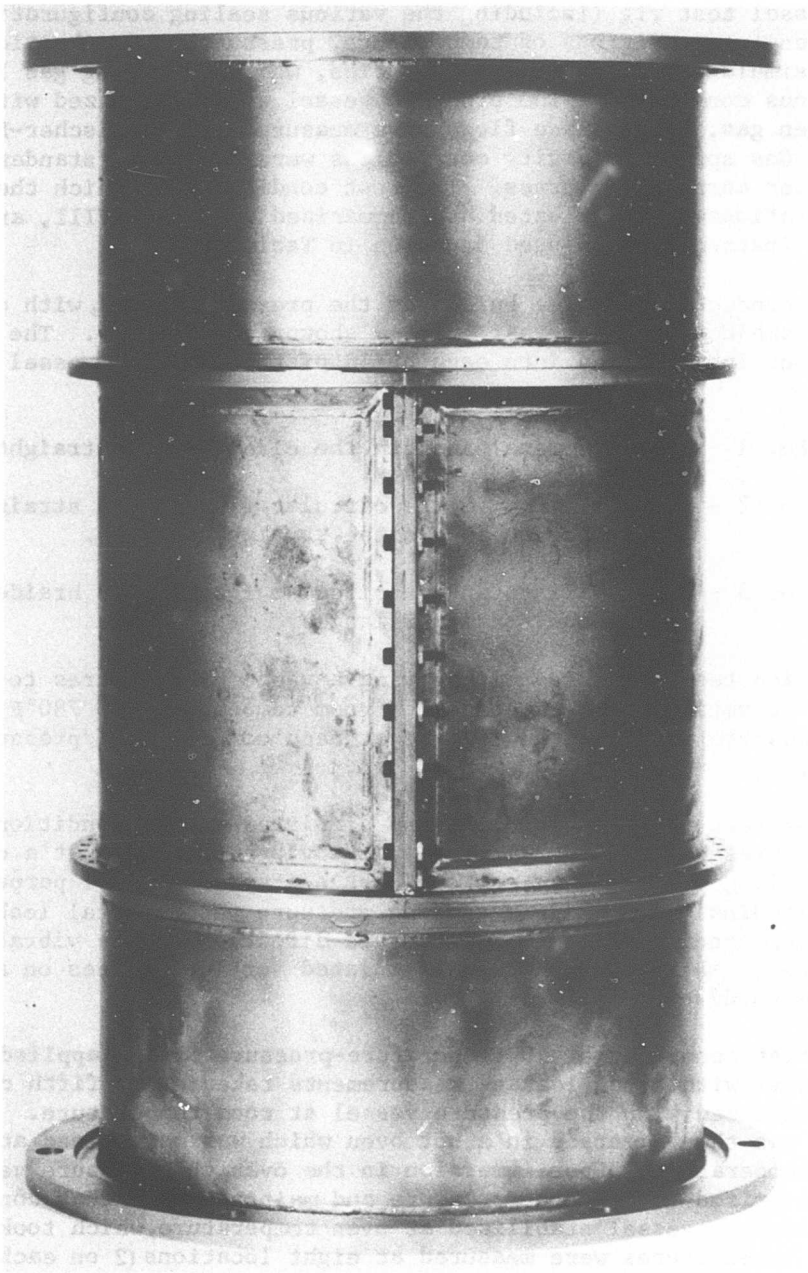

Figure 41. Pressure Vessel Test Rig Assembly.

Test Program

Testing of the engine case split-line seals consisted of subjecting the pressure vessel test rig (including the various sealing configurations) to typical engine conditions of temperature, pressure, and vibration, including 50 simulated engine operating cycles, while measuring gas leakage at the various conditions. The pressure vessel was pressurized with bottled nitrogen gas, and leakage flows were measured with a Fischer-Porter Flowrator. Gas specific gravity corrections were made with standard Fischer-Porter correction curves. The test conditions at which the sealing configurations were evaluated are summarized in Table XVIII, and a list of the instrumentation used is shown in Table XIX.

Testing was conducted in three builds of the pressure vessel, with each build being subjected to the test program shown in the table. The sealing configurations incorporated into each build of the pressure vessel are as follows:

Build No. 1 - Metal-to-metal in both the circular and straight flanges.

Build No. 2 - Metal O-rings in the circular flanges and straight lengths of tubing in the straight flanges.

Build No. 3 - Metal V-rings in the circular flanges and braided packing in the straight flanges.

The calibration test consisted of applying a range of pressures to the pressure vessel at various temperatures from room temperature to 780°F while measuring pressure vessel total leakage at each condition of pressure and temperature.

The vibration test consisted of applying simulated engine conditions of temperature, pressure, and first-order engine vibratory modes at a constant loading of $\pm$ 10 g's applied at one end of the pressure vessel perpendicular to its longitudinal axis while measuring pressure vessel total leakage at each operating condition. The location and direction of the vibratory loads applied to the pressure vessel simulated vertical forces on a cantilever-mounted engine case.

The cyclic test consisted of 50 temperature-pressure cycles applied to the pressure vessel with total leakage measurements taken every fifth cycle. A cycle was initiated with the pressure vessel at room temperature. The pressure vessel was then immersed in a hot oven which was maintained at the desired test temperature. Upon immersion in the oven, the pressure vessel was rapidly pressurized to the test pressure and maintained at that condition until the pressure vessel stabilized at oven temperature, which took 15 to 20 minutes. Temperatures were measured at eight locations (2 on each straight flange and 2 on each circular flange) on the pressure vessel. Temperatures were considered to be stabilized when all locations were within 20°F of the test temperature. Upon achieving the test temperature, the pressure vessel was removed from the oven, the pressure was vented to atmosphere, and

TABLE XVIII. CASE SPLIT-LINE SEAL TEST CONDITIONS

Test Category	Pressure (psig)	Temperature (°F)	Vibration (cps)	Load (G)
A. Calibration	50 to 200	Room Temp	-	-
	50 to 200	140	-	-
	50 to 200	240	-	-
	50 to 200	480	-	-
	50 to 200	650	-	-
	50 to 200	780	-	-
B. Vibration	50	240	580	±10
	100	480	665	±10
	150	650	745	±10
	200	780	830	±10
C. Cyclic (50 Cycles)				
1st Build	200	780	-	-
2nd Build	100	500	-	-
3rd Build	100	500	-	-
D. Leakage Distribution	100 to 200	Room Temp	-	-

TABLE XIX. SPLIT-LINE PRESSURE VESSEL TEST INSTRUMENTATION

Parameter	Location	Instrumentation	Range	Units
Gas Pressure	Upstream of Flowmeter	Gage	0-300	psig
Gas Pressure	Downstream of Flowmeter	Gage	0-300	psig
Gas Pressure	Pressure Vessel Gas Inlet	Gage	0-250	psig
Gas Temp.	Downstream of Flowmeter	I-C Thermocouple	60-90	°F
Metal Temp.	Pressure Vessel Flanges (8 Locations)	C-A Thermocouple	R.T.-800	°F
Gas Flow (Leakage)	Gas Pressurizing Line	Fischer-Porter Flowrator Model 6311-A3592 (two in parallel when required)	0.004-0.019 air at 14.7 psia and 60°F	lb/sec

the pressure vessel was allowed to cool to room temperature; this completed one simulated engine operating cycle. This series of events was repeated 50 consecutive times for the cyclic test.

The oven used to heat the pressure vessel during cyclic testing (and all other elevated temperature testing) is shown in Figure 42. The pressure vessel is shown immersed in the oven in Figure 43 and is shown suspended by a hoist above the oven in Figure 44. The oven is surrounded by an energy absorption shell for safety purposes. Vibratory forces were induced radially at the lower end of the pressure vessel with excitation provided by an MB electromagnetic shaker Model C-10 shown in the photograph. The load is transmitted to the pressure vessel fixture by a connecting rod which passes through the oven wall and protective shell.

The air leakages measured in the calibration, vibration, and cyclic tests were pressure vessel total leakages, including leakage from the circular flanges, straight flanges, and the junctions where the ends of the straight flanges meet the circular flanges, which proved to be a major source of leakage. A method was developed and applied to each of the pressure vessel test configurations to quantitatively identify the level of leakage from each of the possible leakage sources. This method consisted of artificially sealing a particular flange location in the pressure vessel to provide "zero" leakage at that location and performing a leakage calibration over a pressure range. By comparing pressure vessel total leakage with the leakage obtained after artificially sealing some portion of the pressure vessel flanging, the difference in these values represented the leakage of the artificially sealed section. By this method, the effectiveness of the various flange seal configurations could be evaluated. The artificial sealing of the flanges was accomplished by applying a heavy-duty tape internally over the split-line and/or a fiber-filled putty between the flanges at the location to be sealed. The effectiveness of the artificial sealing techniques was established by performing soap-bubble checks of the sealed locations at pressures up to 100 psig prior to conducting the leakage test and then inspecting the sealed locations after completion of the leakage test by the same bubble-check technique and also visually to assure that extrusion of the tape or putty out of the sealed location had not occurred. In all cases, the sealing techniques proved to be satisfactory.

Test Results

The leakage characteristics of the three builds of the pressure vessel test rig incorporating the various flange sealing configurations are shown in Figures 45, 46, and 47, which are plots of total pressure vessel air leakage versus internal air pressure over a range of temperatures from room temperature to 780°F. The first build of the pressure vessel consisting of metal-to-metal flanges in both the circular and straight split-lines displayed a distinct reduction in the rate of leakage with increasing temperature, which is probably related to the reduction in air density at elevated temperature. The second pressure vessel build consisting of silver-plated and internally pressurized metal O-rings in the circular flanges and silver-plated metal tubing in the straight flanges displays less variation

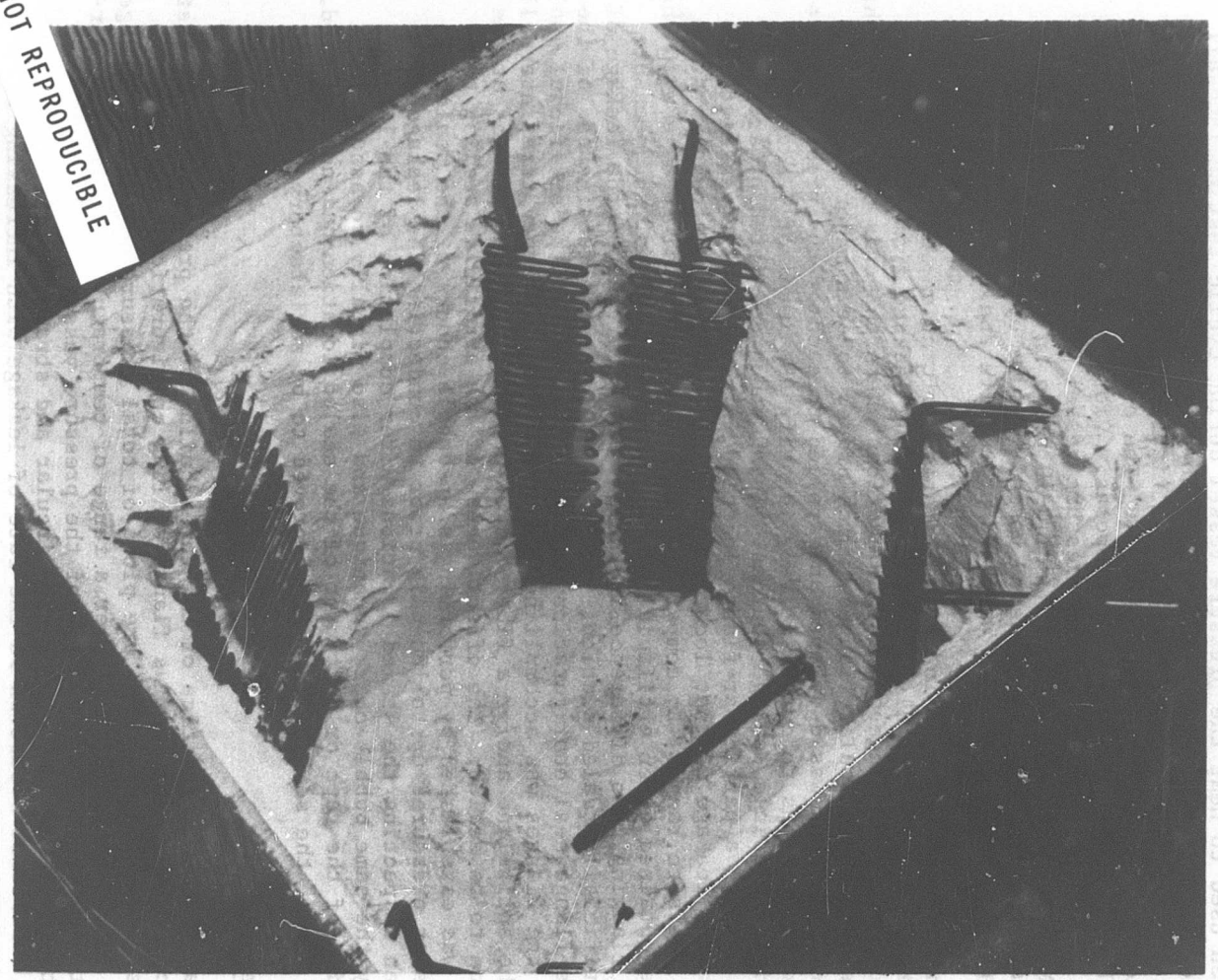

Figure 42. Pressure Vessel Test Rig Oven Arrangement.

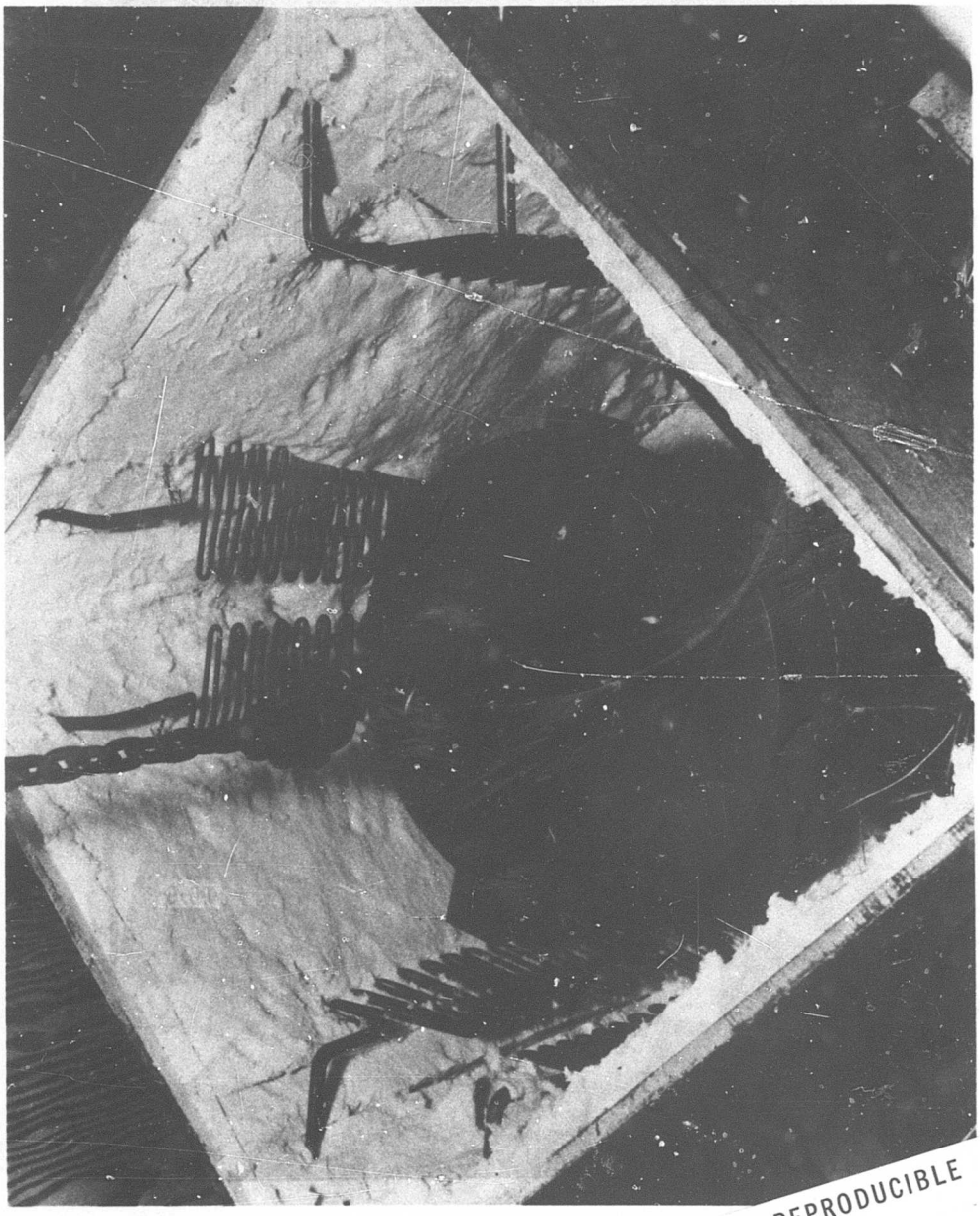

Figure 43. Pressure Vessel Test Rig Immersed in Oven.

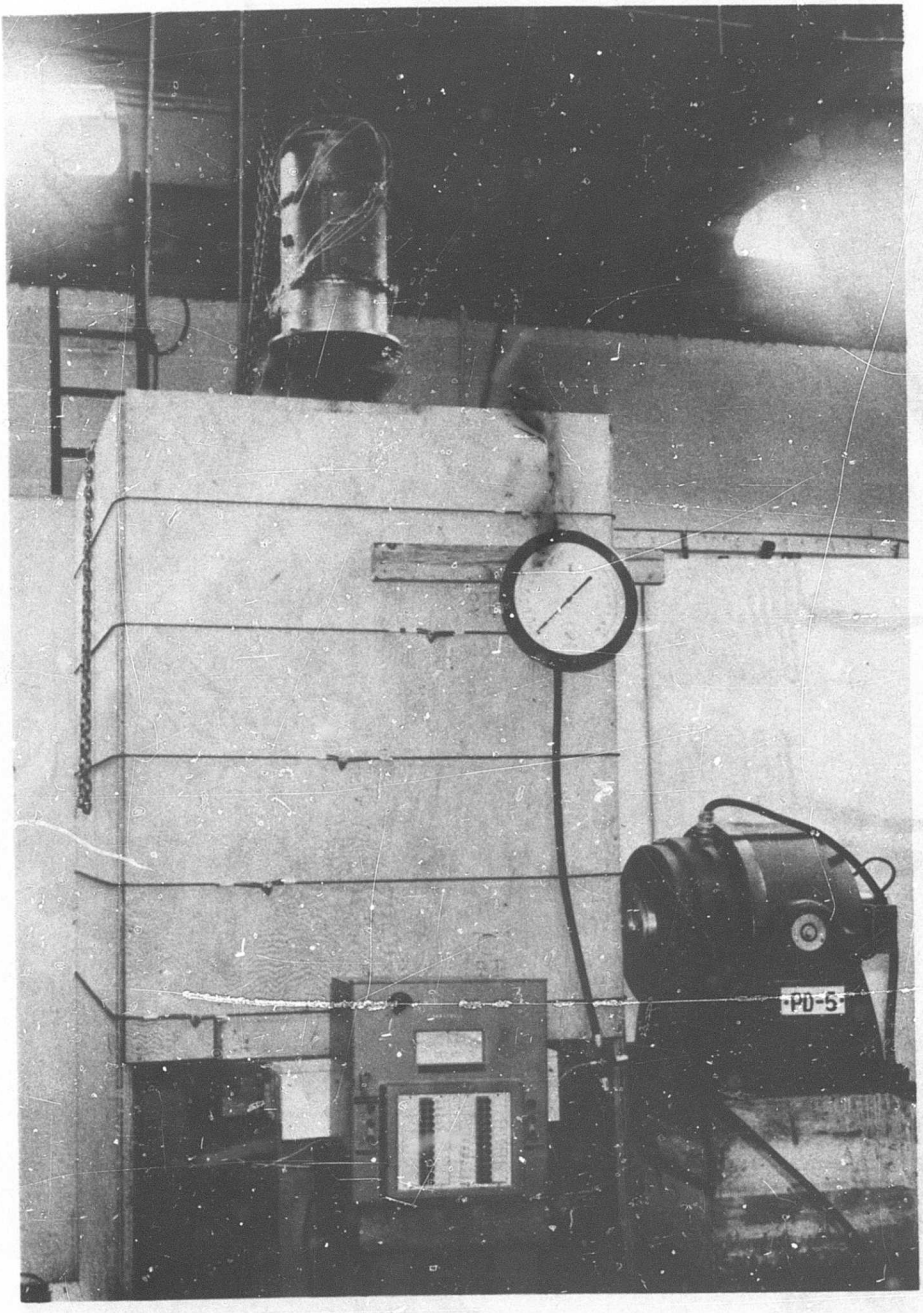

Figure 44. Pressure Vessel Test Rig Suspended Above Oven.

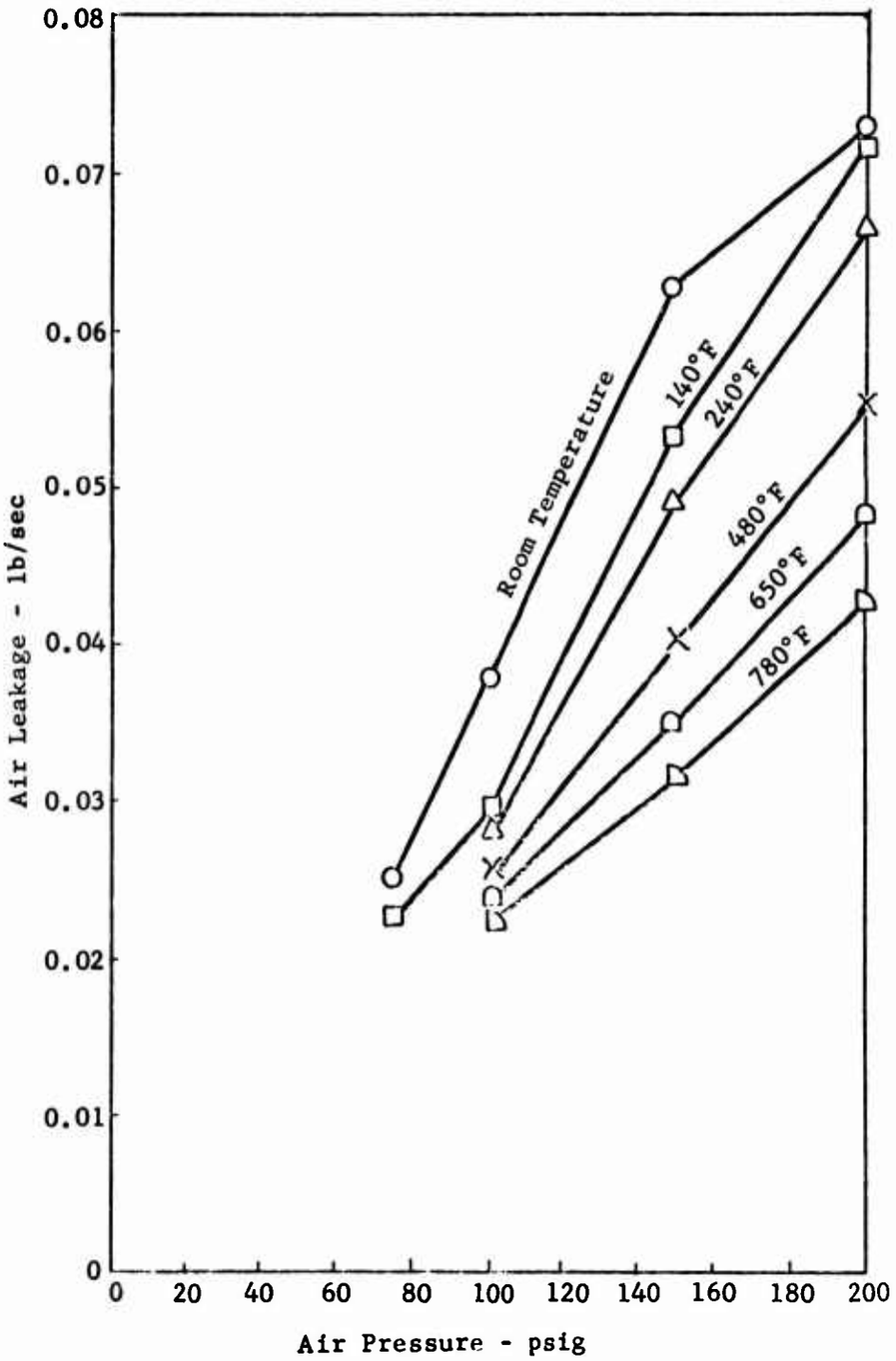

Figure 45. Split-Line Seals, Metal-to-Metal Flange Configuration Leakage Versus Air Pressure.

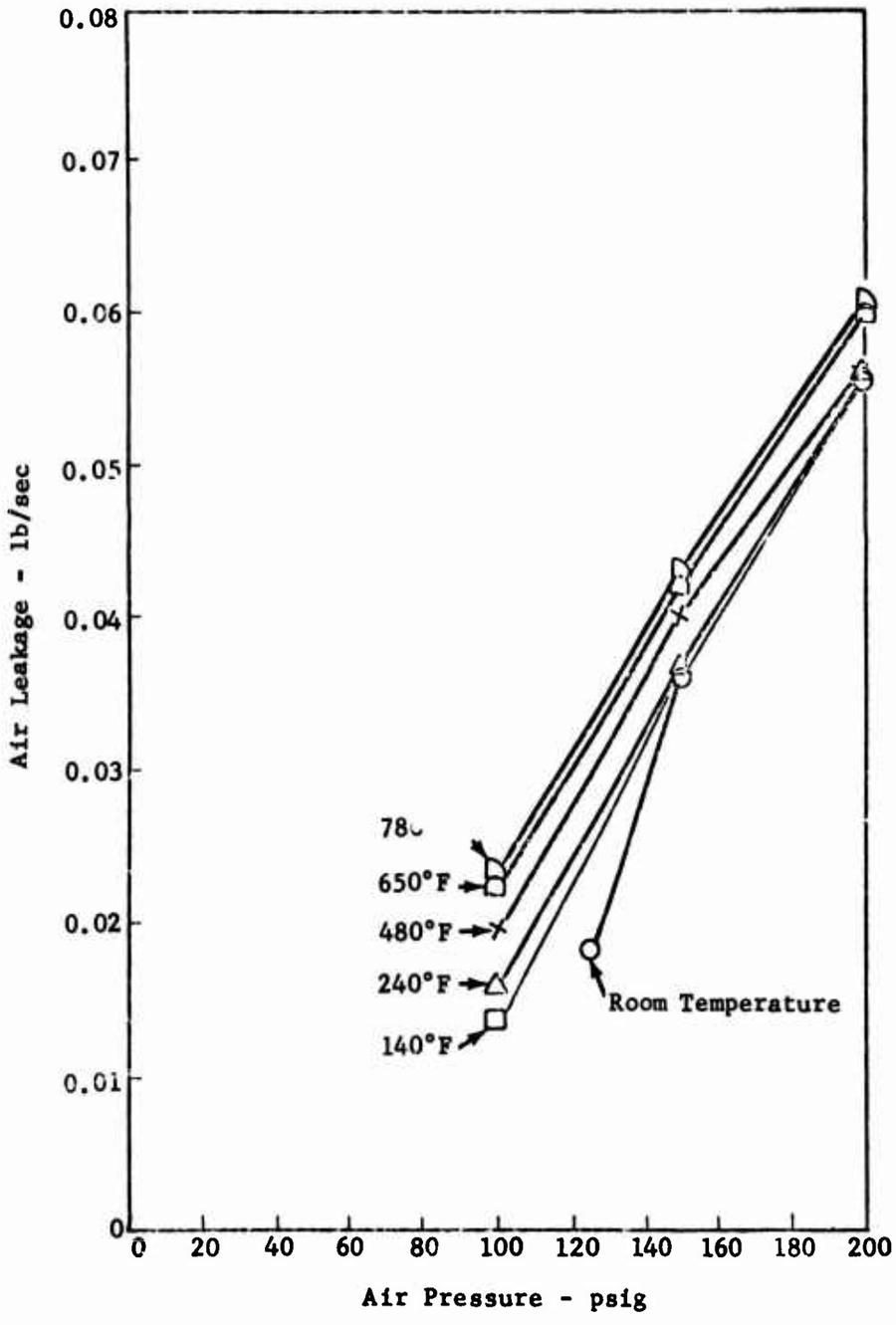

Figure 46. Split-Line Seals, Silver-Plated Metal O-Ring Configuration Leakage Versus Air Pressure.

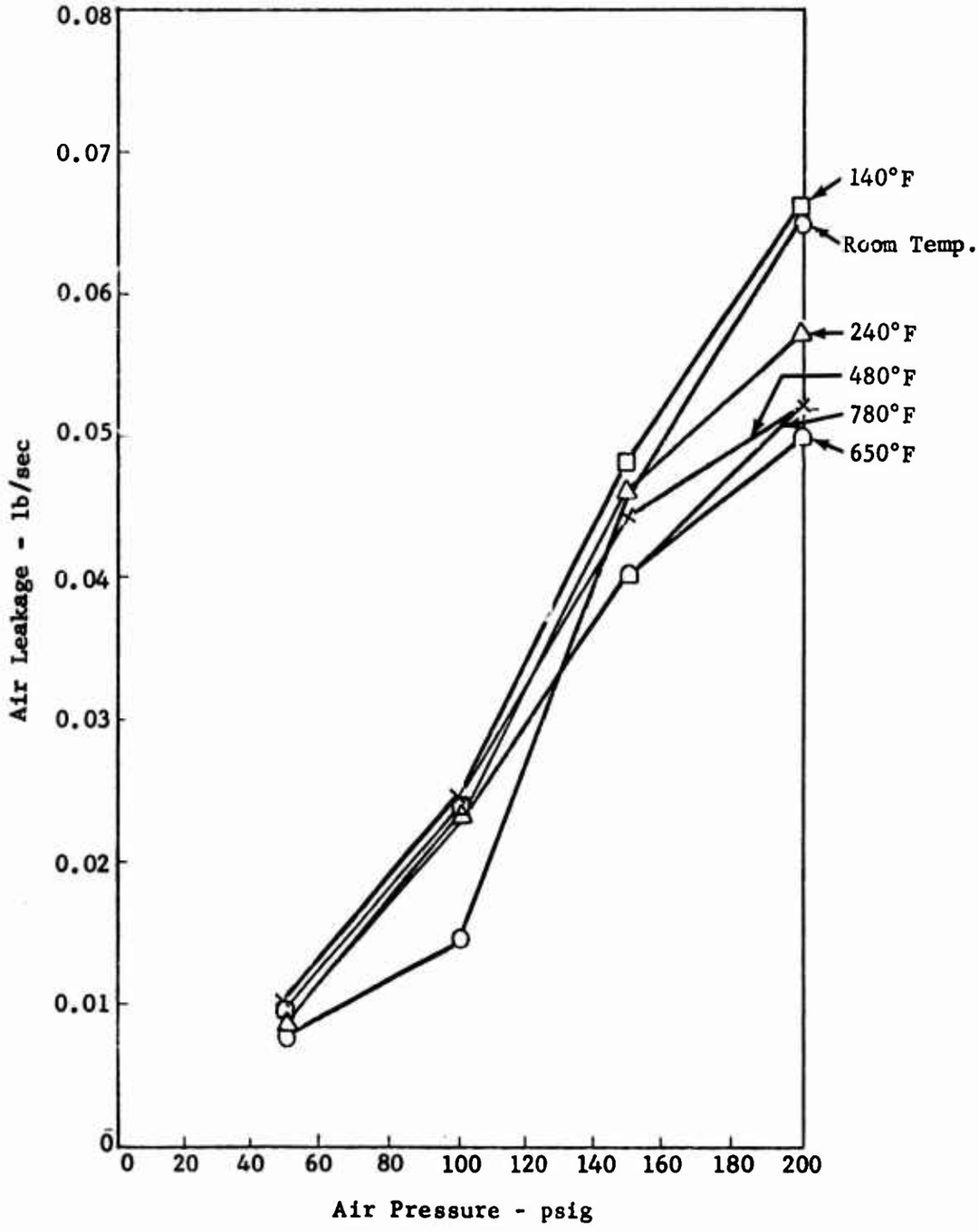

Figure 47. Split-Line Seals, Silver-Plated V-Seals, and Metal-Asbestos Braided Packing Configuration - Leakage Versus Air Pressure.

in leakage with increasing temperature, but the trend is reversed with the rate of leakage increasing with increasing temperature. The O-ring configuration displays a lower leakage at room temperature than the metal-to-metal flange configuration. However, leakage with the O-ring configuration was at a higher rate than the metal-to-metal configuration at the higher temperatures and pressures. This observation may be attributed to (1) increased deflection of the O-ring flange which has a lower stiffness than the original flange and/or (2) permanent deformation of the O-rings with an attendant loss of pinch.

The third build of the pressure vessel, incorporating silver-plated V-rings in the circular flanges and metal-asbestos braided packing in the straight flanges, displays the trend of decreasing leakage with increasing temperature similar to the metal-to-metal configuration. It also displays conditions similar to the O-ring configuration, where the change in leakage with increasing temperature is almost negligible and the leakage is lower at room temperature and higher at elevated temperature than the metal-to-metal configuration.

The vibration test results are shown in Figure 48. Pressure vessel total leakage is plotted versus internal air pressure for the three pressure vessel builds. Also shown are the temperature and vibratory conditions applied to the pressure vessel at the associated pressure condition. For the second build of the pressure vessel, incorporating metal O-ring and metal tubing seals, the leakage at the 50-psig condition was too low to measure, and the point is shown as an extrapolation of the curve down toward zero leakage for the 50-psig point. The curves display only minor variations in pressure vessel total leakage for the different configurations tested, with the metal-to-metal flanges resulting in the lowest leakage at the highest conditions of temperature, pressure, and vibration frequency. All configurations provided approximately the same leakage at the lower ranges of temperature, pressure, and vibration, with the metal O-ring exhibiting the lowest leakage at this condition.

In order to show the effect of vibration on leakage, Figures 49, 50, and 51 were plotted showing pressure vessel total leakage versus internal pressure for each build of the pressure vessel with and without vibratory excitation. Conditions of temperature and pressure are identical for each set of curves, and the temperature associated with each pressure level is shown. It is apparent from this series of curves that vibration had a negligible effect on the leakage rate for each configuration tested.

Plots of pressure vessel leakage versus simulated engine operating cycles are shown in Figure 52 for the three builds of the pressure vessel. No significant change in leakage occurred for any of the configurations throughout the 50-cycle test.

The effects of bolt spacing on flange leakage was evaluated on the first build of the pressure vessel test rig incorporating metal-to-metal flange sealing at all split-lines. The pressure vessel design provides for a bolt spacing of 0.80 inch between bolts in the circular flanges and 0.55 inch

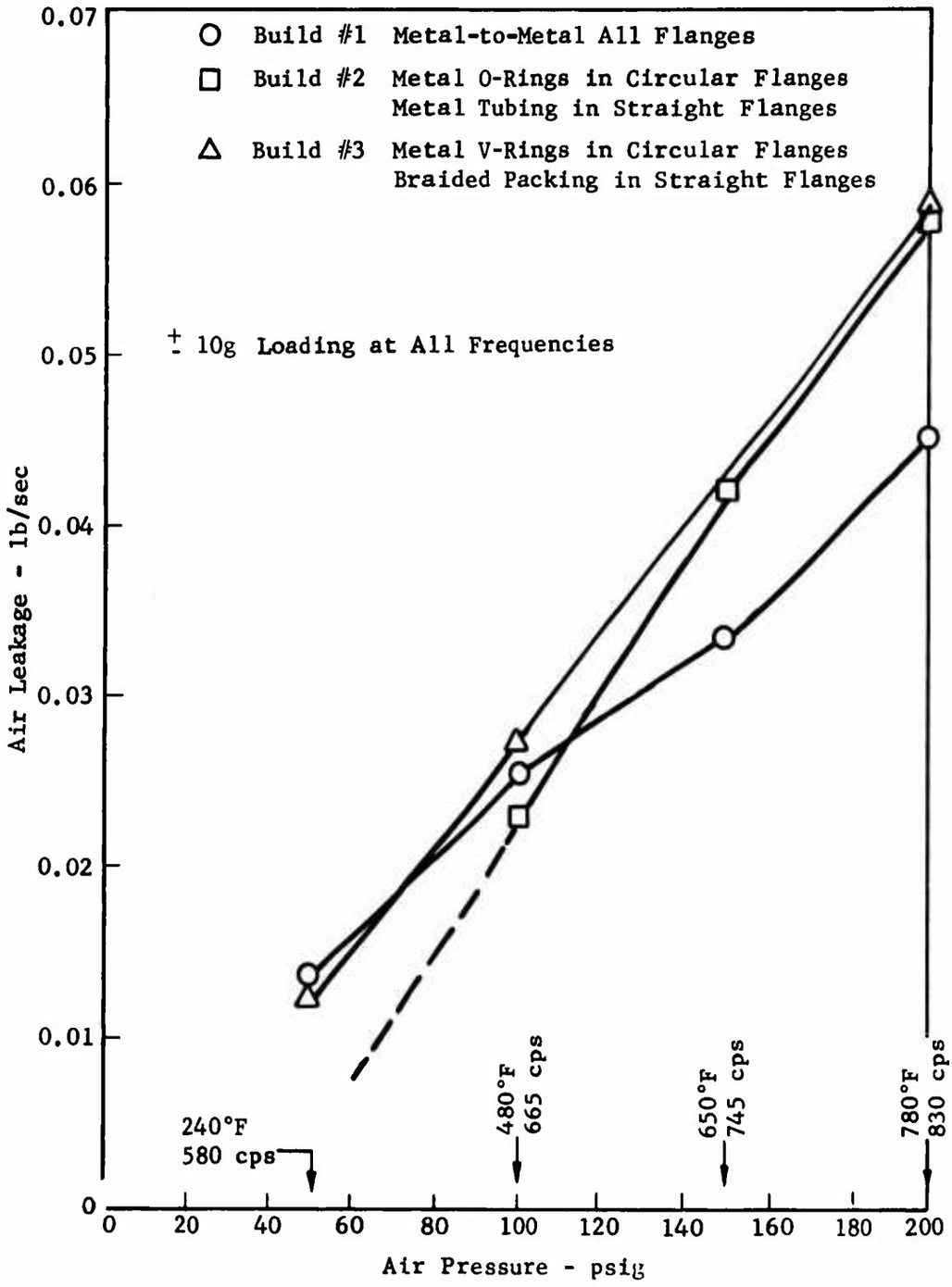

Figure 48. Split-Line Seals Air Leakage Versus Air Pressure for Three Rig Builds Under Temperature and Vibratory Conditions.

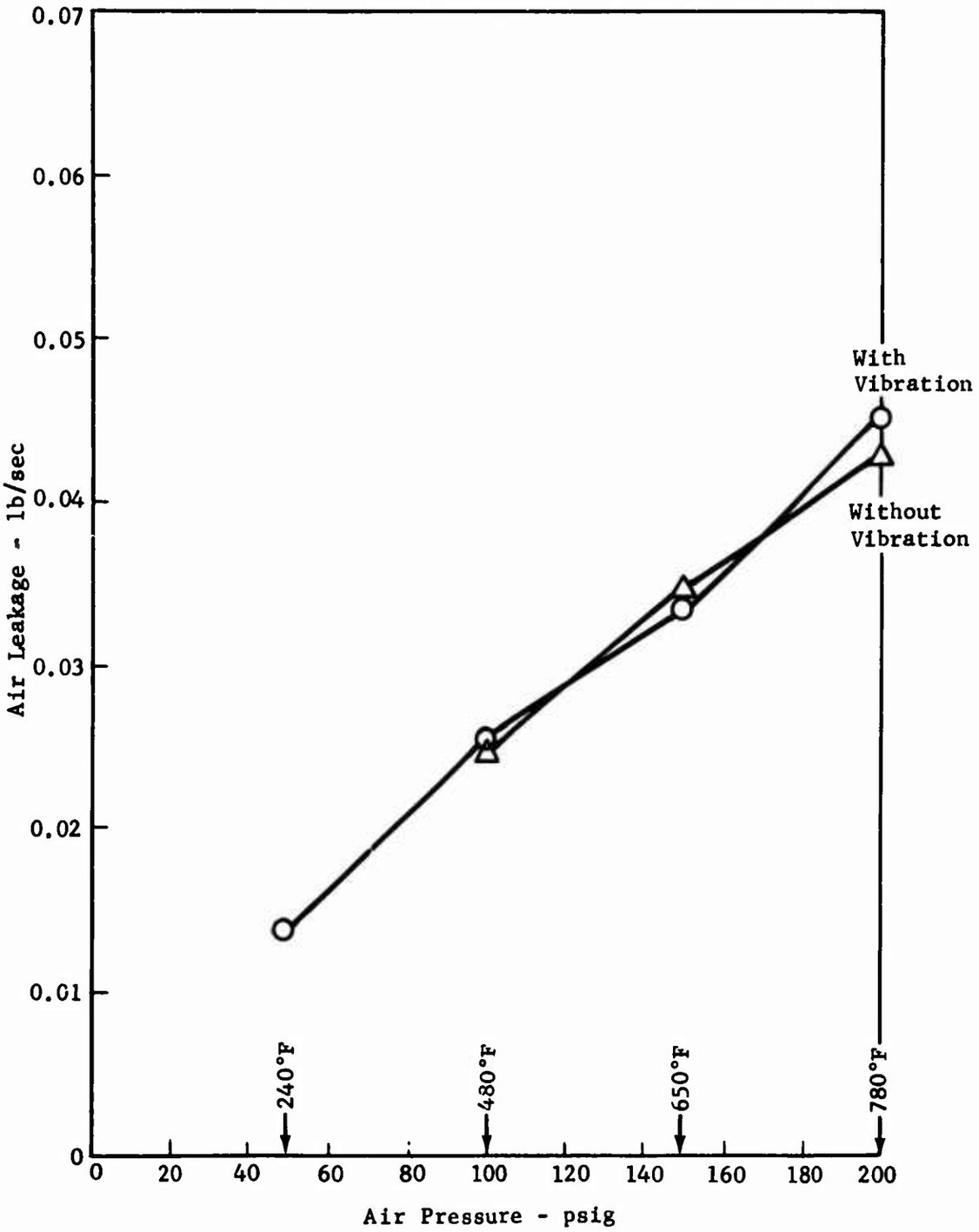

Figure 49. Split-Line Seals, Metal-to-Metal Flange Configuration - Effect of Vibration.

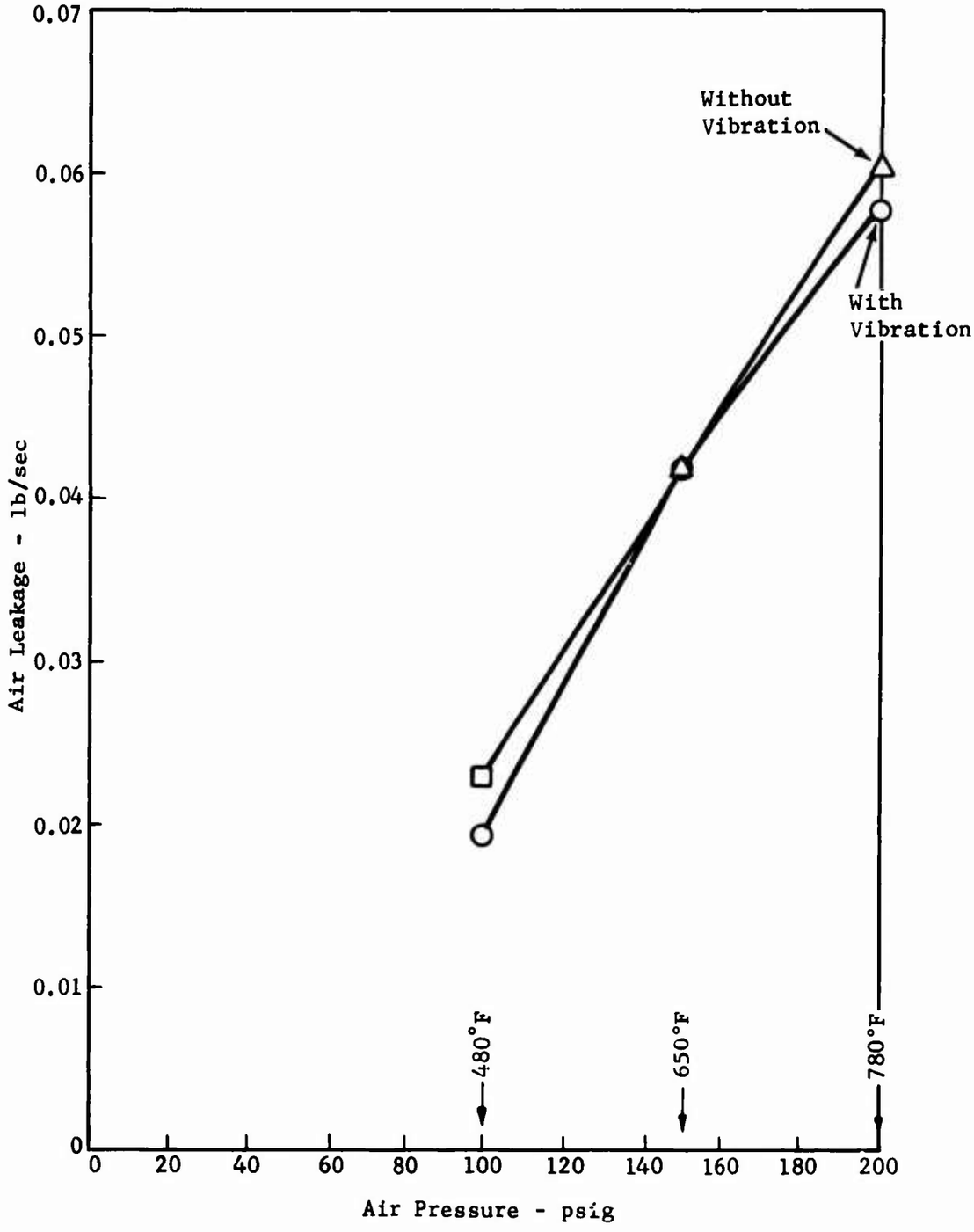

Figure 50. Split-Line Seals, Silver-Plated Metal O-Ring Configuration - Effect of Vibration.

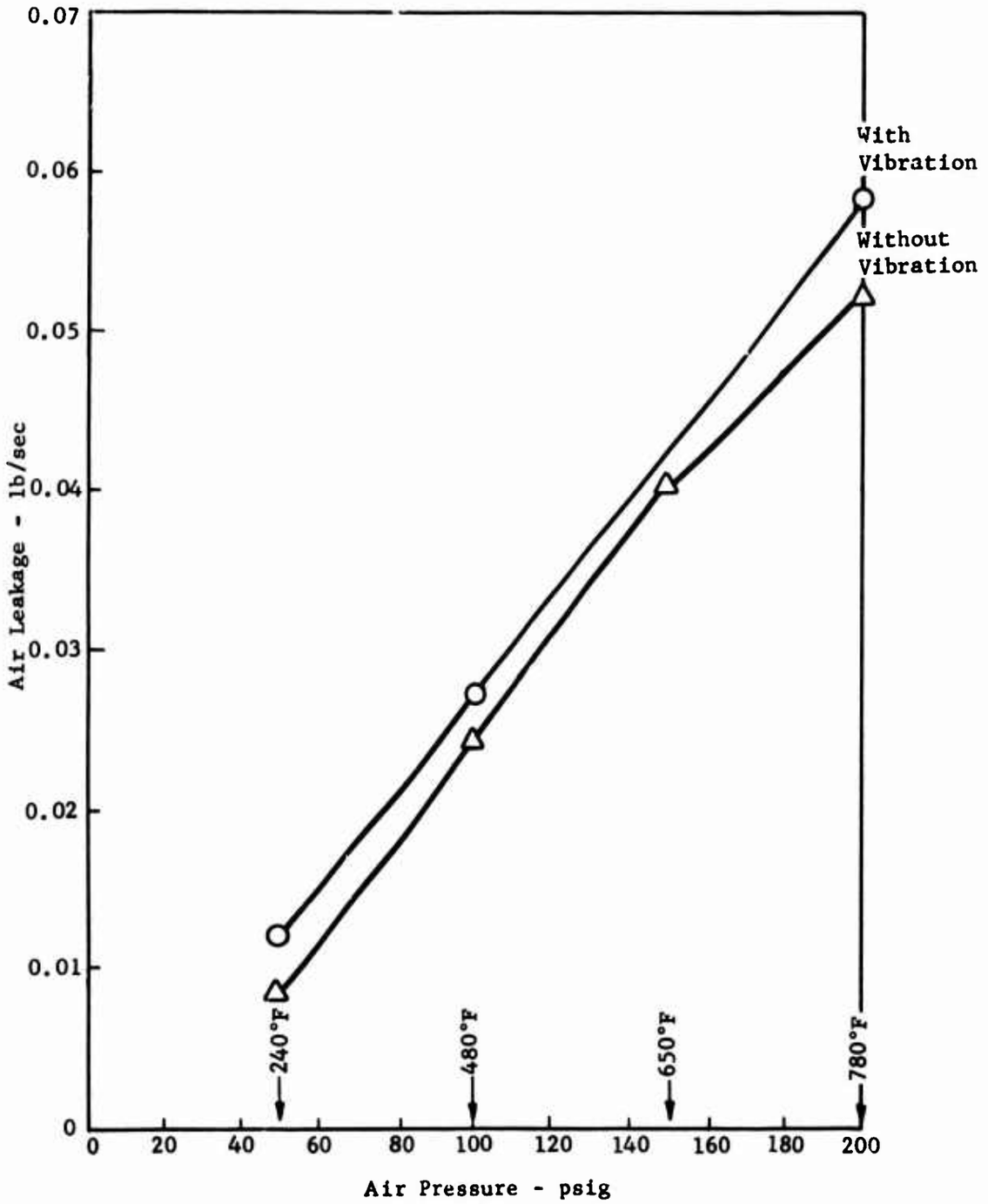

Figure 51. Split-Line Seals, Silver-Plated V-Seals, and Metal Asbestos Braided Packing Configuration - Effect of Vibration.

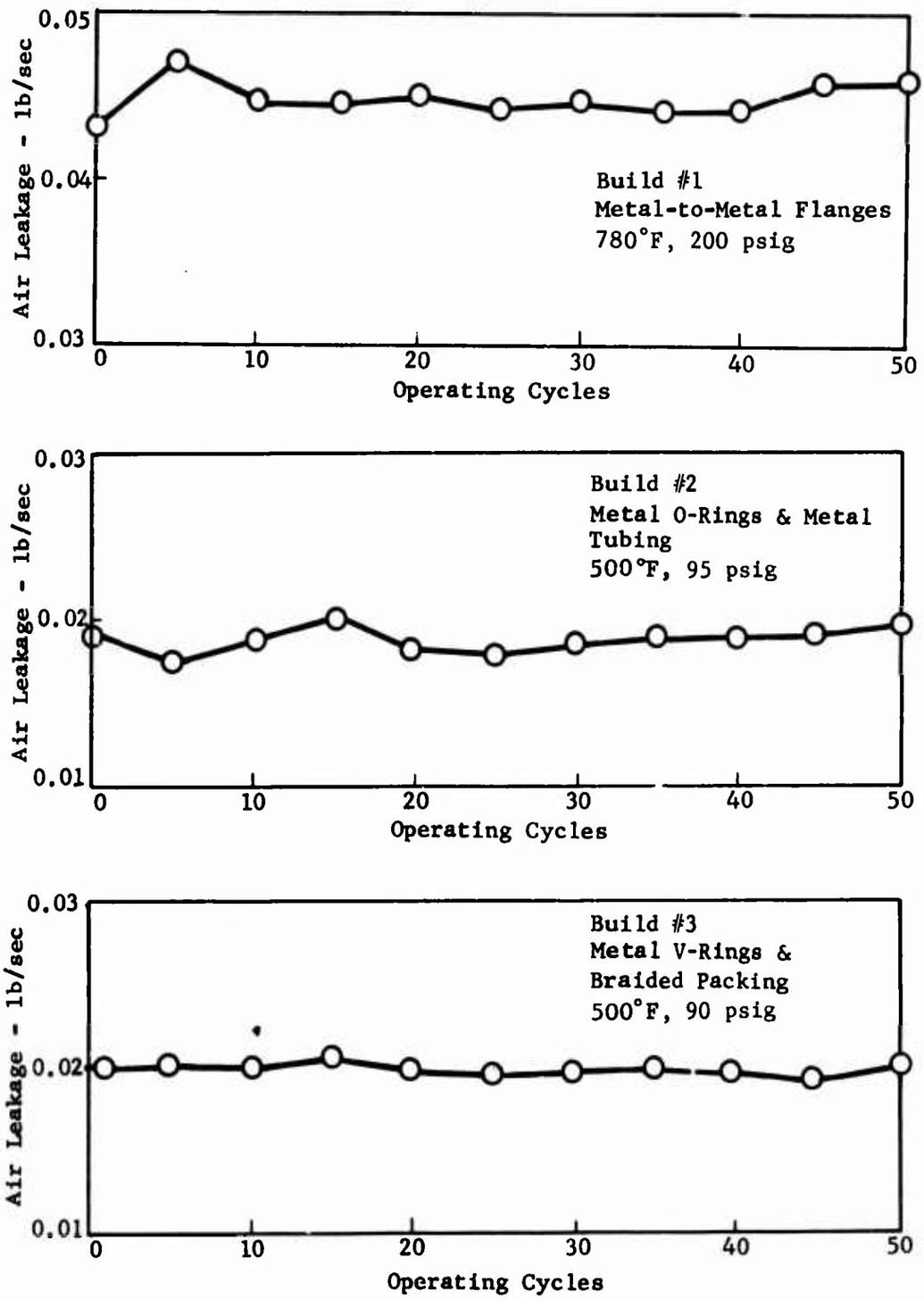

Figure 52. Split-Line Seals Leakage Versus Operating Cycles.

between bolts in the straight flanges. To evaluate the effects of bolt spacing, the distance between bolts was doubled by removing every other bolt on both circular flanges and both straight flanges, allowing only 50 percent of the bolts to remain to provide the flange clamping load. A pressure test at room temperature was conducted, and the total pressure vessel leakage was measured. The results of the test are shown in Figure 53. The test was discontinued at the 80-psig test point because the extremely high leakage encountered indicated possible severe deflection of the flanges. The importance of the bolt spacing on flange sealing characteristics is evident.

The results of room temperature tests conducted to determine the distribution of leakage in the pressure vessel test rig as affected by the various flange sealing configurations are summarized in Table XX for pressure vessel internal pressures of 150 and 200 psig. The table expresses leakage in terms of percentage of pressure vessel total leakage for each split-line location and associated sealing configuration. Flange-end leakage occurs at the four junctions where the ends of the straight flanges in the center section intersect the circular flanges. Circular flange leakage is the sum of the two circular flanges, and straight flange leakage is the sum of the two straight flanges. As indicated in the table, the flange-end leakage in all cases is a significant part of the total leakage. The significance of this leakage is emphasized by considering that in a pressure vessel containing a total of 102 inches of flange length (82 inches of circular flange and 20 inches of straight flange), the leakage from four localized points in these flanges represents in most cases 50 percent or more of the total split-line leakage. In the case of pressure vessel build number 2, a close fit-up of the tubing installed in the straight flanges (tube length was within 0.002 inch of flange length) appears to have created sufficient blockage at the flange ends to substantially reduce leakage at these locations.

The pressure vessel flanges before and after testing are shown in Figures 54, 55, and 56, which show the end-section circular flanges, the center-section circular flanges at the horizontal split-line, and the center section straight flanges respectively. The pretest condition shows the metal-to-metal flange configuration as received and prior to any testing or subsequent reworks. The posttest condition shows the flanges after completion of all pressure vessel testing which included the reworks to incorporate the grooves for subsequent sealing configurations in the faces of the flanges as shown in the photographs. Other than the machining of the grooves, no refinishing of the flange faces occurred between pressure vessel builds. Prior to reassembly of the pressure vessel, the flange faces were cleaned with degreasing solvents only. The flange faces were generally in excellent condition with no apparent changes in surface finish except for minor indications of fretting, which was most evident around some of the bolt holes in the straight flanges. Also visible in the photograph of the straight flanges are surface stains in the groove and its mating flange from the braided packing sealing configuration.

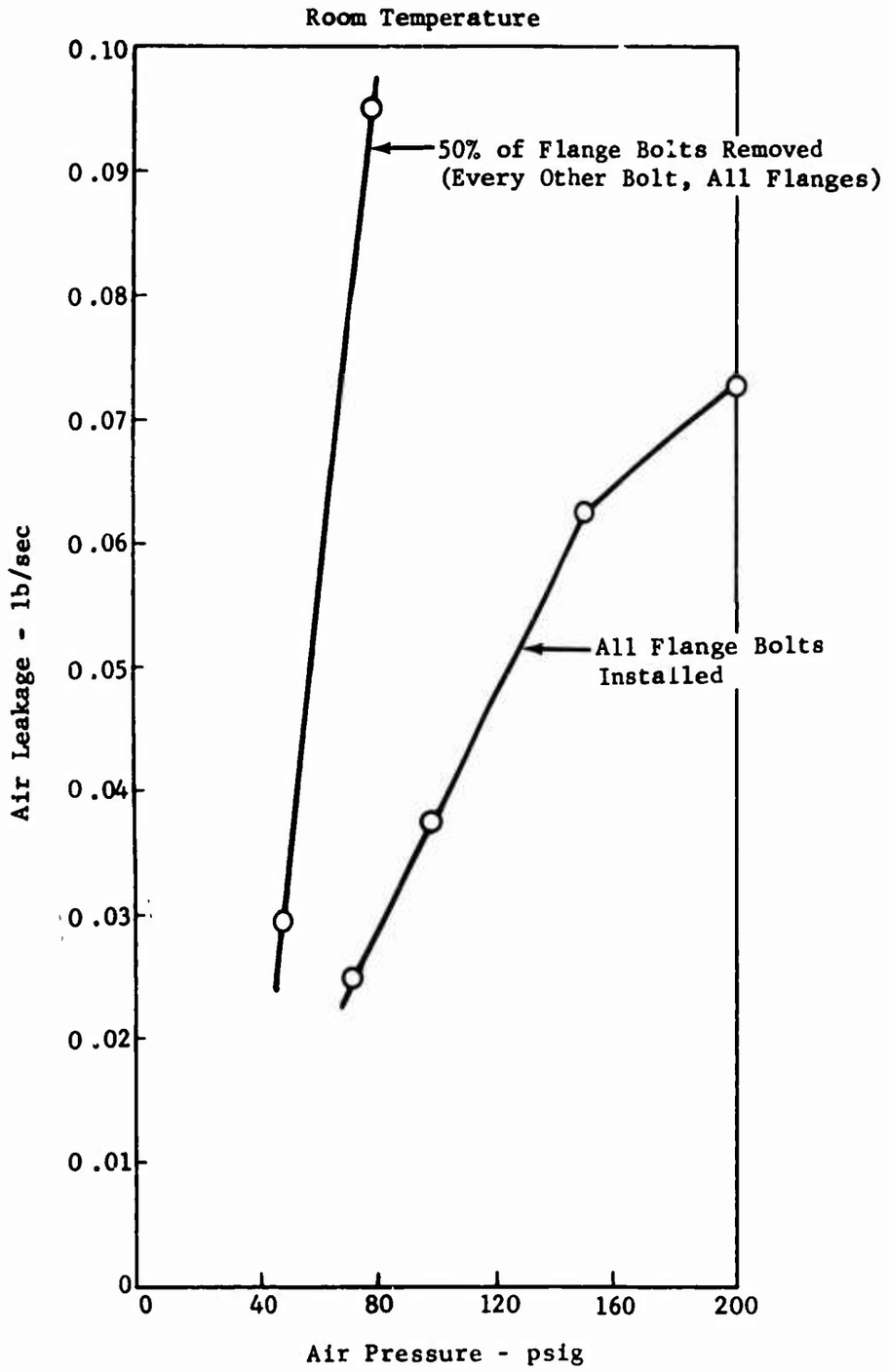

Figure 53. Split-Line Seals, Metal-to-Metal Flange Configuration - Effects of Bolt Spacing.

TABLE XX. CASE SPLIT-LINE SEALS LEAKAGE DISTRIBUTION

Sealing Configurations	Circular Flanges		Straight Flanges		Flange Ends	
	150 psig	200 psig	150 psig	200 psig	150 psig	200 psig
Pressure Vessel Build #1						
Leakage - % of Total Leakage	15	35	nil	8	85	57
Seal Type	Metal-to-Metal		Metal-to-Metal		-	-
Pressure Vessel Build #2						
Leakage - % of Total Leakage	64	76	nil	nil	36	24
Seal Type	Metal O-Ring		Metal Tube		-	-
Pressure Vessel Build #3						
Leakage - % of Total Leakage	23	51	nil	nil	77	49
Seal Type	Metal V-Ring		Braided Packing		-	-

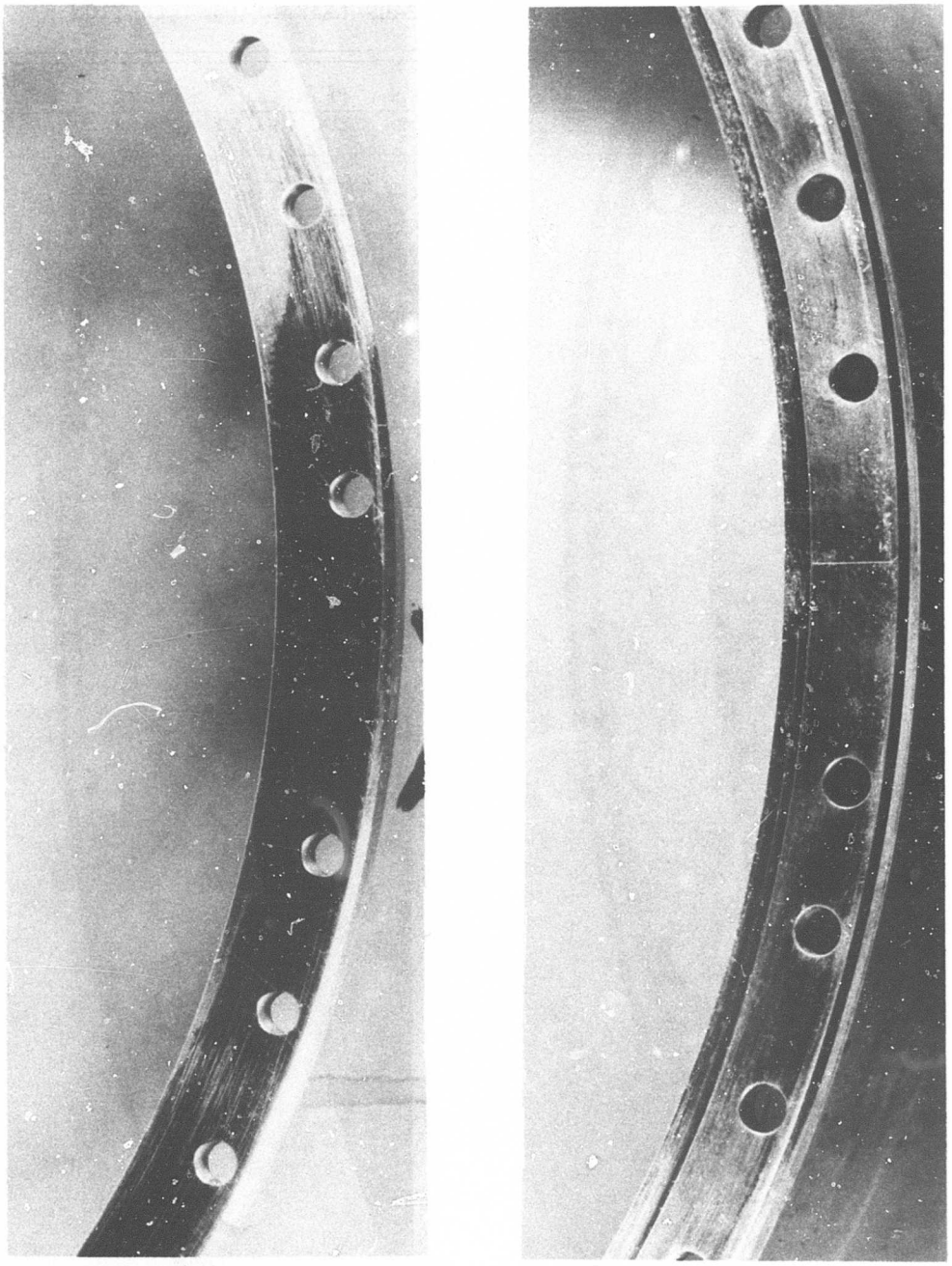

Before

After

Figure 54. Pressure Vessel Test Rig End-Section Circular Flanges Before and After Testing.

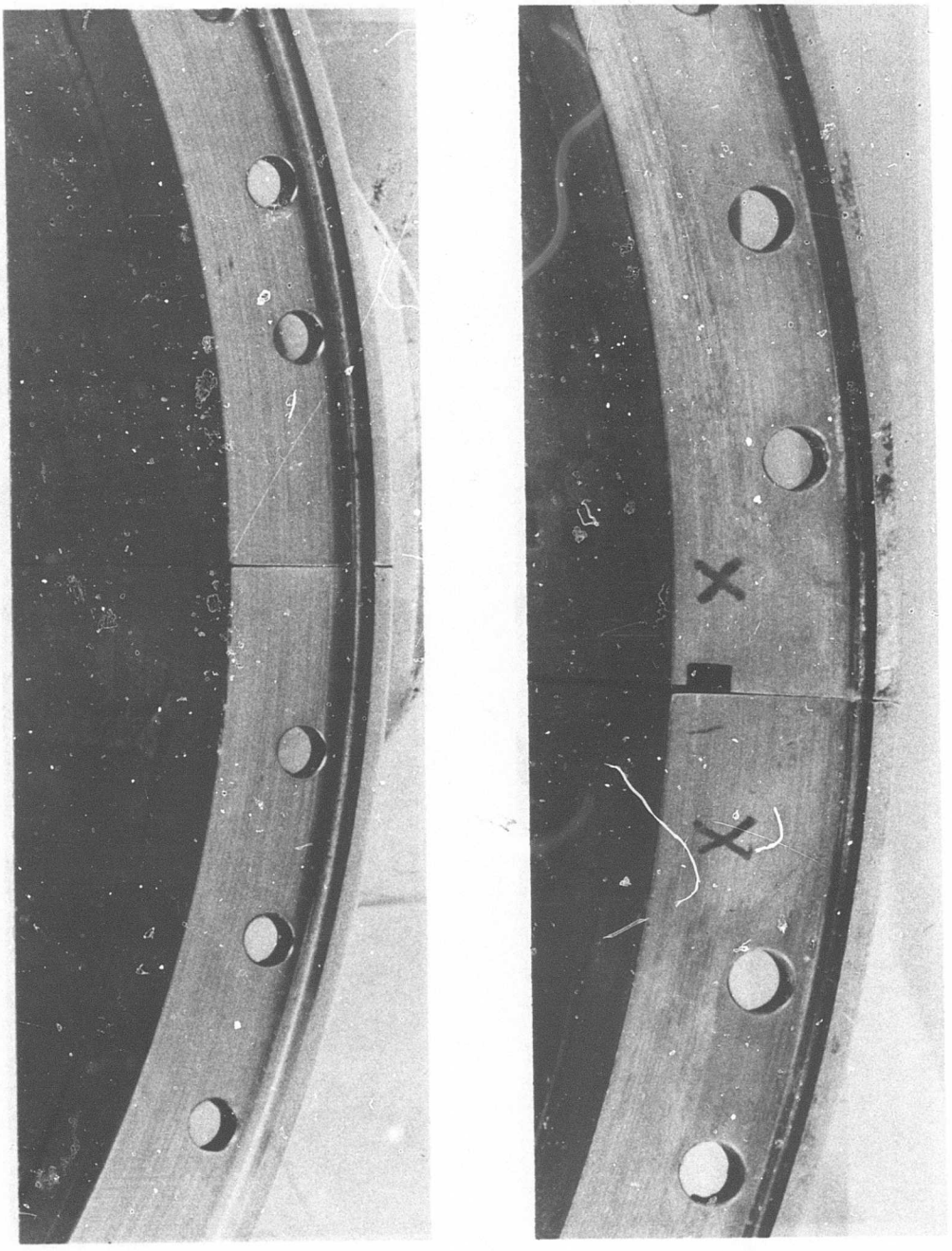

Before

After

Figure 55. Pressure Vessel Test Rig Center-Section Circular Flanges Before and After Testing.

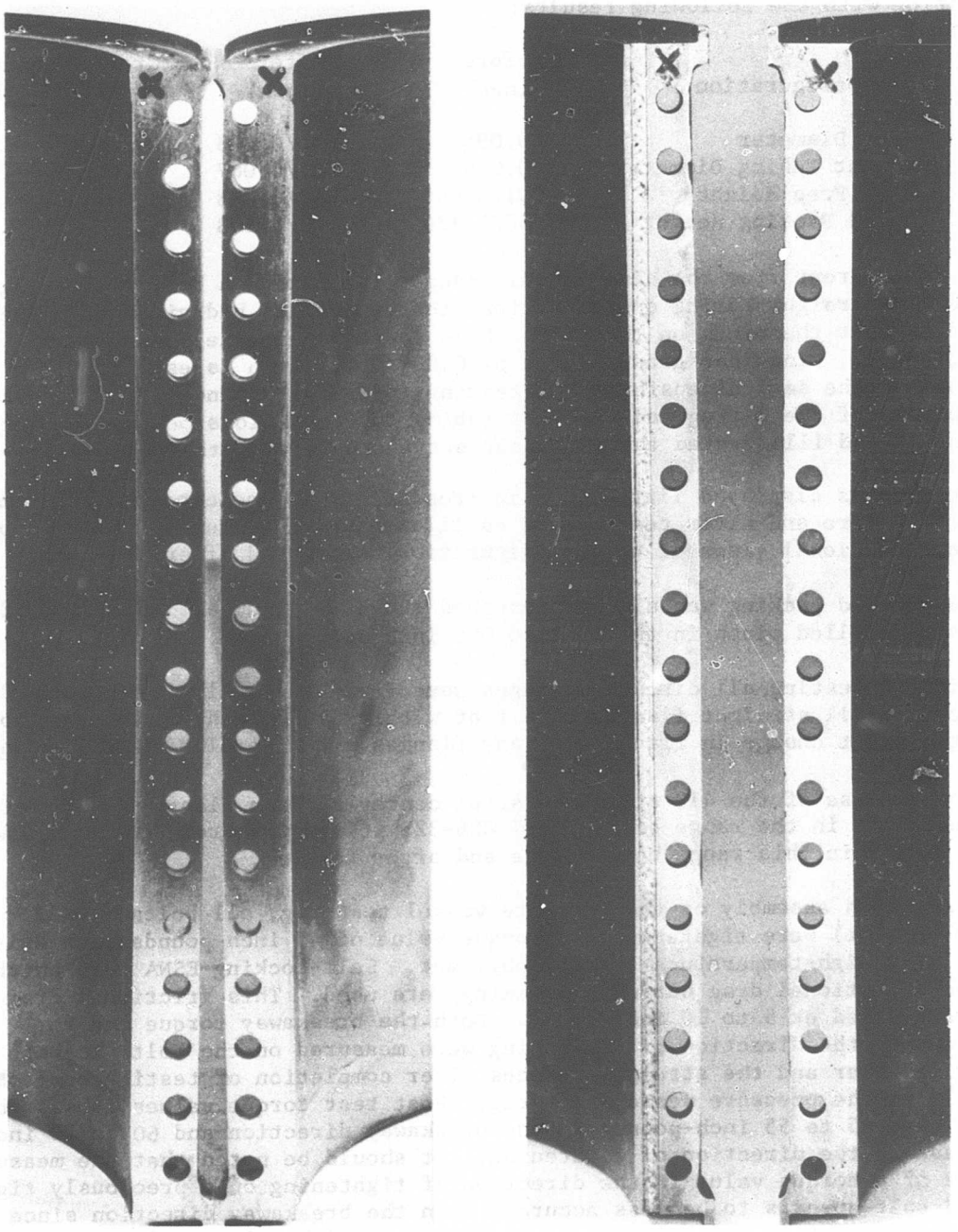

Before

After

Figure 56. Pressure Vessel Test Rig Center-Section Straight Flanges Before and After Testing.

The various flange seal configurations were measured before and after testing with the following results:

Seal Configuration	Before (inch)	After (inch)	Groove Depth (inch)
O-Ring Diameter	0.095	0.070/0.068	0.069/0.065
Straight Tubing Diameter	0.096	0.068/0.067	0.069/0.065
V-Ring Free Height	0.091/0.090	0.090/0.088	0.078/0.076
Braided Packing Height	0.130/0.120	0.112/0.108	0.094/0.090

It is apparent from the dimensional changes indicated on both the O-ring and the straight tubing configurations that the seals had yielded to the extent that the pinch on the seals while installed in the flanges was negligible, since the groove depth of 0.069/0.065 inch is essentially equal to the seal dimension after testing. Figures 57 and 58 show cross sections of the O-ring and straight tubing configurations before and after testing and illustrated the permanent set encountered with these seals.

The V-rings displayed little loss in free height as indicated by the dimensions before and after testing and as illustrated in Figure 59 which shows cross-sectional views of this configuration before and after testing.

The braided packing was slightly crushed but still indicated 0.014/0.022 inch installed pinch in the 0.094/0.090 inch deep groove.

Prior to testing, all circular flanges were found to be flat within 0.003 inch and all straight flanges were flat within 0.002 inch. There was no significant change in flatness of any flanges after completion of testing.

The hardness of the 410 stainless steel center-section flanges was specified to be in the range of Rockwell C26-32; it was measured and determined to be within this range both before and after testing.

During each assembly of the pressure vessel test rig, all bolts (10-32 thread size) were tightened to a torque value of 45 inch-pounds with Fel-Pro C5-A high-temperature thread lubricant. Self-locking ESNA nuts, which have a frctional drag during tightening, were used. This frictional drag was measured at 5 to 10 inch-pound. Both the breakaway torque and the torque in the direction of tightening were measured on the bolts in both the circular and the straight flanges after completion of testing on each build of the pressure vessel test rig. Post test torque values consistently measured 45 to 55 inch-pounds in the breakaway direction and 60 to 70 inch-pounds in the direction of tightening. It should be noted that the measurement of a torque value in the direction of tightening on a preciously tightened bolt appears to be less accurate than the breakaway direction since the first movement of the bolt in the direction of tightening is less apparent than the first movement noted in the directions of loosening or breaking away. However, there appeared to be no loss of torque as a result of testing, and the increase in torque that was noted was to be expected due to loss of the thread lubricant at elevated temperatures. In all cases the bolts were dry after testing.

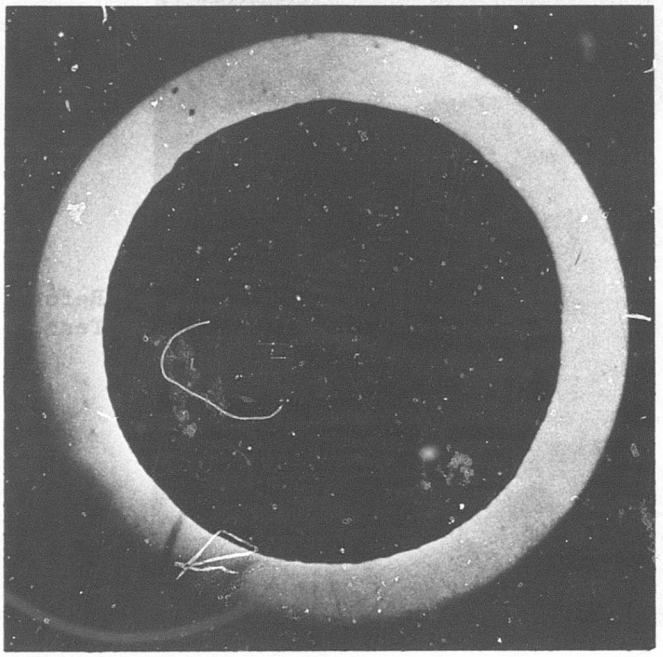

Before
Test

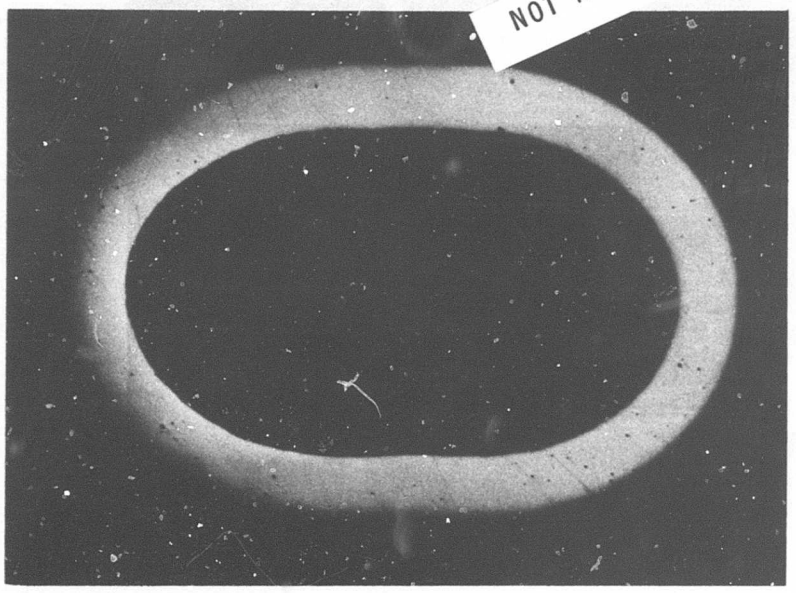

After
Test

Figure 57. Split-Line Seals - Cross-Sections of Metal O-Rings (Silver-Plated Inconel-X).

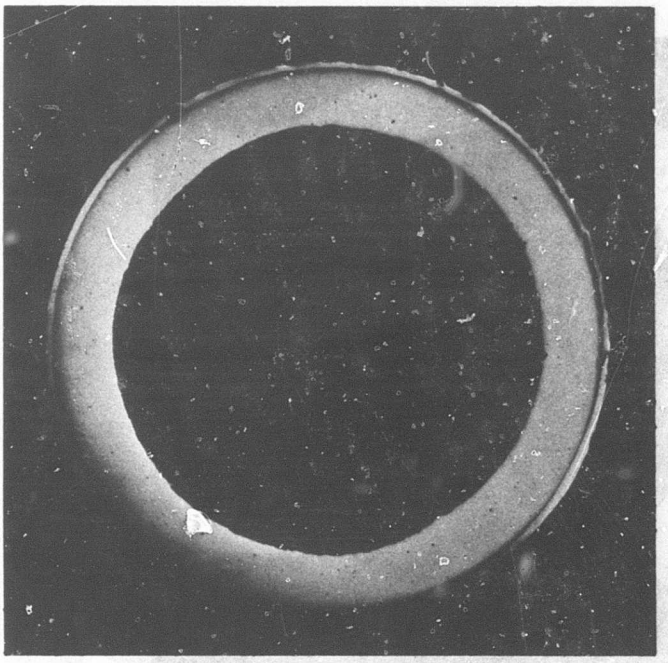

Before Test

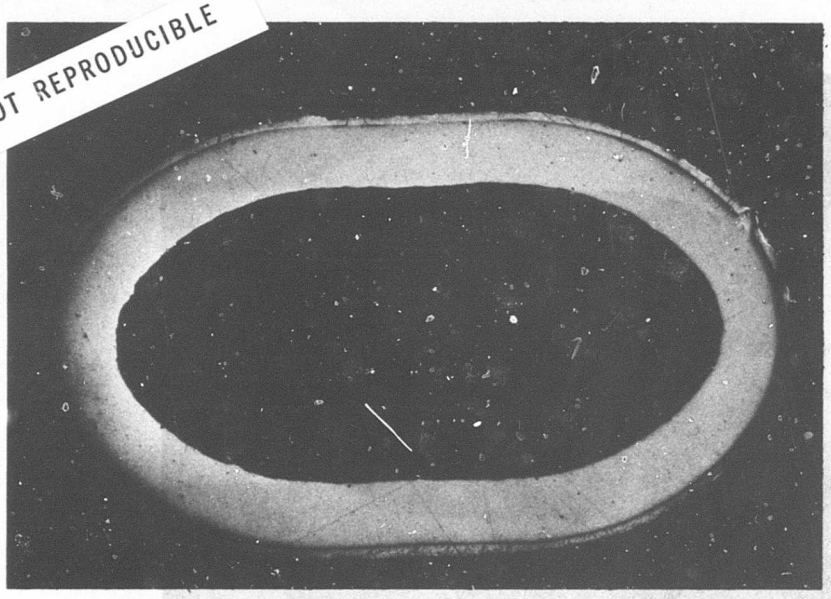

After Test

Figure 58. Split-Line Seals - Cross-Sections of Straight Tubing (Silver-Plated Inconel-X).

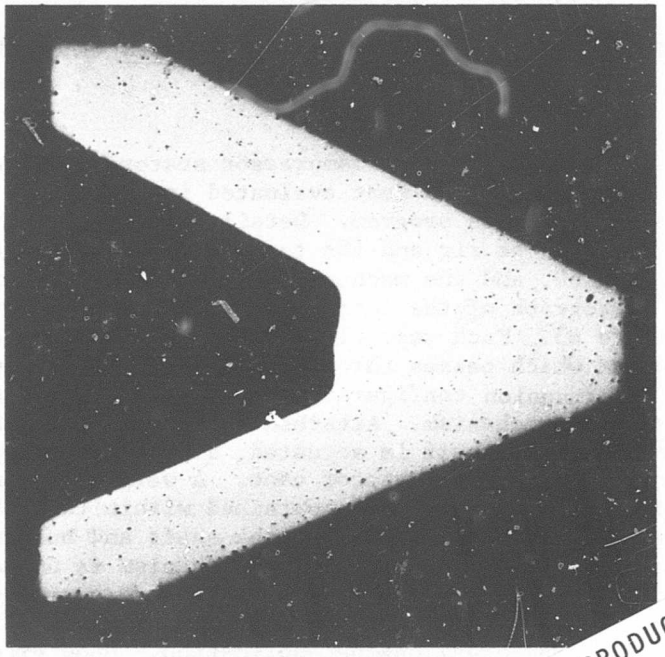

Before Test

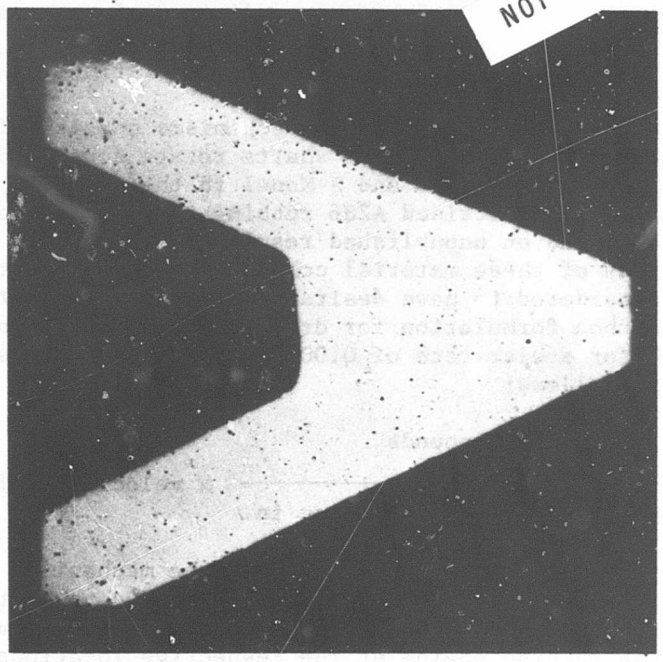

After Test

Figure 59. Split-Line Seals - Cross-Sections of Metal V-Rings (Silver-Plated Inconel-X).

COMPRESSOR AND TURBINE VARIABLE-GEOMETRY MECHANISM SEALS (TASK IV)

Test Rigs

The leakage characteristics of typical compressor stator and power turbine nozzle variable-geometry mechanisms were evaluated in test rigs that were designed and fabricated for this program. Detail drawings of both the compressor variable-geometry test rig and the turbine variable-geometry test rig are shown in Figure 60, and the mechanisms are shown in detail in Figures 61 and 62. A photograph of the test rigs and associated detail hardware is shown in Figure 63. Each test rig consists essentially of a shaft and bushing arrangement which passes through the wall of a pressure-tight housing simulating the trunnion configuration of either a compressor or a turbine variable-geometry mechanism. Attached to one end of each shaft is a lever arm through which the shaft is actuated, simulating the positioning of a variable compressor or turbine stator vane. A weight is cantilevered at the opposite end of each shaft and is contained within the test rig housing. This weight, which is supported by the shaft and bushing arrangement, simulates the gas load to which the vane mechanism is normally subjected. The test rig housing is pressurized to simulate engine pressures, and leakage through the trunnion mechanism is representative of leakage which may be expected in an actual engine application. Upon externally applying heat to the test rig housings and providing controlled actuation of the trunnion mechanisms, the combined engine conditions of temperature, pressure, gas loading, and mechanical actuation as they apply to the compressor and turbine variable-geometry trunnion configurations are simulated.

The shafts in each of the variable-geometry mechanisms consist of nitrided A286 material. The bushings in which the shafts rotate consist of Rulon-A material in the compressor mechanism and S-Monel in the turbine mechanism. The material combinations of nitrided A286 rubbing against S-Monel and Rulon-A were selected based on unpublished results of wear tests which indicated the superiority of these material combinations compared to several other combinations considered to have desirable wear characteristics. Rulon-A is a fluorocarbon formulation for dry bearing applications having a PV value of 20,000 for a wear rate of 0.005 inch per 1000 hours. The PV value is expressed as follows:

$$PV = \frac{\text{load in pounds}}{\text{projected bearing area in sq in.}} \times \text{velocity in ft/min}$$

The weights simulating aerodynamic gas loading of the mechanisms were 22 pounds for the compressor mechanism and 10 pounds for the power turbine mechanism. Both loads are typical of the aerodynamic loads encountered in an actual small gas turbine engine at the respective locations. The load applied to the compressor mechanism is unusually severe compared to those encountered in conventional compressor designs since the loading is representative of the highly loaded supersonic compressor configuration of USAAVLABS Contract DA 44-177-AMC-392(T).

BLANK PAGE

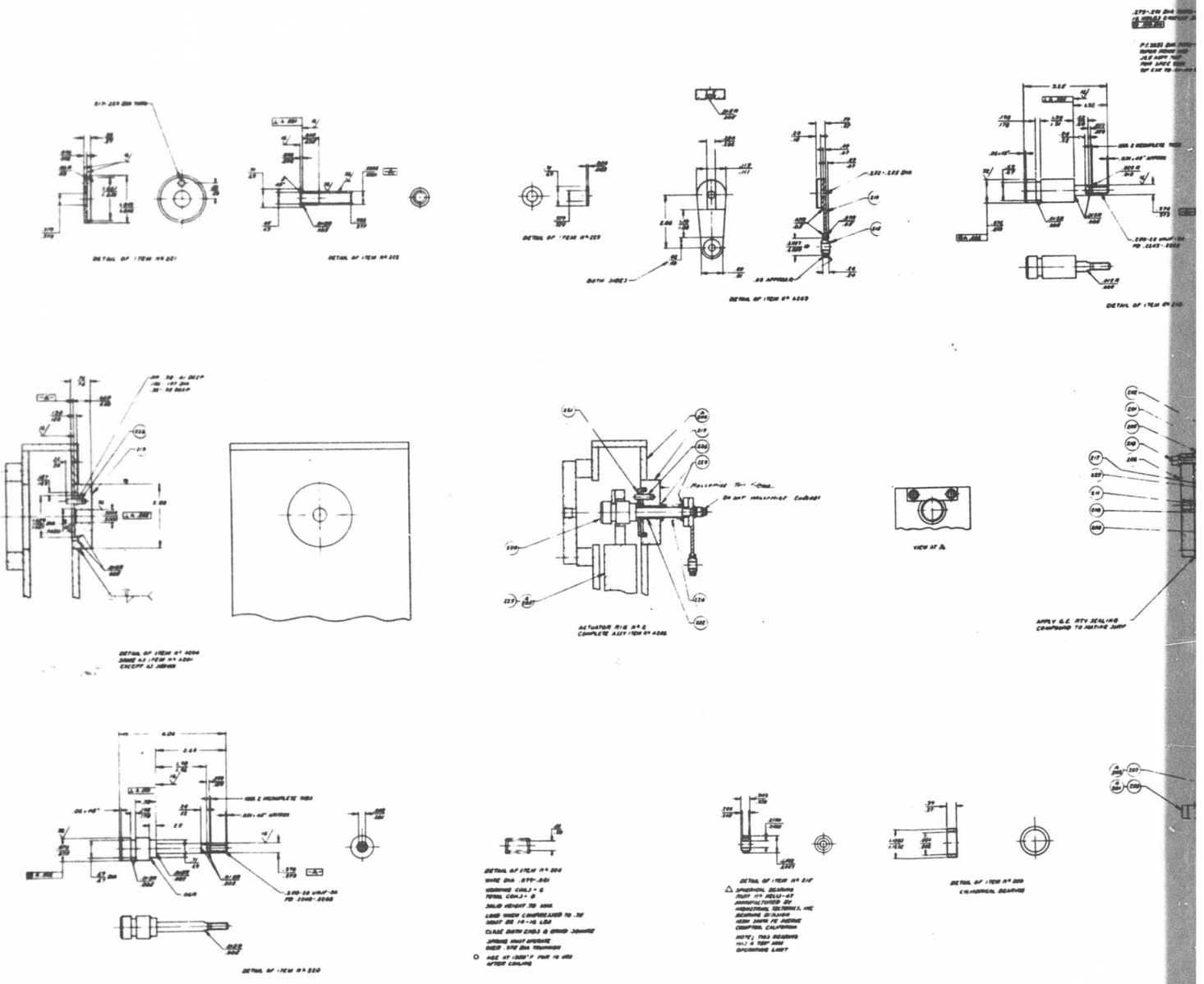

Figure 60. Compressor and Turbine Variable-Geometry Trunnion Test Rigs.

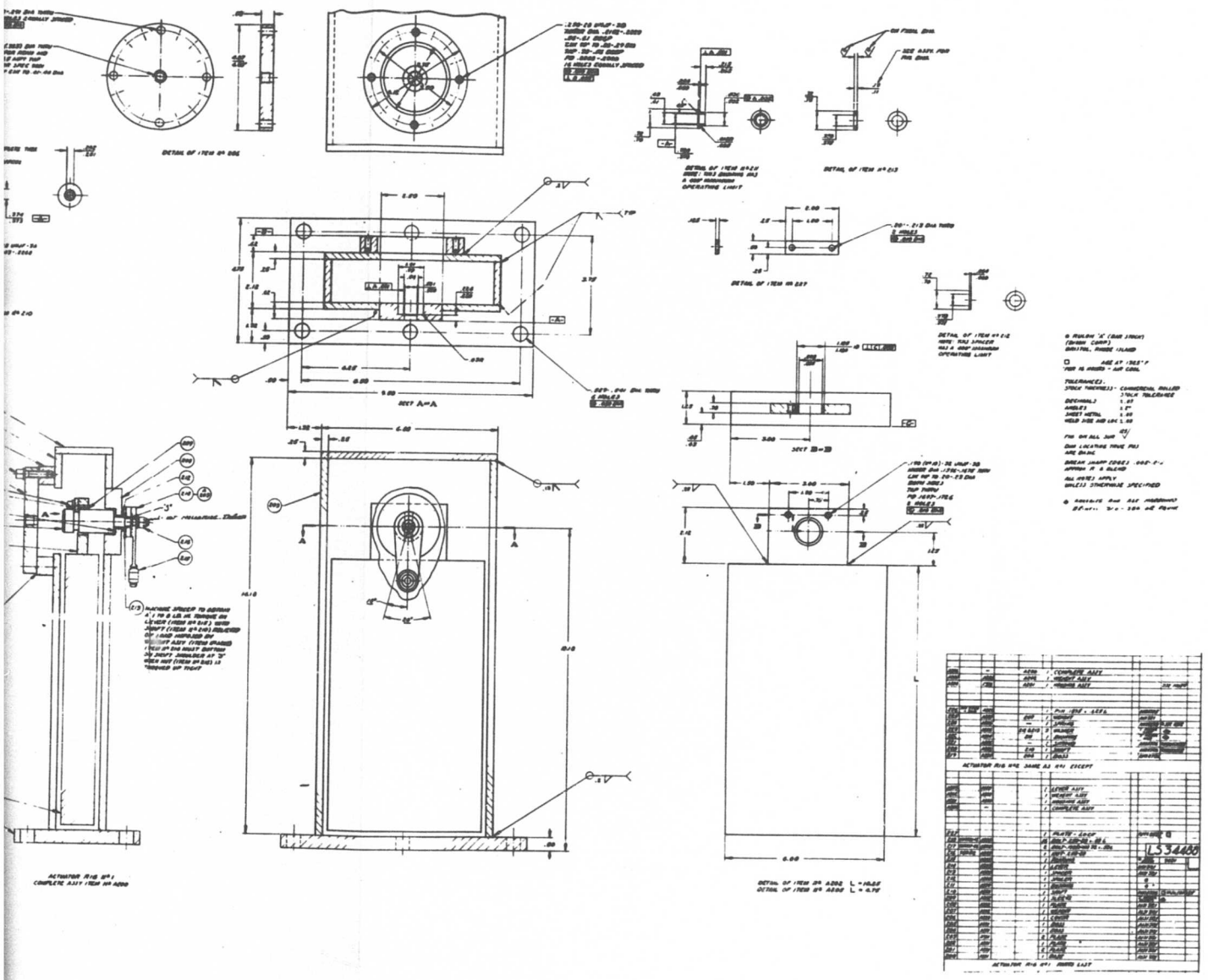

DETAIL OF ITEM 4A 006

DETAIL OF ITEM 4A 013

SECT A-A

SECT B-B

DETAIL OF ITEM 4A 2A2 L = HEAT
DETAIL OF ITEM 4A A206 L = 0.75

ACTUATOR RIG 4A 1
COMPLETE ASSY ITEM NO A200

ACTUATOR RIG 4A2 SAME AS 4A1 EXCEPT

1534486

BLANK PAGE

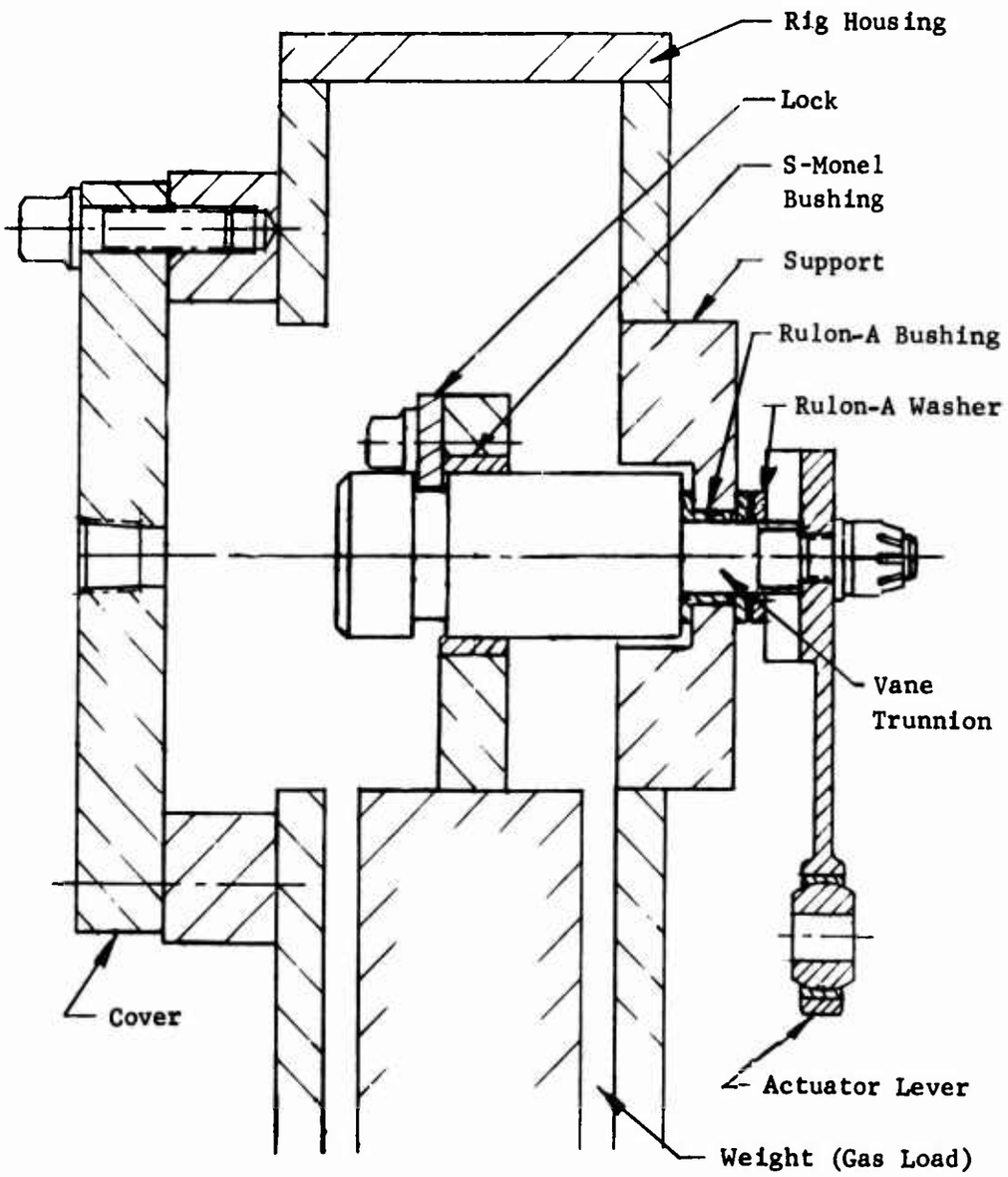

Figure 61. Compressor Variable-Geometry Mechanism.

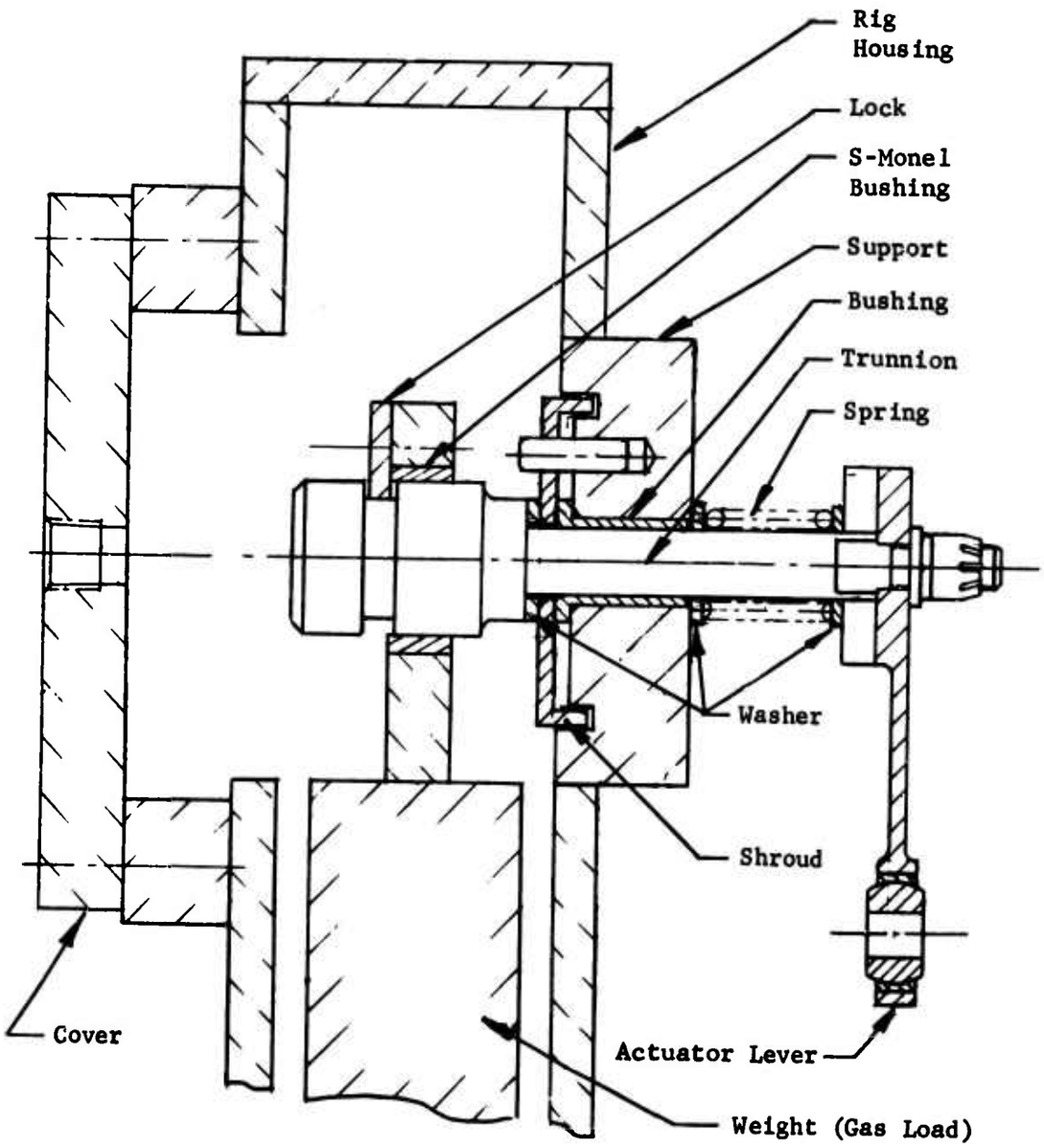

Figure 62. Turbine Variable-Geometry Mechanism.

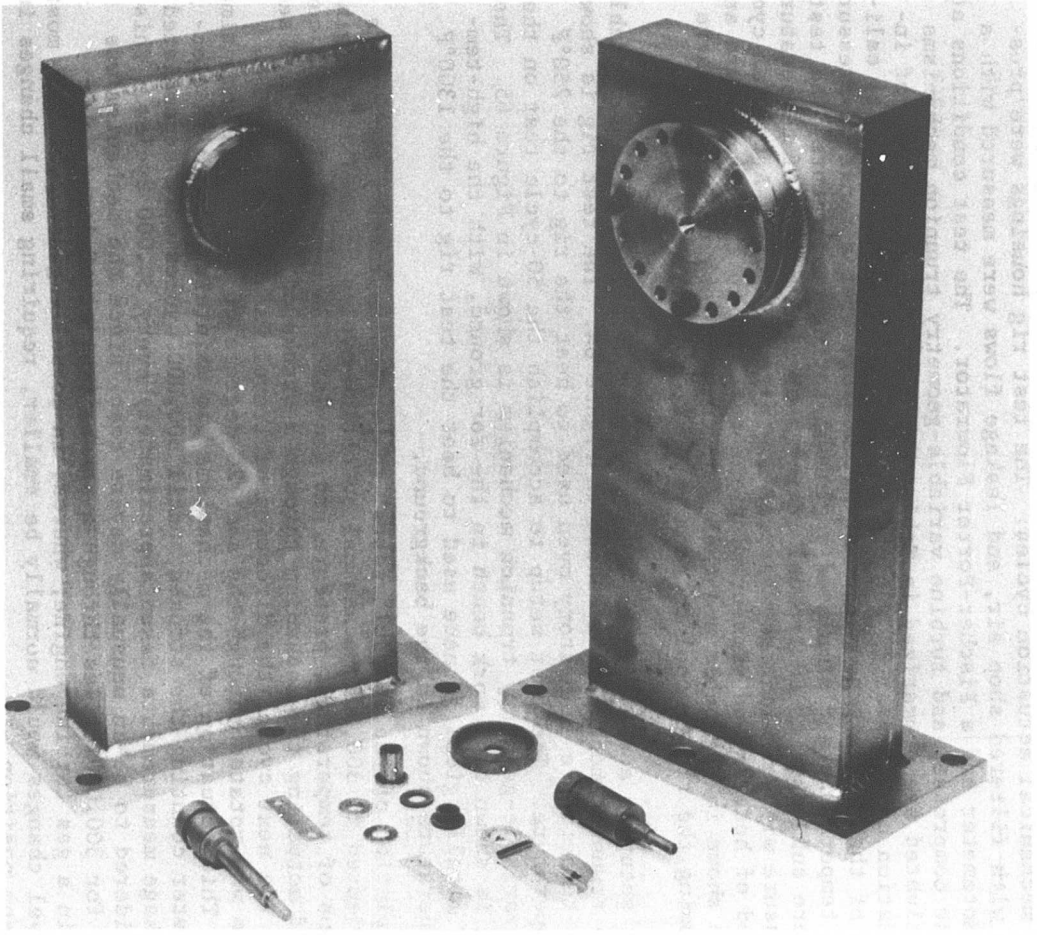

Figure 63. Compressor and Turbine Variable-Geometry Trunnion Test Rigs.

Test Programs

Testing of the compressor and turbine variable-geometry trunnion mechanisms consisted of subjecting the test rigs, under simulated gas loading, to typical engine conditions of temperature, pressure, and mechanical actuation of the mechanisms while measuring gas leakage at the various conditions. Testing included 50 simulated engine operating cycles and 300,000 mechanical actuation cycles. The test rig housings were pressurized with filtered shop air, and leakage flows were measured with a Brooks Rotameter and a Fischer-Porter Flowrator. The test conditions at which the compressor and turbine variable-geometry trunnion mechanisms were evaluated are summarized in Tables XXI and XXII, and lists of instrumentation used appear in Tables XXIII and XXIV. After initial calibration of the mechanisms, measuring air leakage over a range of pressures at room temperature and simulated engine operating temperature, the test rings were subjected to 50 typical engine operating cycles of temperature and pressure with air leakage measured every tenth cycle. A typical cycle consisted of heating and pressurizing the test rig to the temperature and pressure shown in the table and then venting the pressure to atmosphere and allowing the rig to cool to room temperature.

The test setup to accomplish the 50-cycle test on the compressor variable-geometry trunnion mechanism is shown in Figure 64. The test rig is shown in a low-temperature laboratory oven used to heat the rig to the 250°F test temperature. The test setup to accomplish the 50-cycle test on the turbine variable-geometry trunnion mechanism is shown in Figure 65. The test rig is shown on a work bench in the foreground, with the high-temperature metallurgical furnace used to heat the test rig to the 1300°F test temperature shown in the background.

Upon completion of the 50-cycle tests, the variable-geometry mechanisms were subjected to 300,000 mechanical actuation cycles at simulated engine conditions of temperature, pressure, and gas load. A mechanical cycle consisted of actuating the mechanism through a stroke of 20 degrees in 1 second. For the next cycle, the direction of travel was reversed and the mechanism was rotated through the same 20 degrees of arc in the same time period. This actuation of the mechanisms was maintained, with an electronic meter counting the strokes, until 300,000 cycles were accumulated with leakage measurements taken approximately every 30,000 cycles. This was considered to be an unusually severe test, since the mechanism was actuated for 300,000 cycles through a stroke typical of large power changes in a gas turbine engine; whereas in actual engine operation, most power level changes would normally be smaller, requiring small changes in stator vane position.

A view of the test setup to accomplish the 300,000 actuation cycles is shown in Figure 66. The compressor variable-geometry test rig is shown in the foreground being heated by infrared lamps. The turbine variable-geometry test rig is in the background enclosed in a heating chamber constructed of firebrick and asbestos composition board. Electric-resistance heaters within the chamber maintained the turbine variable-geometry test.

TABLE XXI . COMPRESSOR VARIABLE-GEOMETRY TRUNNION TEST CONDITIONS

Test Category	Pressure (psig)	Temperature (°F)	Gas Load (lb)
A. Calibration	5 to 30	Room Temp	22
	5 to 30	250	22
B. Thermal Cycles (50 Cycles)	13	250	22
C. Mechanical Cycles (300,000)	13	250	22

TABLE XXII. TURBINE VARIABLE-GEOMETRY TRUNNION TEST CONDITIONS

Test Category	Pressure (psig)	Temperature (°F)	Gas Load (lb)
A. Calibration	5 to 30	Room Temp	10
	5 to 30	1300	10
B. Thermal Cycles (50 Cycles)	25	1300	10
C. Mechanical Cycles (300,000)	25	1000	10

TABLE XXIII. COMPRESSOR VARIABLE-GEOMETRY MECHANISM TEST INSTRUMENTATION

Parameter	Location	Instrumentation	Range	Units
Gas Pressure	Upstream of Flowmeter	Gage	0-50	psig
Gas Pressure	Downstream of Flowmeter	Gage	0-50	psig
Gas Pressure	Rig Housing Gas Inlet	Gage	0-50	psig
Gas Temp.	Downstream of Flowmeter	I-C Thermocouple	60-90	°F
Metal Temp.	Rig Housing (2 locations)	I-C Thermocouple	R.T.-300	°F
Gas Flow (Leakage)	Gas Pressurizing line	Brooks Flowmeter Model 1040	0.1-1.5 air at 14.7 psia and 70°F	SCFH

TABLE XXIV. TURBINE VARIABLE-GEOMETRY MECHANISM TEST INSTRUMENTATION

Parameter	Location	Instrumentation	Range	Units
Gas Pressure	Upstream of Flowmeter	Gage	0-50	psig
Gas Pressure	Downstream of Flowmeter	Gage	0-50	psig
Gas Pressure	Rig Housing Gas Inlet	Gage	0-50	psig
Gas Temp.	Downstream of Flowmeter	I-C Thermocouple	60-90	°F
Metal Temp.	Rig Housing (2 Locations)	C-A Thermocouple	R.T.-1300	°F
Gas Flow (Leakage)	Gas Pressurizing Line	Fischer-Porter Flowrator Model 6506-A5169	0.1-2.9 air at 90 psig and 100°F	SCFM

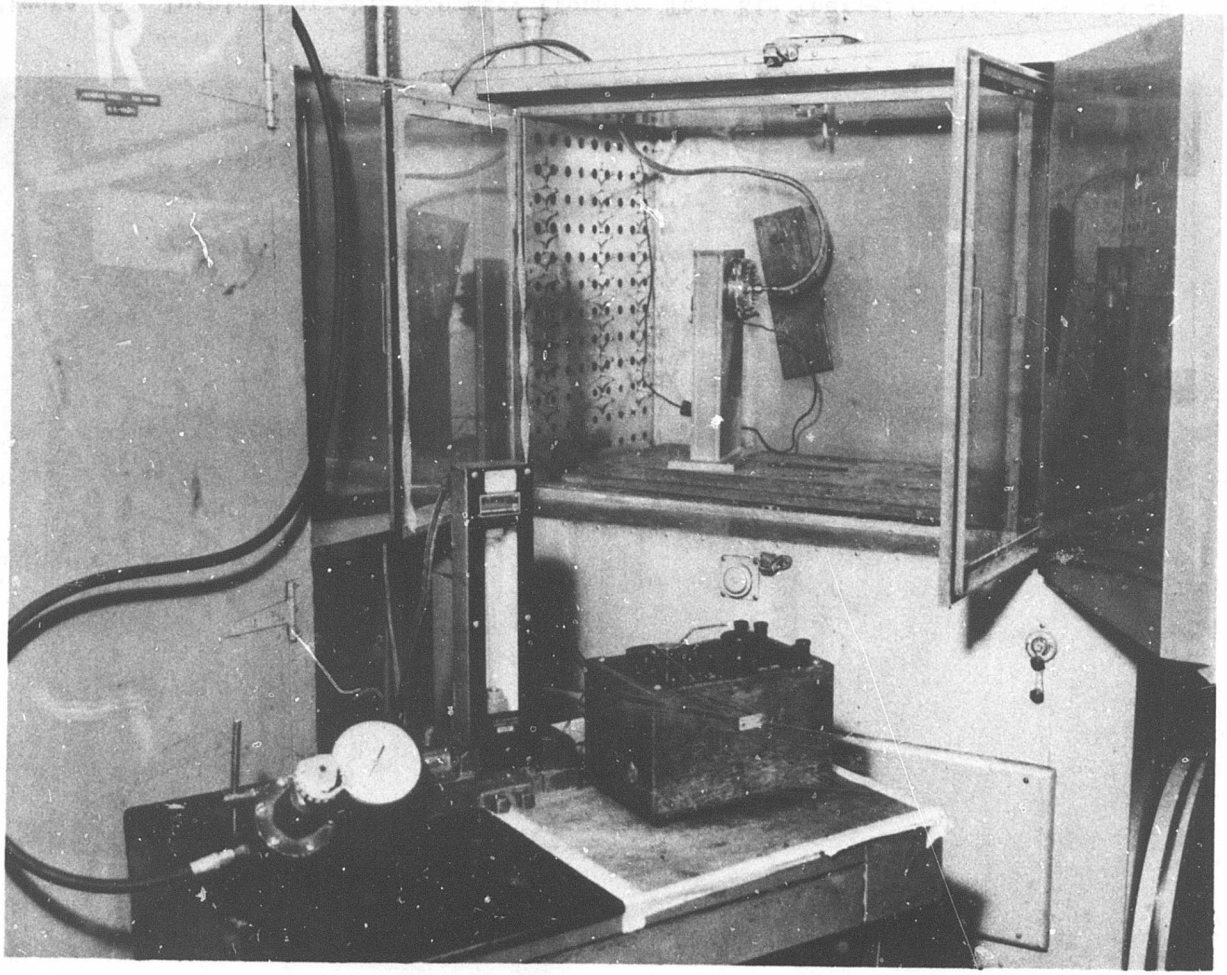

Figure 64. Compressor Variable-Geometry Trunnion Test Rig Thermal Cycling Test Setup.

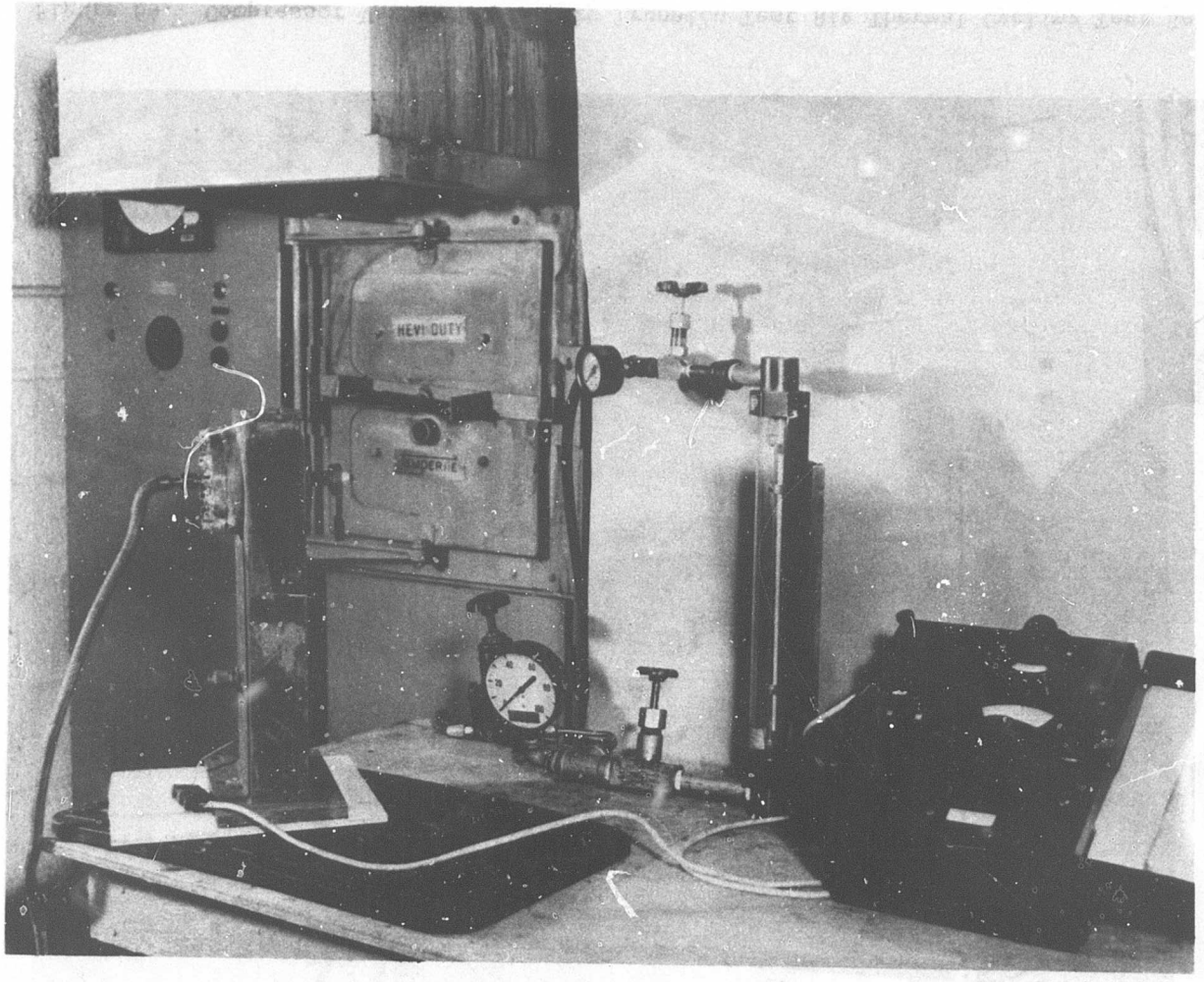

Figure 65. Turbine Variable-Geometry Trunnion Test Rig Thermal Cycling Test Setup.

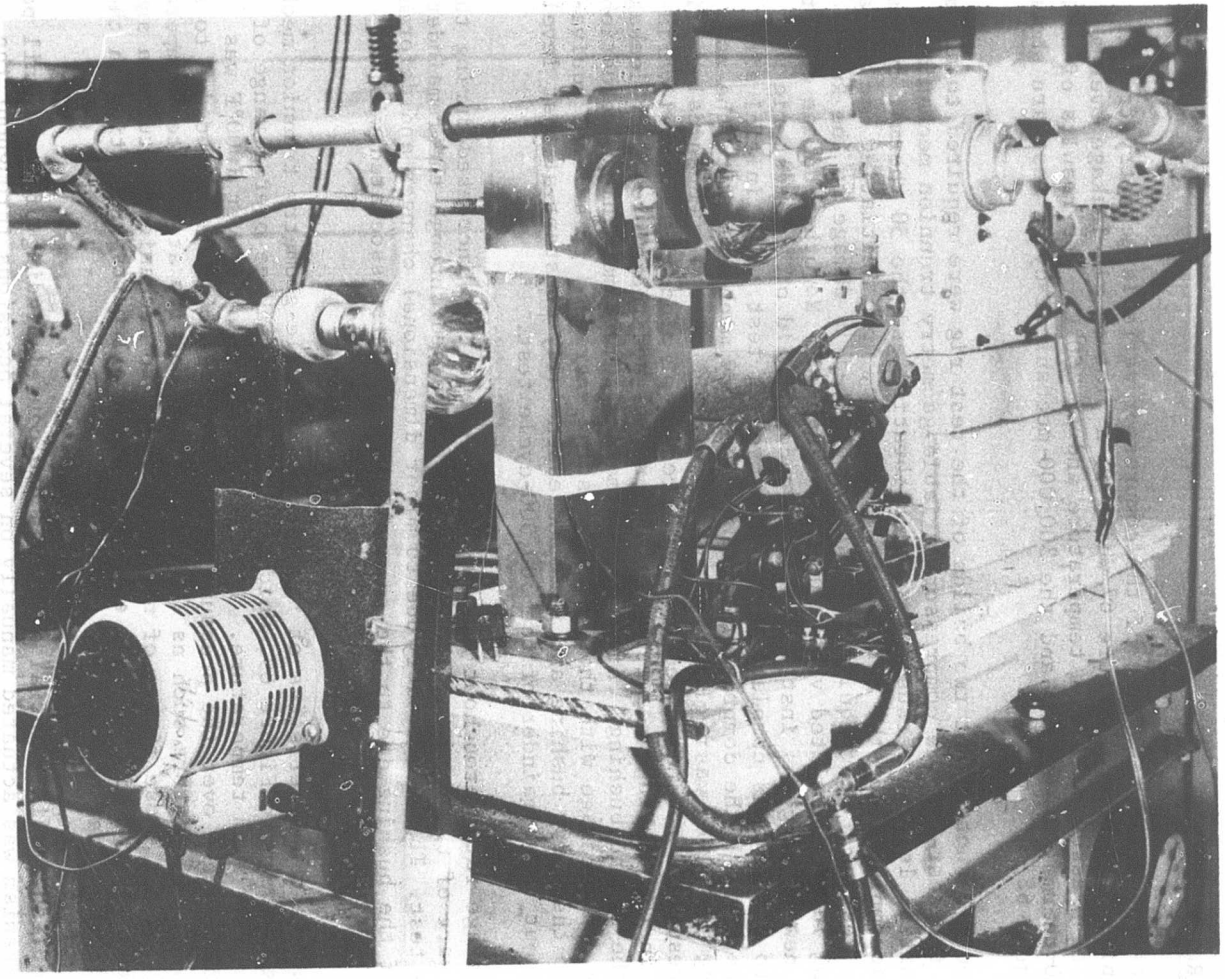

Figure 66. Compressor and Turbine Variable-Geometry Trunnion Test Rigs Mechanical Cycling Test Setup.

rig at the test temperature. The lever arms on each of the variable-geometry mechanisms were attached to a common driving device consisting of a solenoid-actuated pneumatic piston which was operated by means of a timing device. A microswitch arrangement controlled the piston stroke.

Test Results

The leakage characteristics of the compressor variable-geometry trunnion mechanism are shown in Figure 67, which is a plot of air leakage over a range of pressures at room temperature and at 250°F. The results of both the 50-thermal-cycle test and the 300,000-mechanical-cycle test are shown in Figure 68.

It should be noted that two builds of the test rig were required to accomplish the tests on the compressor variable-geometry trunnion mechanism. The initial leakage versus pressure calibration and the 50 thermal cycles were accomplished on the first build. However, upon initiating mechanical cyclic testing, a test equipment failure resulted in damage to the Rulon bushing in the simulated vane trunnion mechanism. No other damage occurred and a new bushing was installed. This second build of the test rig was used to perform the complete mechanical cycling test. The initial air leakage through the compressor variable-geometry mechanism with the new bushing installed was negligible, as shown in the plot of mechanical cycling test results. This appeared to be the result of minor dimensional variations in the bushings resulting in closer fits and therefore lower leakage with the second bushing. After approximately 20,000 mechanical actuation cycles, the leakage with this second bushing increased to a level equivalent to the first bushing and remained essentially constant at that level throughout the remainder of the 300,000-cycle test.

The leakage rate throughout the 50-thermal-cycle test increased during the early part of the test and then gradually decreased through the remainder of the test. This is probably due to minor dimensional changes and deformation of the bushing due to the temperature gradients associated with the test.

The leakage characteristics of the turbine variable-geometry trunnion mechanism are shown in Figure 69, which is a plot of leakage over a range of pressures at room temperature. Leakage at temperatures over 1000°F was essentially zero over the pressure range. This is believed to be due to a combination of factors such as (1) the low gas density at elevated temperatures, (2) the close fit-up of new parts prior to mechanical actuation and wear, and (3) the differential expansion of detail parts, resulting in the reduction of clearances.

To establish if differential expansion had caused binding of the detail parts, the mechanism was actuated manually on several occasions throughout the 50-cycle test at temperatures above 1000°F and found to be actuating freely. Binding did eventually occur between the shaft and the S-Monel bushing in the weight that represented the gas load on the mechanism, because of a loss of clearance as a result of oxidation. However, this bushing was

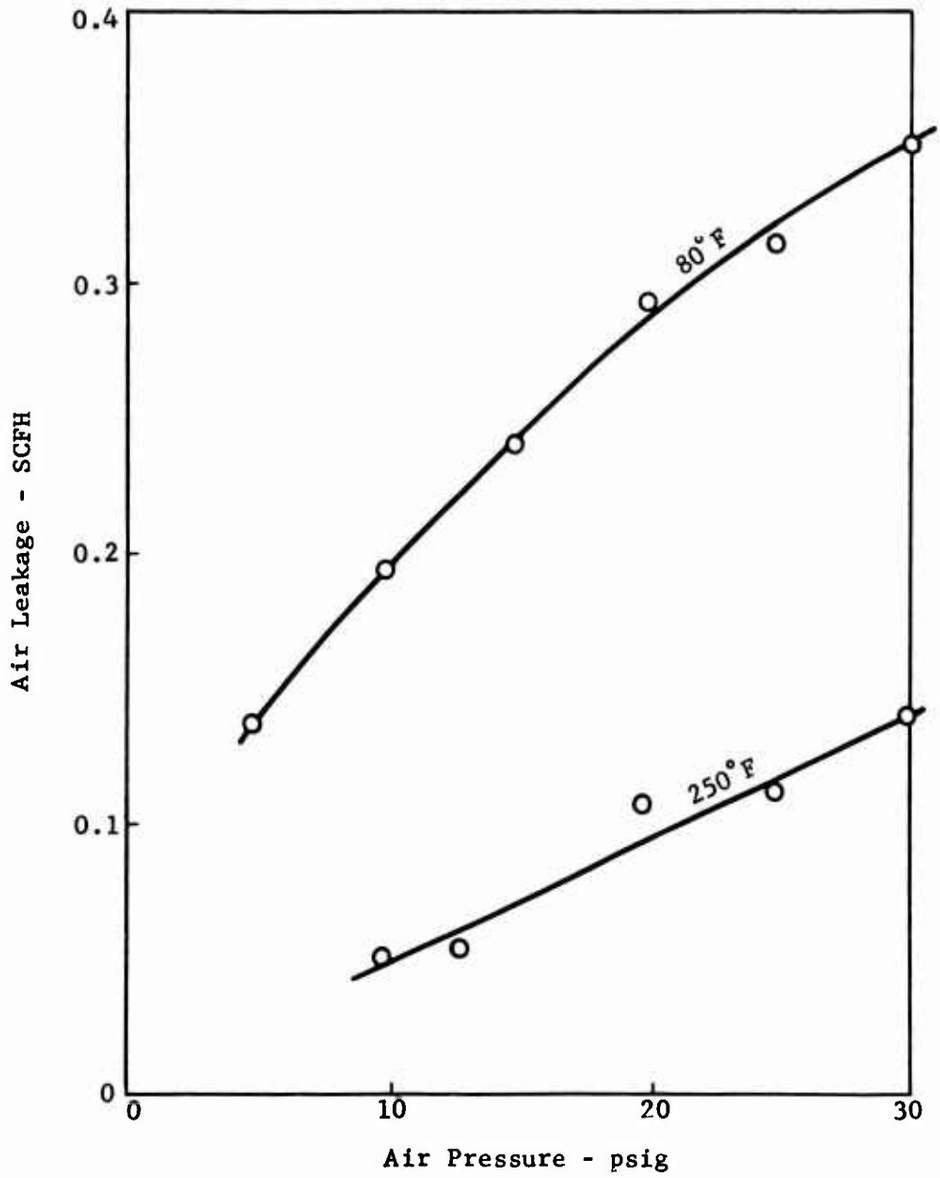

Figure 67. Compressor Variable-Geometry Trunnion Seal Air Leakage Versus Air Pressure.

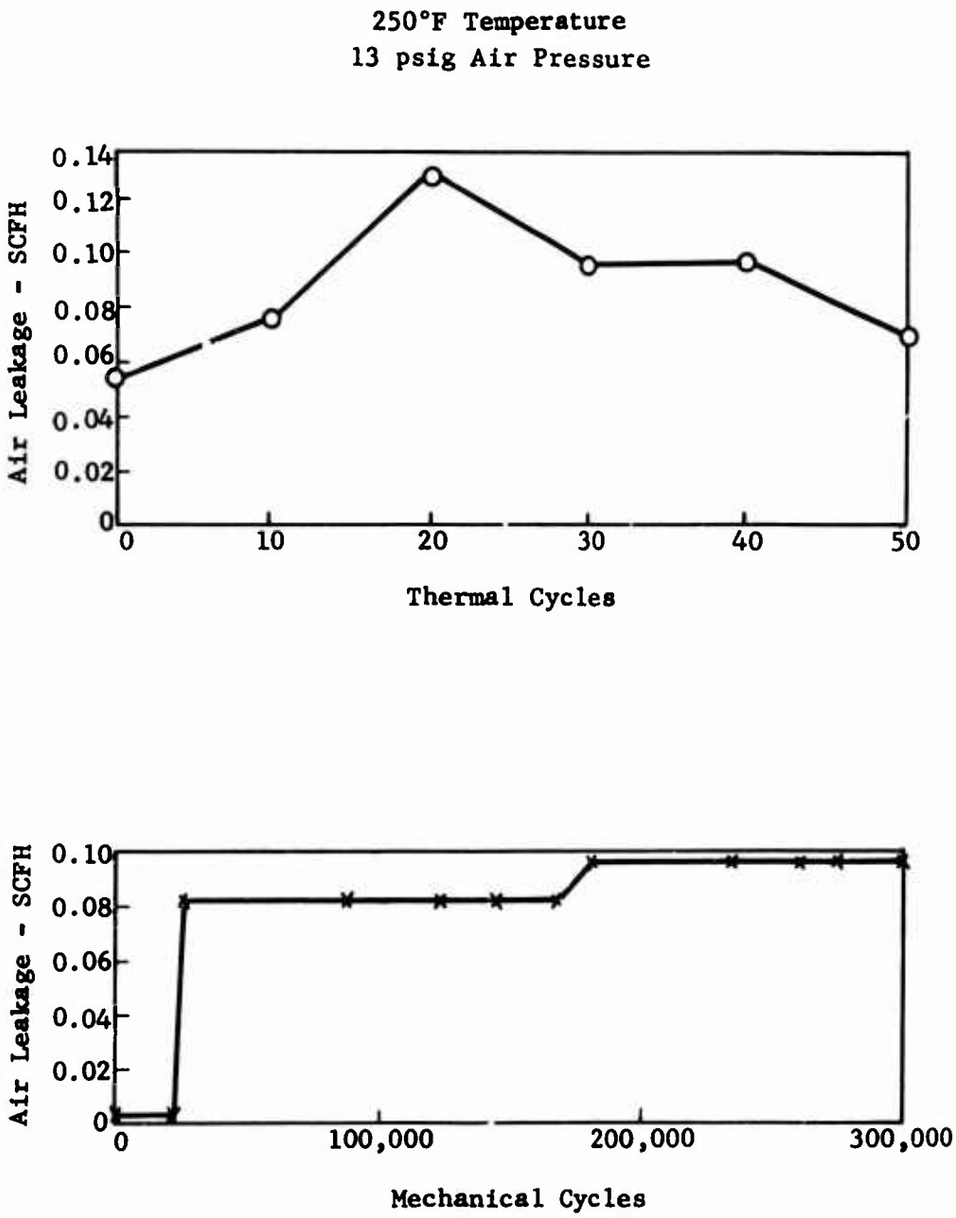

Figure 68. Compressor Variable-Geometry Trunnion Seal Thermal and Mechanical Cycling Test Results.

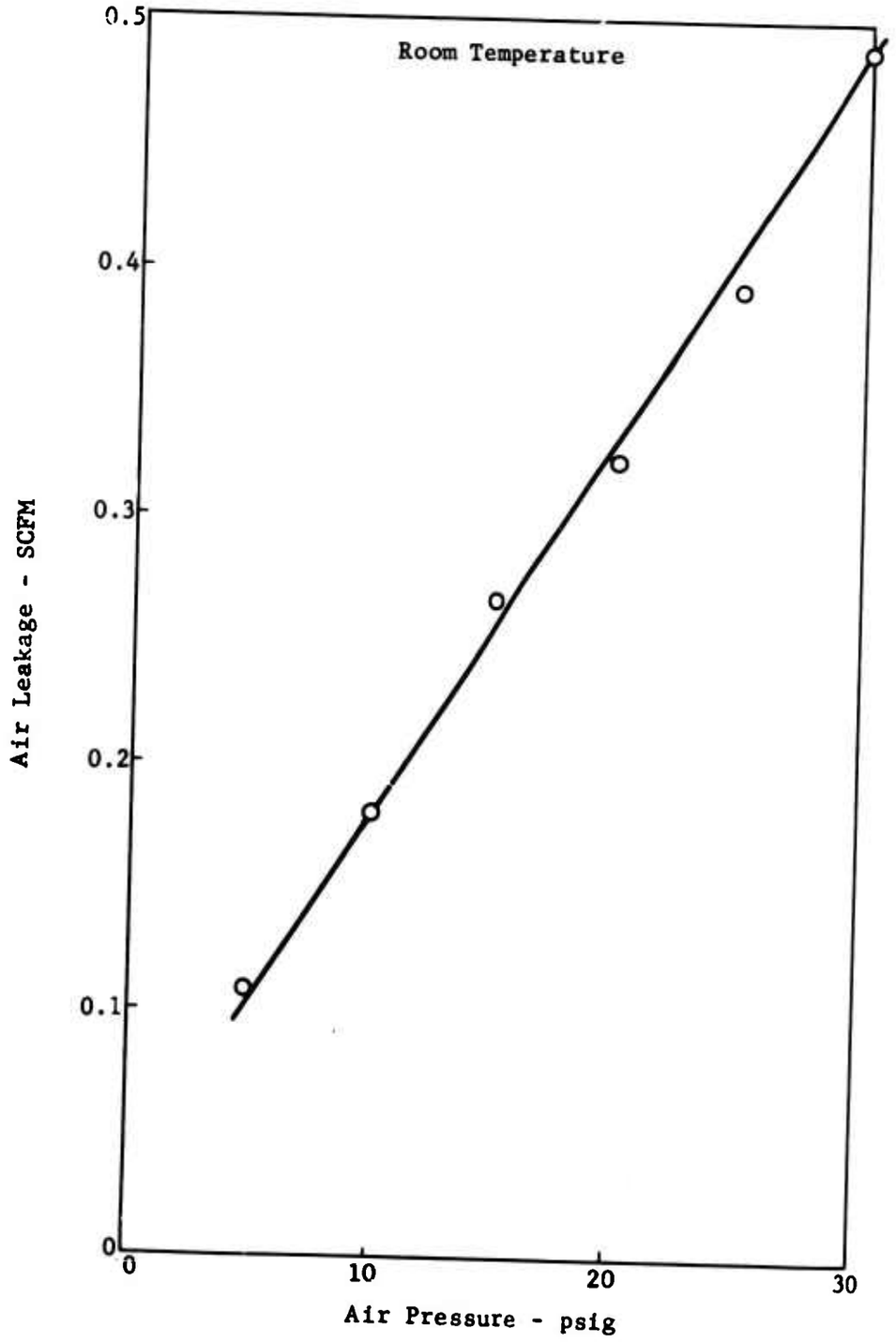

Figure 69. Turbine Variable-Geometry Trunnion Seal Air Leakage Versus Air Pressure.

considered a test equipment item and was bored to an oversized condition, which eliminated binding at this location for the remainder of the test.

Test results for the 50 thermal cycles and 300,000 mechanical cycles are shown in Figure 70. Since the leakage at high temperature was too low to measure during the 50-cycle test, room temperature leakage data were obtained and are shown in the plot of test results, which indicates no change in the leakage characteristic as a result of thermal cycling. Mechanical cycling of the turbine variable-geometry trunnion mechanism caused sufficient wear to increase clearances, resulting in an increase in leakage between 20,000 and 45,000 cycles as shown in the plot of test results.

In order to maintain continuity with earlier data obtained only at room temperature, both room-temperature and elevated-temperature leakage data were obtained throughout the 300,000 cycle test. As shown in the plot of air leakage versus mechanical cycles, the leakage increased over the first 45,000 cycles and remained essentially constant thereafter. The room temperature leakage approximately tripled during this early part of the test, and the leakage at elevated temperature increased sufficiently to come within measuring range.

Details of the compressor variable-geometry trunnion mechanism after 300,000 mechanical actuation cycles are shown in Figure 71. The details consist of a Rulon-A bushing and washer which assemble to the smaller diameter of the nitrided A286 shaft. Generally, the parts were in good condition upon completion of the test. The shaft gave no evidence of scoring and had a high polish, as shown in the photograph, with no change in diameter at the bushing location. The plastic bushing and washer showed a variety of dimensional changes due to a combination of wear and plastic deformation of the material but primarily due to plastic deformation. The O.D. of the washer and the larger O.D. of the bushing were slightly oval in shape with local increases in diameter from 0.037 to 0.068 inch. The washer showed a loss of thickness from 0.008 to 0.027 inch and showed evidence of extruding into the housing bore, which can be seen in the photograph as a small step in the face of the washer. The I.D. of the bushing and its mating surface on the shaft had a highly polished appearance, but there was no measurable wear of the bushing I.D. surface. The wear and plastic deformation observed on the bushing and washer appear to be the result of axial loads imposed on the mechanism rather than the radial load at the shaft O.D. and bushing I.D. location. The sources of these axial loads are (1) the designed axial preload provided by the stack-up of details to minimize clearances, and (2) the cantilever-supported weight simulating the engine gas load.

The driving torque for the compressor variable-geometry trunnion mechanism at the start of the 300,000-cycle test was 8 inch-pounds; upon completion of the test, it was 2 inch-pounds. This reduction in the driving torque is an indication of loss of the axial preload due to wear and extrusion of the Rulon-A bushing and washer. There was no change in vane mechanism driving torque as a result of the 50 thermal cycles.

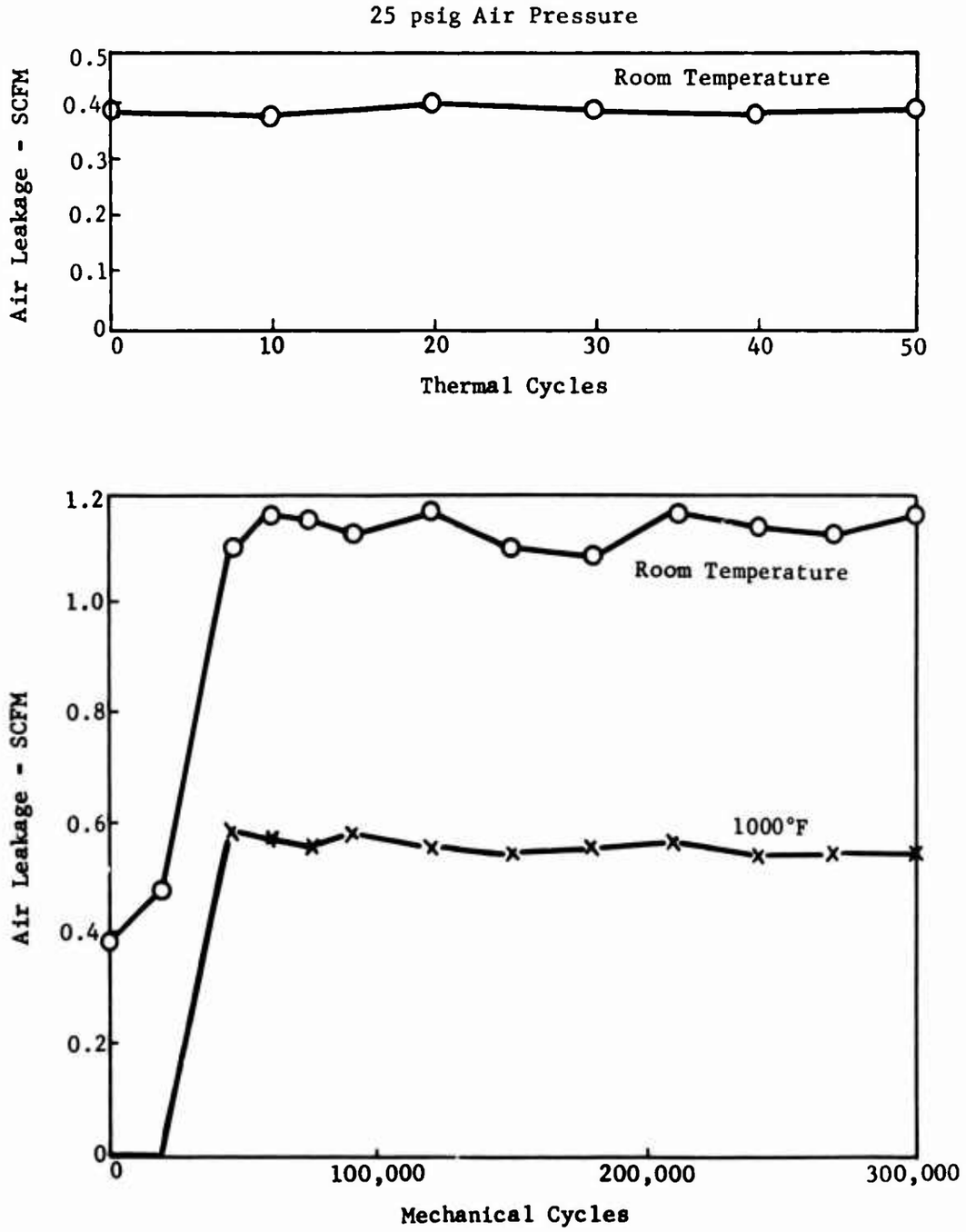

Figure 70. Turbine Variable-Geometry Trunnion Seal Thermal and Mechanical Cycling Test Results.

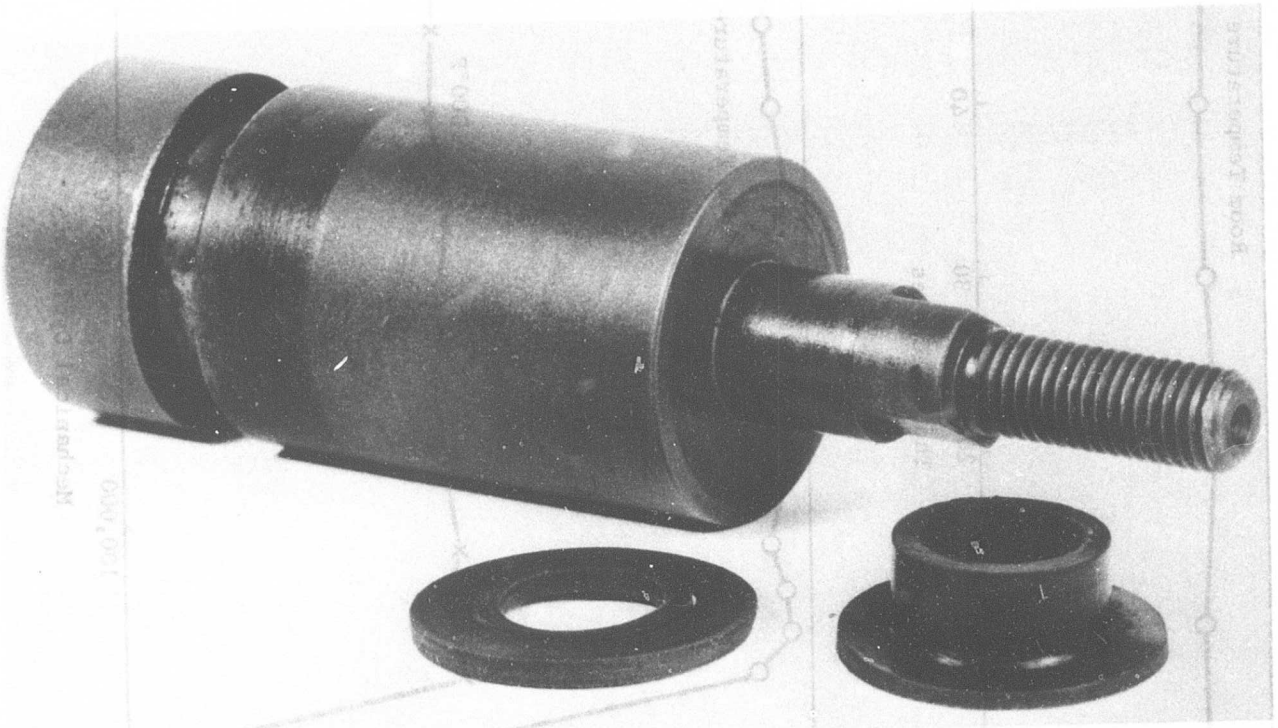

Figure 71. Compressor Variable-Geometry Trunnion Mechanism After Testing.

Details of the turbine variable-geometry trunnion mechanism after 300,000 mechanical actuation cycles are shown in Figure 72. The details consist of the S-Monel bushing and washers and a nitrided A286 shaft. The parts were in good condition upon completion of the test. The shaft showed two points of wear located 180 degrees apart at opposite ends of the bushing location. The wear points were attributed to the forces on the shaft and bushing arrangement counteracting the simulated gas load. Shaft wear was measured at a maximum of 0.002 inch, with the surface showing a high polish and no scoring or galling. The I.D. of the S-Monel bushing showed evidence of corrosion and light scoring at the ends of the bushing matching the wear points on the shaft. Bushing wear near the ends was measured at a maximum of 0.004 inch.

The driving torque for the turbine variable-geometry trunnion mechanism measured at room temperature prior to testing was 20 inch-pounds and at the completion of all testing had increased slightly to 24 inch-pounds. At the completion of all testing, the driving torque was measured also at 1000°F and was determined to be 12 inch-pounds.

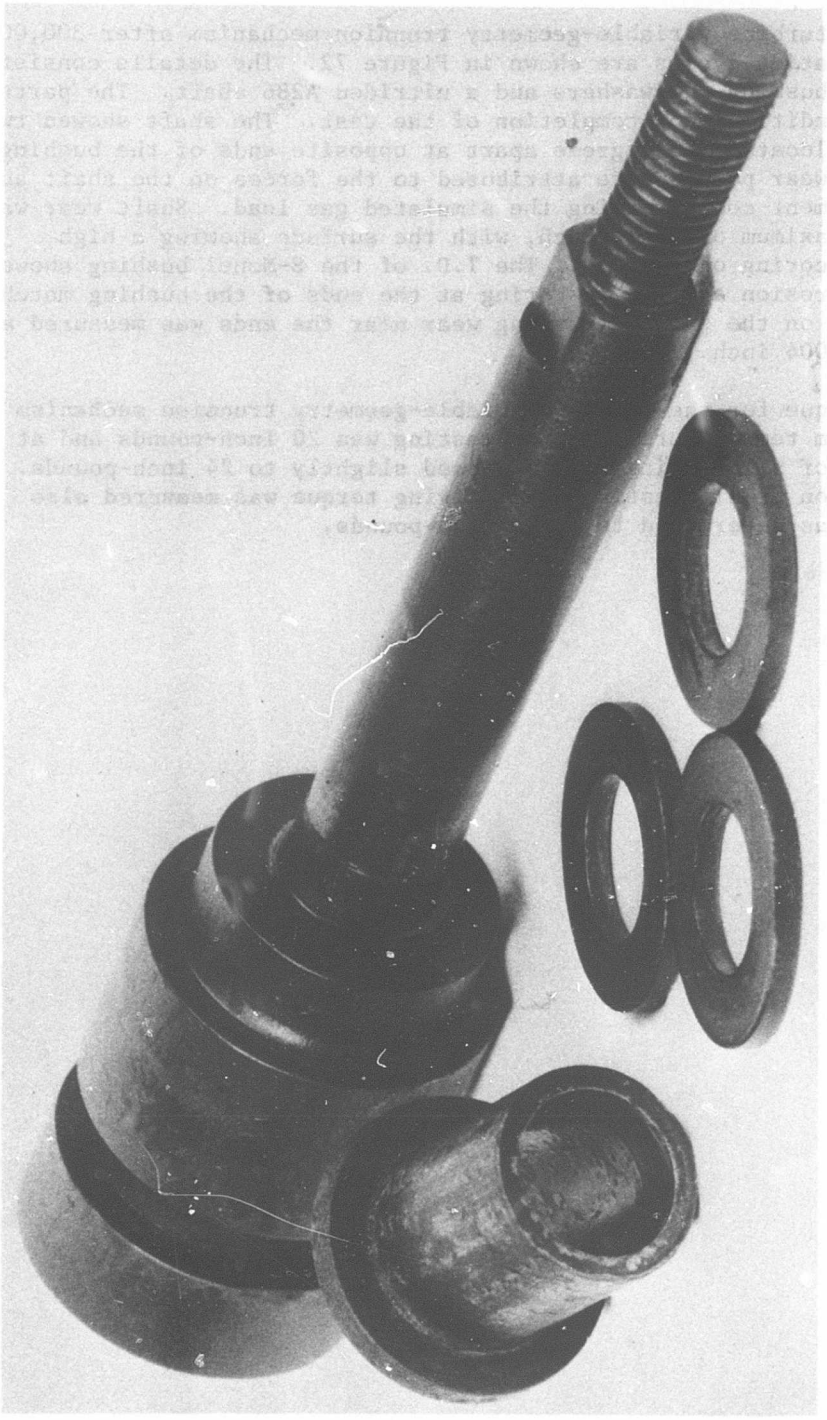

Figure 72. Turbine Variable Geometry Trunnion Mechanism After Testing.

ANALYSIS OF LEAKAGE EFFECTS ON ENGINE PERFORMANCE (TASK V)

Cycle Analysis

An analysis was performed to determine the effect of leakage on engine performance based on the leakages measured during testing conducted in Tasks II, III, and IV. The design point characteristics and component performances of the turboshaft engine selected for the air/gas seal leakage evaluation are as follows:

Engine Airflow	5 pounds per second
Compressor Pressure Ratio	Variable (8:1 to 2:1)
Compressor Efficiency	82 percent
Combustor Efficiency	99 percent
Combustor Pressure Drop	3 percent
Turbine Inlet Temperature	2300°F
Gasifier Turbine Efficiency	86 percent
Power Turbine Efficiency	90 percent

The effects of leakage on engine power output and specific fuel consumption were evaluated for three leakage classifications as follows:

A. Leakage Overboard - flow that has been compressed in the compressor and does no work in the turbines.

B. Leakage which bypasses the compressor turbine but returns to the main stream before the power turbine.

C. Leakage which bypasses the combustor but returns to the main stream before the compressor turbine.

The results of this analysis, expressed as percent loss in power per 1 percent leakage and percent increase in BSFC per 1 percent leakage for the three leakage classifications and over a range of pressure ratios, are shown in Figure 73. These curves were obtained by determining the power output and BSFC at zero leakage and then repeating the procedure for each of the leakage categories while introducing an amount of leakage of each type equal to 1 percent of the engine airflow. The change in power output and BSFC as a result of the 1 percent of leakage for each leakage category was then expressed as a percent change from the zero leakage condition and plotted as shown.

This procedure was repeated for the design condition and several part throttle conditions corresponding to cycle pressure ratios of 20, 17, 14, 11, and 8:1 in order to indicate the effects of leakage over a range of pressure ratios. Off-design or part-power operation was obtained by reducing turbine inlet temperature and, consequently, speed and airflow. The effects of leakage on performance were evaluated by holding the turbine inlet temperature (T.I.T.) constant as each of the three categories of leakage was applied. For example, at a 14:1 cycle pressure ratio, the turbine inlet temperature was held constant as the effect of overboard leakage was evaluated. Then,

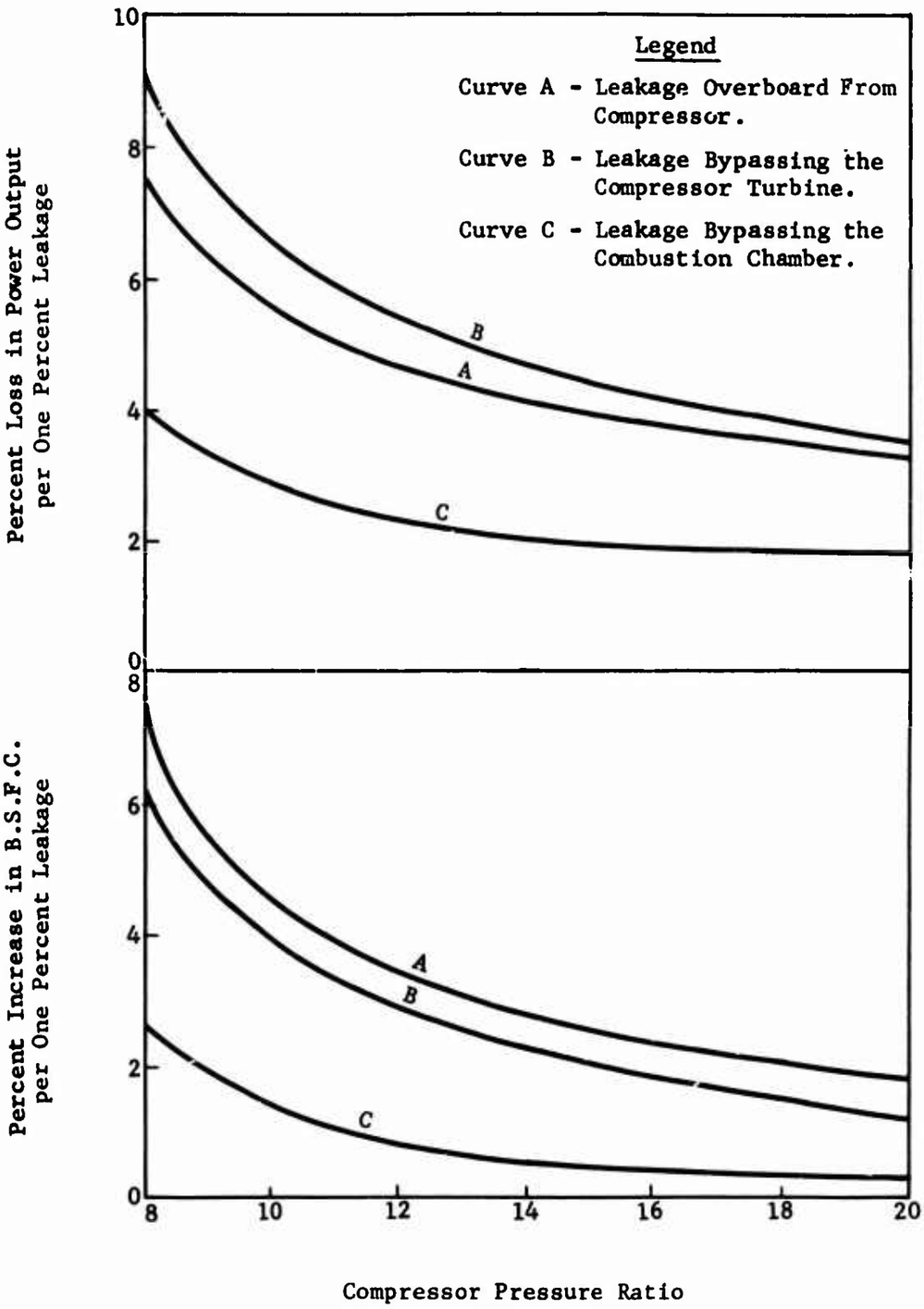

Figure 73. Leakage Effects on the Performance of a Small Gas Turbine Engine.

at the same T.I.T. with no overboard leakage, the effect of bleed air bypassing the compressor turbine was calculated. Finally, the effect of leakage bypassing the combustion chamber was determined at the same T.I.T. and with no leakage in the other categories. In all cases the engine speed was allowed to change (decrease) to properly rematch the components in the cycle, i.e., provide continuity and power balance.

The analysis was conducted as though the leakage was unanticipated during the design phase. In all instances, the effects on performance of these unexpected leakages would be more pronounced at higher pressure ratios and are larger than if the amount of leakage were predetermined in the original engine design and allowance were made in terms of correctly sizing the turbine flow area. If the areas were adjusted in the original design such that design rotor speed and design T.I.T. were maintained for a predetermined leakage, the loss in power would be less than it would be with the unexpected leakage. For example, a 1-percent overboard leakage at the design condition causes an 0.85-percent decrease in gas generator shaft speed. If the same leakage were to occur past the compressor turbine but return to the power turbine, the result would be a 1.43 percent decrease in shaft speed, since under this condition the leakage acts as a back-pressure on the gas generator, causing it to slow down (similar in effect to a smaller exhaust nozzle). Consequently, a higher power loss occurs as indicated in Figure 73. However, anticipation of this leakage flow and sizing of the power turbine to accommodate the flow would reduce the backpressure on the gas generator and reduce the power loss.

Performance Effects

Based on the test results obtained on the various types of seals evaluated in Tasks II, III, and IV, leakages in a hypothetical small gas turbine engine were established and the resultant performance effects were determined. A summary of the leakages and associated performance losses is presented in Table XXV. The engine stations, leakage sources, and engine state conditions are the same as those established in Task I and discussed earlier. In addition to leakages based on the test results of Tasks II, III, and IV, the estimated leakages from Task I have been included in this table for comparison purposes. However, the performance losses shown in the table are based entirely on the measured leakages from Tasks II, III, and IV. Also shown in the table is the leakage category for each leakage source: (1) leakage overboard, (2) leakage bypassing the compressor turbine, and (3) leakage bypassing the combustion chamber.

The basis for the measured leakage rates appearing in the table is as follows:

1. All labyrinth seal leakages are based on Task II test data for the labyrinth seal in the aligned condition, after the 50-cycle test, at 250°F temperatures and at 400 feet per second peripheral velocity. A plot of labyrinth seal air leakage versus air pressure for these conditions is presented in Figure 17. Where necessary, extrapolations were made directly from the curve for

pressure condition other than those imposed in the test program. In cases where the engine temperature is significantly different from the 250°F test temperature, the mass rate of leakage was adjusted to reflect the density change by multiplying by the square root of the ratio of the test temperature to the engine temperature (absolute). Also, the leakage rate was adjusted for the difference in diameter between the engine seal and the test seal to account for the difference in peripheral length of gap. The diameter used for each engine labyrinth seal is shown in the table.

2. All carbon-face seal leakages are based on Task II test data for the carbon-face seal in the aligned condition, after the 50-cycle test, at 500°F temperatures and at 320 feet per second rubbing velocity. A plot of carbon-face seal air leakage versus air pressure for these conditions is presented in Figure 30. The curve was extrapolated where necessary for pressure-flow determinations, and adjustments were made to the leakage rate for density changes due to temperature and for seal size as described above for the labyrinth seal. The diameters used for the engine face seals are shown in the table.

3. All split-line leakages are based on Task III test data for the metal-to-metal flange configuration. Curves of air leakage versus air pressure for this configuration at various temperatures are presented in Figure 45. Leakage adjustments were made for the flange length, and the engine flange lengths used are shown in the table. The existence of horizontal split-lines was assumed for the compressor casing, and leakage at the ends of the straight flanges was included in this region in the same proportions encountered during testing since these flange-ends proved to be a significant source of leakage (see Table XX). Leakage from the remainder of the horizontal split-lines was ignored since it proved to be insignificant during testing. Where necessary, curves were extrapolated for pressure-flow determinations, and temperature-density adjustments were made where engine temperatures were out of the range of the test temperatures.

4. All compressor and turbine variable-geometry trunnion seal leakage is based on Task IV test results after stabilization of the leakage rates during the 300,000 mechanical cycling tests. Plots of these test results for the compressor and turbine variable-geometry mechanisms are presented in Figures 68 and 70. No adjustments to the leakage data were made because of the physical size of the hardware, since the mechanisms tested were approximately the actual size that might be used in a small gas turbine. Extrapolations for pressure were not necessary, and density adjustments were made for temperature. A total of 39 vanes was assumed for the compressor variable-geometry arrangement; 31 vanes each were assumed for both turbine variable-geometry locations.

BLANK PAGE

TABLE XXV. TYPICAL SMALL GAS TURBINE LEAKAGES

Engine Section	Type Seal	Seal Dimensions	Leakage Category	E T (
STATION 2A - Axial Compressor				
a. Axial compressor front hsg. flange to axial compressor rear hsg. flange.	Metal-to-metal flanges	23.6-inch circular flange length plus two flange-ends	A	2
b. Second axial compressor stage variable vane trunnion seal (39 vanes).	Rulon-A bushing	As tested in Task IV	A	2
c. Interaxial compressor stage labyrinth seal.	Labyrinth	2.5-inch fin diameter	-	2
STATION 2B - Axial to Centrifugal				
a. Axial compressor rear hsg. flange to centrifugal compressor hsg. front flange.	Metal-to-metal flanges	18.5-inch circular flange length plus two flange-ends	A	3
b. Axial to centrifugal compressor interstage labyrinth seal.	Labyrinth	2.1-inch fin diameter	-	3
STATION 3 - Centrifugal Compressor				
a. Centrifugal compressor hsg. rear flange to combustor hsg. front flange.	Metal-to-metal flanges	56-inch circular flange length	A	7
b. Centrifugal compressor outlet circumferential fin labyrinth seal.	Labyrinth	7.0-inch fin diameter	B	7 -
c. Number 2 bearing coolant supply cavity labyrinth seal.	Labyrinth	2.9-inch fin diameter	A	3
d. Carbon-ring bearing seal.	-	-	-	-
e. Carbon-face bearing seal.	Carbon face	1.6-inch face diameter	A	8

TURBINE LEAKAGES AND EFFECT ON PERFORMANCE

Leakage Category	Engine State Conditions Temp. (°F)	Engine State Conditions ΔP (psi)	Leakage Rate Estimated (Task I) (lb/sec)	Leakage Rate Measured (Task II, III or IV) (lb/sec)	Leakage Rate Measured (Task II, III or IV) (%)	BSFC Increase (%)	Horsepower Loss (%)
A	250	17	0.002	0.0025	0.06	0.14	0.23
A	250	13	0.0004	0.00008	nil	nil	nil
-	250	8	0.0052	0.003	-	-	-
A	350	37	0.0024	0.004	0.09	0.21	0.34
-	350	12	0.0053	0.003	-	-	-
A	794	211	0.028	0.011	0.024	0.55	0.91
B	794	206	0.098	0.174	-	-	-
	-	or	or	or			
		75	0.066	0.055	1.22	2.20	5.12
A	300	11.5	0.0055	0.0041	0.09	0.21	0.34
-	-	-	0.0024	-	-	-	-
A	800	135	0.0014	0.0015	0.03	0.07	0.11

B

TABLE XXV - C

Engine Section	Type Seal	Seal Dimensions	Leaka Categ
STATION 4A - 1st-Stage Turbine			
a. 1st-stage turbine coolant axial labyrinth seal.	Labyrinth	5.2-inch fin diameter	C
b. Number 3 bearing coolant supply cavity labyrinth seal.	Labyrinth	2.6-inch fin diameter	A
c. Carbon-ring bearing seal.	-	-	-
d. Carbon-face bearing seal.	Carbon face	1.6-inch face diameter	A
e. Turbine stator support rear flange to 1st-stage rotor shroud front flange.	Metal-to-metal flanges	22.7-inch circular flange length	C
STATION 4B - 2nd-Stage Turbine Stator			
a. 1st-stage rotor shroud rear flange to 2nd-stage stator vane support front flange.	Metal-to-metal flanges	23.2-inch circular flange length	C
b. 2nd-stage turbine stator coolant axial fin labyrinth seal.	Labyrinth	3.3-inch fin diameter	C
STATION 4C - 2nd-Stage Turbine Rotor			
a. 2nd-stage rotor coolant axial fin labyrinth seal.	Labyrinth	3.3-inch fin diameter	C
STATION 5 - 2nd-Stage Turbine			
a. 2nd-stage rotor shroud rear flange to combustor outer hsg. rear flange.	Metal-to-metal flanges	25.2-inch circular flange length	B
b. Combustor outer hsg. rear flange to power turbine transition duct front flange.	Metal-to-metal flanges	25.2-inch circular flange length	A

BLE XXV - Continued

ns	Leakage Category	Engine State Conditions Temp. (°F)	Engine State Conditions ΔP (psi)	Leakage Rate Estimated (Task I) (lb/sec)	Leakage Rate Measured (Task II, III or IV) (lb/sec)	Leakage Rate Measured (Task II, III or IV) (%)	BSFC Increase (%)	Horsepower Loss (%)
	C	800	110	0.07	0.06	1.33	0.40	2.53
	A	800	210	0.04	0.066	1.47	3.38	5.58
	-	-	-	0.0022	-	-	-	-
	A	400	35	0.0005	0.00035	0.01	0.02	0.04
;e	C	800	110	0.011	0.0023	0.05	0.02	0.10
;e	C	800	110	0.011	0.0023	0.05	0.02	0.10
	C	900	26	0.016	0.0086	0.19	0.06	0.36
	C	900	57	0.021	0.019	0.42	0.13	0.80
e	B	790	170	0.012	0.0039	0.09	0.16	0.38
e	A	1600	36	0.0021	0.0007	0.02	0.05	0.08

TABLE XXV - Con

Engine Section	Type Seal	Seal Dimensions	Leakage Categor
STATION 5- 2nd-Stage Turbine (Continued)			
c. 2nd-stage rotor rear axial labyrinth seal.	Labyrinth	4.7-inch fin diameter	A
d. Number 4 bearing coolant supply cavity labyrinth seal.	Labyrinth	3.3-inch fin diameter	A
e. Carbon-ring bearing seal.	-	-	-
f. Carbon-face seal.	Carbon face	1.6-inch face diameter	A
STATION 6 - Power Turbine			
a. Variable turbine vane trunnion seals (31 vanes).	S-Monel bushing	As tested in Task IV	A
b. Carbon-ring bearing seal.	-	-	-
c. Carbon-face seal.	Carbon face	2.5-inch face diameter	A
STATION 6A - 1st-Stage Power Turbine			
a. 1st-stage power turbine stator support rear flange to rotor shroud front flange.	Metal-to-metal flanges	28.6-inch circular flange length	A
STATION 6B - 2nd-Stage Power Turbine			
a. Interstage power turbine labyrinth seal.	Labyrinth	3.3-inch fin diameter	-
b. 2nd-stage power turbine variable stator vane trunnion seal (31 vanes).	S-Monel bushing	As tested in Task IV	A

BLE XXV - Continued

ns	Leakage Category	Engine State Conditions Temp. (°F)	Engine State Conditions ΔP (psi)	Leakage Rate Estimated (Task I) (lb/sec)	Leakage Rate Measured (Task II, III or IV) (lb/sec)	Leakage Rate Measured (Task II, III or IV) (%)	BSFC Increase (%)	Horsepower Loss (%)
	A	1600	31	0.0144	0.012	0.027	0.062	1.03
	A	400	30	0.009	0.012	0.27	0.62	1.03
	-	350	16	0.0013	-	-	-	-
	A	350	16	-	0.0002	nil	nil	nil
	A	1570	25	0.0013	0.02	0.44	1.01	1.67
	-	700	50	0.0026	-	-	-	-
	A	700	50	-	0.0008	0.02	0.05	0.08
	A	1572	14	0.0013	0.0003	0.01	0.02	0.04
	-	1290	7.3	0.003	0.0021	-	-	-
	A	1290	3.7	0.0008	0.0016	0.04	0.09	0.15

The performance losses shown in the table were obtained by converting the Task II, III, and IV leakages to percentages of engine airflow and then applying the curves of percent change in performance per percent leakage for the different leakage categories. The high-performance losses associated with labyrinth seal leakages are apparent in the table.

To more clearly display the relative significance of the various leakage sources, the performance losses were grouped and totaled by type of seal and leakage category and plotted in Figure 74 for loss of power output and in Figure 75 for increase in BSFC. In both areas of performance degradation and in all leakage categories, labyrinth seal leakage appears as the most serious form of engine leakage. The overboard leakage (Category A) is the most serious form of leakage, with the total performance loss due to overboard leakage being more than twice as much as the combined Category B and C leakages for both types of performance losses.

The overall power loss due to leakage in the hypothetical small gas turbine engine is a total of 21.02 percent, with 16.79 percent attributable to labyrinth seals; the overall increase in BSFC is a total of 10.03 percent, with 7.62 percent attributable to labyrinth seals. Typically, labyrinth seals serve as the centrifugal compressor outlet seal, the first-stage turbine coolant seal, and the number 3 bearing coolant supply cavity seal. Since these seals are large-diameter and/or high-pressure seals, they contribute a large percentage of the total engine leakage. Therefore, close attention is required at the component and/or engine system design levels to minimize leakage from these sources.

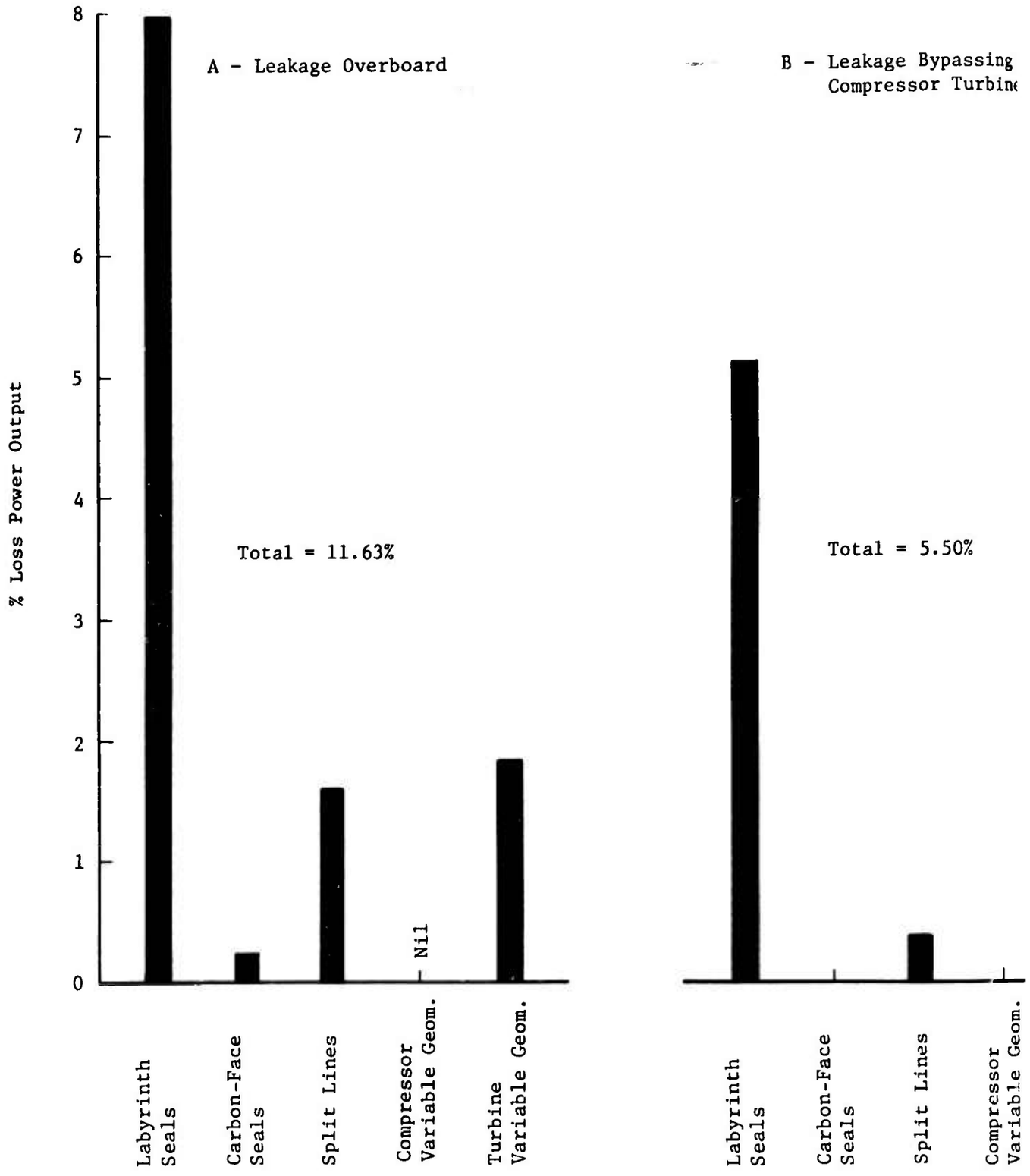

Figure 74. Effects of Engine Leakage on Power Output.

passing
Turbine

C - Leakage Bypassing
Combustion Chamber

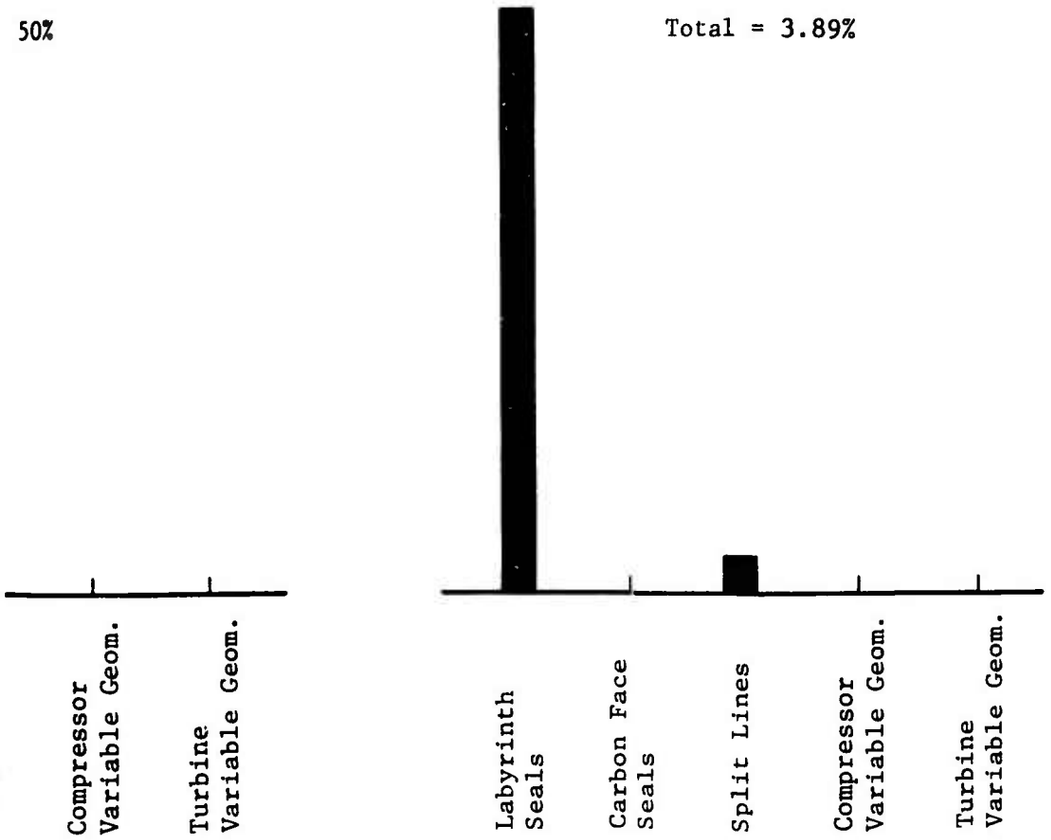

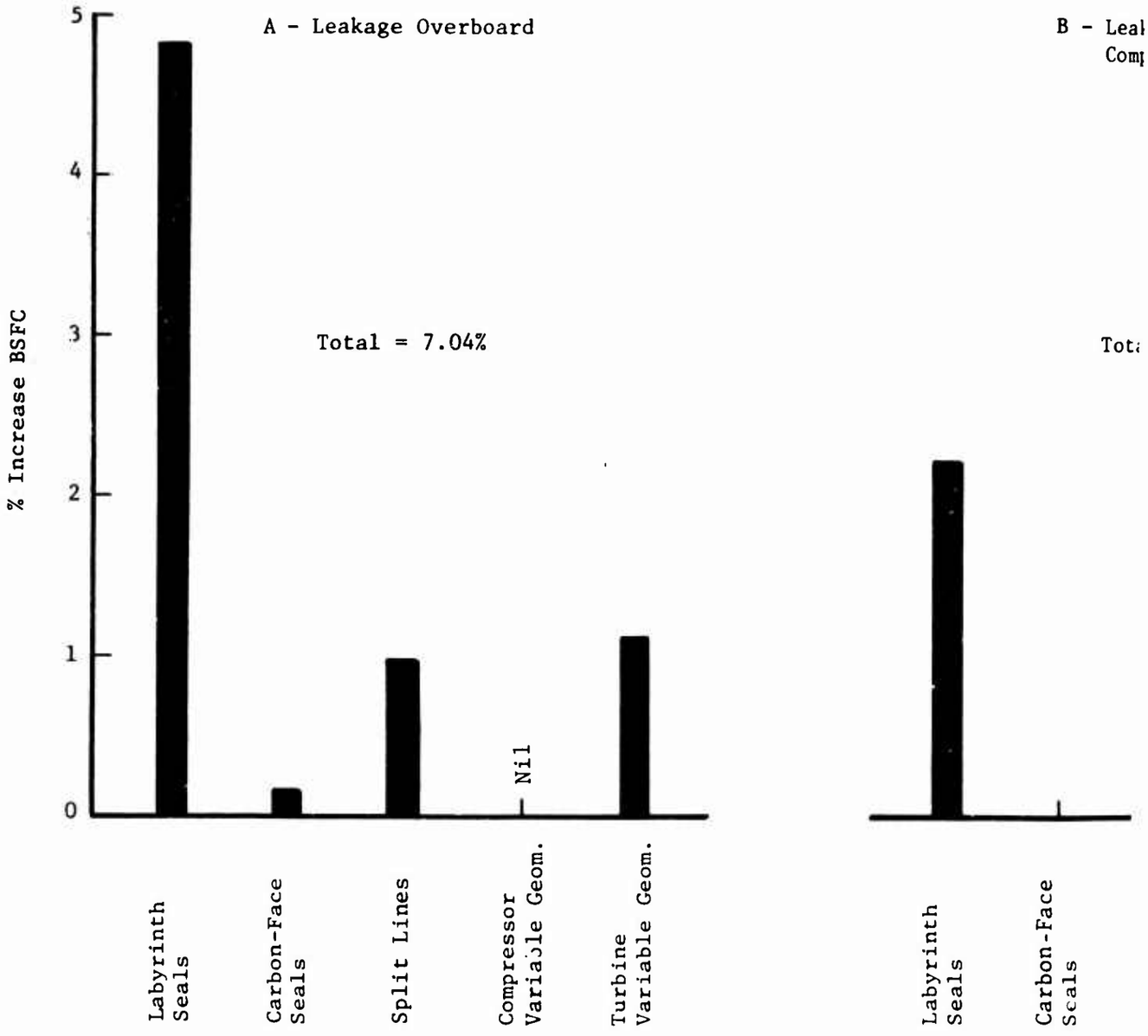

Figure 75. Effects of Engine Leakage on BSFC.

- Leakage Bypassing
Compressor Turbine

Total = 2.36%

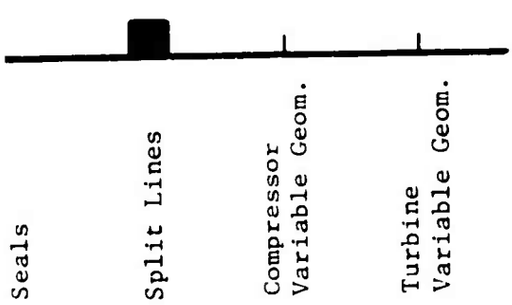

C - Leakage Bypassing
Combustion Chamber

Total = 0.63%

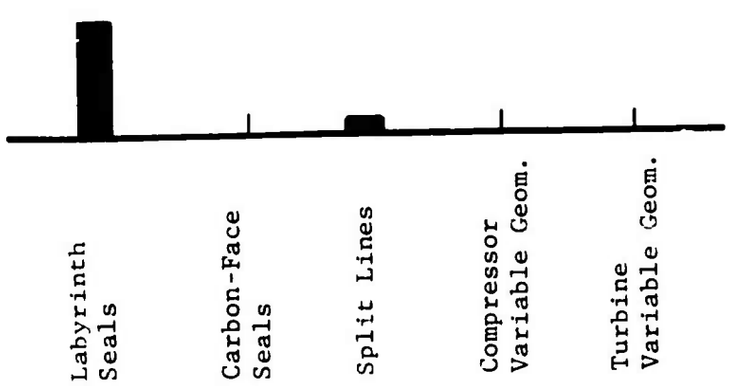

CONCLUSIONS

1. Analysis shows that a power loss of up to 21 percent and an increase in specific fuel consumption of up to 10 percent are possible in a small, high performance gas turbine engine if air and gas leakages are not predicted and accounted for in the engine cycle.

2. The most significant sources of leakage are the labyrinth seals. More than 75 percent of the performance losses associated with leakage in a small gas turbine engine are attributable to these seals.

3. The leakage as a percent of main airflow for the casing flanges and rotating seals in the small engine is substantially higher than in the large engine since the main airflow increases approximately as the square of the diameter, whereas the leakage is only proportional to the diameter. The use of a centrifugal compressor further increases the casing flange leakage of a given airflow small engine.

4. Regarding leakage paths in the small engine and resultant performance losses, overboard leakage represents more than twice the losses associated with all other types of engine leakage.

5. The pressure-energized, static seal configurations tested for engine case split-lines produced no significant reduction in leakage over that encountered with metal-to-metal flanges.

6. Significant contributors to split-line leakage are the flange-end locations where the horizontal split-lines intersect the vertical split-lines as in a typical compressor casing.

7. The low leakage characteristics of the carbon face contact seals make them desirable for use at bearing cavity locations.

8. Misalignment had a significant effect on the leakage rates of the labyrinth and carbon face seals tested.

9. A variable geometry compressor vane seal, consisting of a nitrided A286 shaft in a Rulon-A bushing, proved to be a durable and effective sealing arrangement.

10. A variable geometry turbine vane seal, consisting of an S-Monel bushing and a nitrided A286 shaft, proved to be durable for operation in a high temperature environment but the overboard leakage from this mechanism resulted in significant performance losses.

RECOMMENDATIONS

It is recommended that:

1. The effects of leakage on engine performance be minimized by assuring that:
   (a) Air/gas leakage is reduced to a minimum and accurately predicted.
   (b) Leakages are accurately accounted for in the engine cycle.
   (c) Particular attention is given to sources of overboard leakage.
   (d) Internal leakage is used as efficiently as possible elsewhere in the engine system.

2. Advanced sealing techniques suitable as replacements for labyrinth seals be investigated.

3. A sealing technique for the intersection of the compressor case horizontal and vertical split-lines be developed.

4. The sealing effectiveness of the variable-geometry turbine vane trunnion seal be improved.

SELECTED BIBLIOGRAPHY

Zabriskie, W., and Sternlight, B., LABYRINTH-SEAL LEAKAGE ANALYSIS, Journal of Basic Engineering, Transactions of the ASME, September 1959, pp. 332-340.

Johnson, D. L., THE CONTROLLED GAP AND SEGMENTAL SEALS, National Conference on Fluid Power, 1965, pp. 39-43.

Hamaker, J., NEW MATERIALS IN MECHANICAL END FACE SEALS. National Conference on Fluid Power, 1965, pp. 58-65.

Benrnd, L. H., SURVEY OF THE THEORY OF MECHANICAL FACE SEALS, Parts I, II, and III, Lubrication Engineering, October, November, December 1968, pp. 479- 484, 525-530, 597-604.

Ewbank, W. J., DYNAMIC SEALS - A REVIEW OF THE RECENT LITERATURE, ASME Publication 67-WA/LUB-24, November 1967.

Shevchenko, R. P., SHAFT, BEARING AND SEAL SYSTEMS FOR A SMALL ENGINE, SAE Publication 670064, January 1967.

Heck, J. A., THE CIRCUMFERRENTIAL SEAL: ITS APPLICATION, ITS PLACE IN THE SEAL SPECTRUM RELATIVE TO GAS TURBINES, SAE Publication 670062, January 1967.

Hawkins, R. M., DEVELOPMENT OF COMPRESSOR END SEALS, STATOR INTERSTAGE SEALS AND STATOR PIVOT SEALS IN ADVANCED AIR-BREATHING PROPULSION SYSTEMS, Pratt and Whitney Aircraft Report PWA-3597, January 1969, NASA Contract NAS3-7605.

Smoley, E. M., SEALING WITH GASKETS, Machine Design, October 1966, pp. 172-185.

Bialkowski, L. S., and W. J. Le Blanc, A METALLIC SEAL DESIGN FOR ADVANCED SYSTEMS, SAE Publication 523B, April 1962.

Baskey, R. H., AN INVESTIGATION OF SEAL MATERIALS FOR HIGH-TEMPERATURE APPLICATION, ASLE Transactions, April 1960, pp. 116-123.

Wallach, J., et Al., CALCULATION OF LEAKAGE BETWEEN METALLIC SEALING SURFACES, ASME Publication 68-LUB-15, October 1968.

Roth, A., and Inbar, A., A NEW METHOD OF EXPRESSING AND MEASURING THE SEALING ABILITY OF GASKET MATERIALS, Journal of Materials, Vol. 2, No. 3, September 1967, pp. 567-580.

Alford, J. S., and Lawson, G. W., DIMENSIONAL STABILITY AND STRUCTURAL INTEGRITY OF LABYRINTH SEALS, SAE Publication 660048, January 1966.

DYNAMIC SEALING: THEORY AND PRACTICE, Koppers Company, Inc., Baltimore, Maryland.

Gardner, J. F., COMBINED HYDROSTATIC AND HYDRODYNAMIC PRINCIPLES APPLIED TO NON-CONTACTING FACE SEALS, ASLE, FICFS Preprint No. 36, 1969.

Taschenberg, E. J., et al., EVALUATION OF DESIGNS AND MATERIALS FOR HIGH SPEED - HIGH TEMPERATURE SHAFT SEALS FOR TURBOJET ENGINE APPLICATIONS, WADC Technical Report 56-267, Part I May 1956, Part II December 1958.

Spooner, R. B., Lagarias, J. S., and Pfoutz, B. D., EVALUATION OF SEAL-LUBRICANT DEPOSIT FORMATIONS UNDER HIGH-TEMPERATURE CONDITIONS, U.S.A.F. Aerospace Fluids and Lubricants Conference, 1963, pp. 80-92.

Brown, P. F., Gordon, N., and King, W. J., A TEST METHOD FOR EVALUATING GAS TURBINE ENGINE SEAL MATERIALS, Lubrication Engineering, January 1966, pp. 7-16.

APPENDIX
METHODS OF ESTIMATING LEAKAGES

A. Labyrinth Seal Leakage*

$$W = \frac{(C_D C_L)\ (D)\ (P_1)\ (N)}{(.6)\ \ (\sqrt{T})}$$

W = Flow - lb/sec

$C_D C_L$ = Flow Function

D = Fin Diam - inch

P_1 = Upstream Press. - psia

N = Restriction Factor

T = Air Temp - °R

B. Flange Leakage

Assume leakage equation approximates a labyrinth seal with one fin operating against a flat plate.

B. Leakage by Trunnion Bushing or Controlled Gap Circumferential Seal**

$$q = \frac{.00108}{1728} (1000C)^3 \frac{dP}{\mu L}$$

q = flow - cu. ft/min.

C = radial clearance - inch

P = Δ P across bushing - psi

d = diam. of bushing - inch

L = length of bushing - inch

μ = abs. viscosity of gas - poises

---

*Labyrinth Seal Design Handbook No. XE756, Curtiss-Wright Corporation, Wood-Ridge, N.J., June 30, 1965.

**Mechanical Engineers' Handbook, L. S. Marks, Fifth Edition, 1951, pp. 939.